INVESTIGATIONS ON HIGH GAIN AND BROADBAND CIRCULARLY POLARIZED ANTENNAS FOR 5GHz WI-FI APPLICATIONS

Submitted in partial fulfilment of the requirements of the degree of

DOCTOR OF PHILOSOPHY

by

GUTHI SRINIVAS

(Roll No.717130)

Under the guidance of

Prof. D. VAKULA

DEPARTMENT OF ELECTRONICS AND COMMUNICATION ENGINEERING
NATIONAL INSTITUTE OF TECHNOLOGY WARANGAL
TELANGANA, INDIA-506 004

2022

APPROVAL SHEET

This Dissertation Work entitled "**Investigations on high gain and broadband circularly polarized antennas for 5GHz Wi-Fi applications"** by **Guthi Srinivas, Roll No. 717130** is approved for the degree of Doctor of Philosophy

Examiners

_____

_____

_____

Supervisor

_____

Chairman

_____

Date:_____ Place: _____

DECLARATION

This is to certify that the work presented in the thesis entitled "**Investigations on high gain and broadband circularly polarized antennas for 5GHz Wi-Fi applications**" is a bonafide work done by me under the supervision of **Prof. D. Vakula**, Professor, Department of Electronics and Communication Engineering, National Institute of Technology Warangal and was not submitted elsewhere for the award of any degree.

I declare that this written submission represents my ideas in my own words and where others' ideas or words have been included, I have adequately cited and referenced the original sources. I also declare that I have adhered to all principles of academic honesty and integrity and have not misrepresented or fabricated or falsified any idea/data/fact/source in my submission. I understand that any violation of the above will be a cause for disciplinary action by the Institute and can also evoke penal action from the sources which have thus not been properly cited or from whom proper permission has not been taken when needed.

Guthi Srinivas
(Roll No:717130)
Date:……

DEPARTMENT OF ELECTRONICS AND COMMUNICATION ENGINEERING
NATIONAL INSTITUTE OF TECHNOLOGY, WARANGAL
TELANGANA, INDIA-506 004

CERTIFICATE

This is to certify that the thesis entitled **"Investigations on High Gain and Broadband Circularly Polarized Antennas for 5GHz Wi-Fi Applications "**, which is being submitted by **Mr. Guthi Srinivas (Roll No.:717130)**, in partial fulfilment for the award of the degree of Doctor of Philosophy to the Department of Electronics and Communication Engineering of National Institute of Technology Warangal, is a record of bonafide research work carried out by him under my supervision and guidance and has not been submitted elsewhere for any degree.

Signature of Supervisor

Prof. D. Vakula
Department of ECE
NIT Warangal
Warangal, Telangana,
India-506004

ACKNOWLEDGEMENTS

First and foremost, I owe my deepest gratitude to my research supervisor, Prof. D. Vakula, Professor, Department of Electronics and Communication Engineering, National Institute of Technology Warangal who has been my mentor not only in research, but for many other things in life for her help, kindness, patience, unwavering support and constant encouragement more than I could ever ask for throughout my years as a graduate student. She has been instrumental in often returning me to the correct point of view at various points during my research. Her advice and guidance on matters both academic and non-academic have proved invaluable time. I feel very thankful not only for the research guidance but also for the humanity shown on me.

I am also grateful to Prof. P. Srihari Rao, Head, Department of Electronics and Communication Engineering, for his invaluable assistance and suggestions that he shared during my research tenure.

I take this privilege to thank all my Doctoral Scrutiny Committee members, Prof. Y. N. Reddy, Professor of Department of Mathematics, Dr. A. Prakasa Rao, Associate Professor of Department of Electronics and Communication Engineering, and Dr. G. Arun Kumar, Assistant Professor of Department of Electronics and Communication Engineering for their detailed review, constructive suggestions and excellent advice during the progress of this research work.

I am also thankful to Prof. N. V. S. N Sarma for giving valuable suggestions during his tenure and I am also very grateful to the former Heads of the ECE department Prof. L. Anjaneyulu and Prof. N. Bheema Rao for their suggestions. I would also like to thank all the faculty members and research scholars of the ECE department, and also friends for their continuous support and encouragement.

I thank the Government of India and MHRD for financial support.

I also thank the team of Microwave wing headed by Mr. Rakesh Kumar Singh, RCI, Hyderabad, the team of Antenna wing headed by C. Sai ram, DLRL, Hyderabad and M/s Cosmic Enterprises, Hyderabad for providing measurement and fabrication facility.

I would like to acknowledge my biggest debt to my family members for their continuous support.

Guthi Srinivas

ABSTRACT

Nowadays, the internet is the primary medium of information and people communicate from anywhere with an internet connection. Now people are connected to the internet through wireless without any cable which is possible by Wi-Fi (IEEE 802.11). Wi-Fi is used by a wide range of devices, including smartphones, laptops and tablets. Many Wi-Fi antennas are available in the market such as 2.4GHz Wi-Fi antenna, 5GHz Wi-Fi antenna and 2.4/5GHz Wi-Fi antenna. These antennas are working at 2.4GHz (2.402GHz-2.483GHz) and 5GHz (5.150GHz-5.850GHz). Some of them are designed to work at both frequencies.

In the thesis, the antennas are designed to work at the entire 5GHz Wi-Fi frequency with high gain directional radiation patterns and circular polarization. In addition, the broadband and high gain circularly polarised antennas with compact sizes are realised. Gain and bandwidth enhancement techniques are applied simultaneously and also circular polarization is realized.

A high gain and broadband circularly polarized antenna is designed for 5GHz Wi-Fi applications. Conventional structures like a pentagonal patch and square patch are truncated to get circular polarization. The impedance bandwidth of the antenna is improved by adding RIS structure as a ground plane and the gain of an antenna is improved by placing a superstrate approximately half wavelength above the antenna. The pentagonal patch antenna is combined with the RIS structure and FSS superstrate to increase both gain and impedance bandwidth. Furthermore, the truncated corner square patch is combined with RIS structure and high dense dielectric sheet as superstrate to improve both gain and impedance bandwidth.

In order to achieve broadband axial ratio bandwidth, unconventional structures like H, C, E and S structures are designed with RIS structure as a ground plane. The S-shaped structure with RIS structure is providing good impedance matching over H, C and E structures. Moreover, the superstrate is placed above an S-shaped patch with RIS structure to get improvement in impedance bandwidth, gain and axial ratio bandwidth.

In order to design a high gain and broadband circularly polarized antenna in the single-layer substrate, the metasurface with aperture CPW feed technique has opted. Initially, the metasurface is designed with a 3x3 array of circle patches on the top face of the substrate and L shaped aperture CPW feed is designed on the bottom face of the substrate. The stubs are added across the slot and the central patch size in the metasurface is reduced to further enhance the impedance bandwidth and an axial ratio bandwidth.

In the case of uniform aperture CPW feed, the changes are made in the metasurface to design high gain and broadband circularly polarized antenna in a single layer substrate. The

metasurface is designed with a 3x3 array of truncated corner square patches or a 3x3 array of 45^{o} tilted slot-loaded square patches on the top face of the substrate and stub-loaded uniform aperture CPW feed is designed on the bottom face of the substrate.

High-frequency structure simulator simulations are used for the design and realization of the antenna configuration. All the antenna designs are fabricated, evaluated and measured results are validated with simulation results.

The outcome of the research work led to the development of novel techniques for high gain and broadband circularly polarized antennas. The impedance bandwidth is improved using RIS structure and the gain of the antenna is improved using superstrate. In addition to that, circular polarization is achieved using conventional and unconventional structures. The compact antenna in a single layer substrate is designed using a metasurface with aperture CPW feed for the high gain and broadband circular polarization.

All the antennas developed have promising applications in 5GHz Wi-Fi and Wi-Max applications.

CONTENTS

LIST OF FIGURES

LIST OF TABLES

LIST OF ABBREVIATIONS

RF	Radio Frequency
Wi-Fi	Wireless Fidelity
Wi-Max	Worldwide Interoperability for Microwave Access
WLAN	Wireless Local Area Network
IEEE	Institute of Electrical and Electronics Engineering
VNA	Vector Network Analyzer
RIS	Reactive Impedance Surface
HIS	High Impedance Surface
PRS	Partially Reflecting Surface
FSS	Frequency Selective Surface
FPR	Fabry Perot Resonator
CPW	Coplanar Waveguide
NRI	Negative Refractive Index
LHM	Left Handed Material
NZRI	Near Zero Refractive Index
SRR	Split Ring Resonator
HFSS	High-Frequency Structure Simulator
SMA	Sub Miniature version A
FCC	Federal Communications Commission
VSWR	Voltage Standing Wave Ratio
AR	Axial Ratio
CP	Circular Polarization
PEC	Perfect Electric Conductor
LHCP	Left Hand Circular Polarization
RHCP	Right Hand Circular Polarization
TM	Transvers Magnetic
EM	Electro Magnetic
GHz	Giga Hertz
MHz	Mega Hertz

LIST OF SYMBOLS

λ	Wavelength
f	Frequency
ε	Permittivity
ε_o	Free Space Dielectric Constant
ε_r	Relative Dielectric Constant
μ	Permeability
μ_o	Free Space Permeability
μ_r	Relative Permeability
Γ	Reflection Coefficient
φ	Reflection Phase
$\tan\delta$	Loss tangent
D	Directivity
G	Gain

Chapter 1

Introduction

1.1 Overview

Nowadays there is an increasing number of applications emerging in wireless communications. The antenna is the fundamental component in any wireless system. It converts the electrical signal to electromagnetic waves and vice versa as shown in fig. 1.1. The transmitting antenna has to radiate the field towards the target without interfering with the other communication systems [1-3]. The receiving antenna converts an incoming electromagnetic wave to an electrical signal, preferably with the exclusion of all other electromagnetic signals in the vicinity.

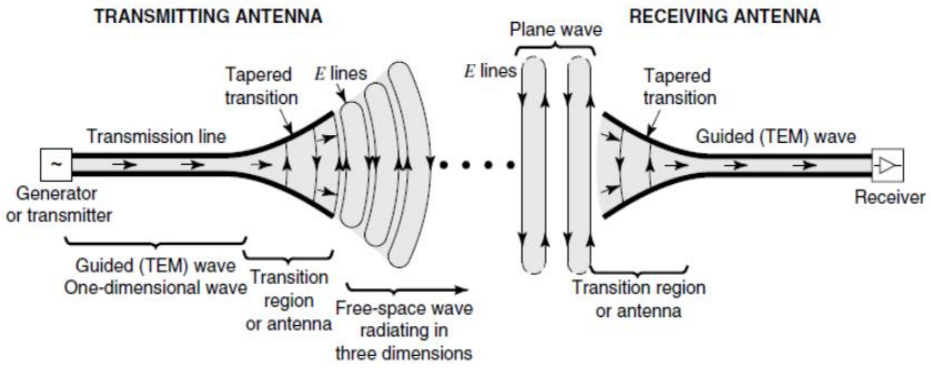

Fig.1.1. Basic radio communication system [3]

The dipole antenna is made up of half-wavelength wire cut into two-quarter wavelengths as shown in fig. 1.2. The source is connected at the centre of the wire. The vertically oriented antenna has a vertical polarized electric field. They produce omni directional radiation patterns. It looks like a doughnut-shaped pattern as shown in fig. 1.3.

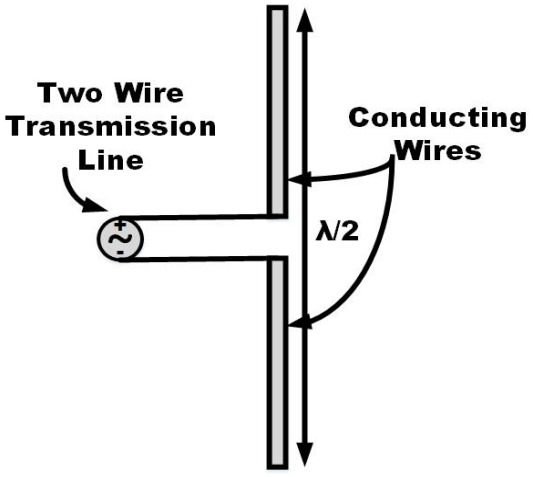

Fig.1.2. Half -wave dipole antenna

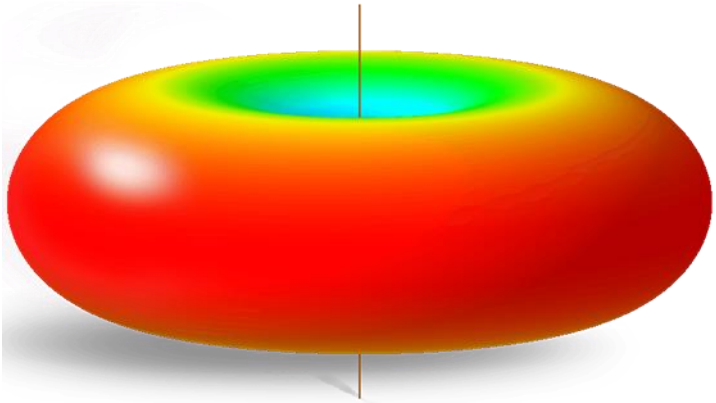

Fig.1.3. 3D radiation pattern of vertically oriented dipole antenna [80]

The slot antenna is dual of a dipole antenna, it is made up of cutting half wavelength slot from the conducting sheet as shown in fig 1.4. Its radiation pattern is similar to a dipole antenna whereas the vertically oriented slot antenna has a horizontal electric field component. These slot antennas also produce an omni-directional radiation pattern.

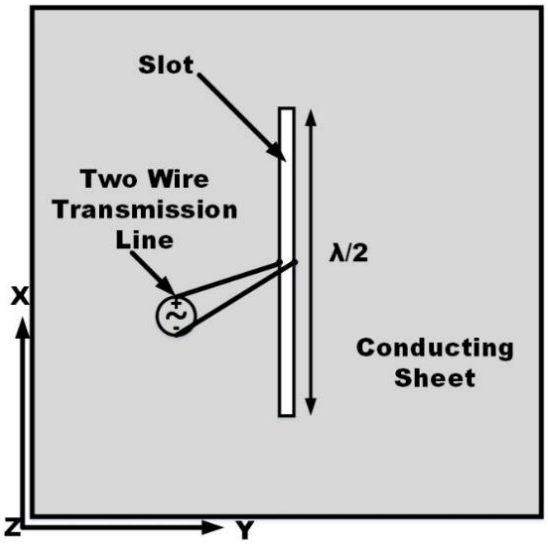

Fig.1.4. Slot antenna

Microstrip patch antennas consist of a radiating patch on a grounded dielectric substrate as shown in fig 1.5. When the patch is excited, the waves generated within the dielectric form reflections and are emitted from the edges of the radiating patch [4]. The microstrip patch antennas radiate in the broadside direction due to the radiation of fringing fields and they are simple to design and fabricate

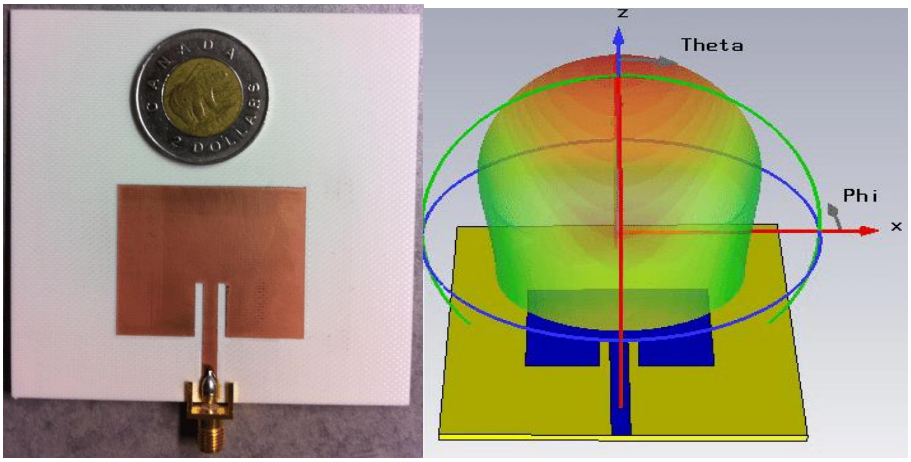

Fig. 1.5.Microstrip patch (a) Prototype [81] (b) 3-D Radiation pattern [82]

Some other types of antennas are available depending on the radiation phenomenon such as yagi-uda antennas which consist of folded dipole antenna as a source, reflectors and directors as shown in fig. 1.6a. They radiate in the direction of directors. Horn antennas radiate from the aperture of the flared waveguide as shown in fig. 1.6b. Parabolic reflector antennas collimate the rays from the radiating source as shown in fig. 1.6c. The radiating source may be a dipole antenna or slot antenna.

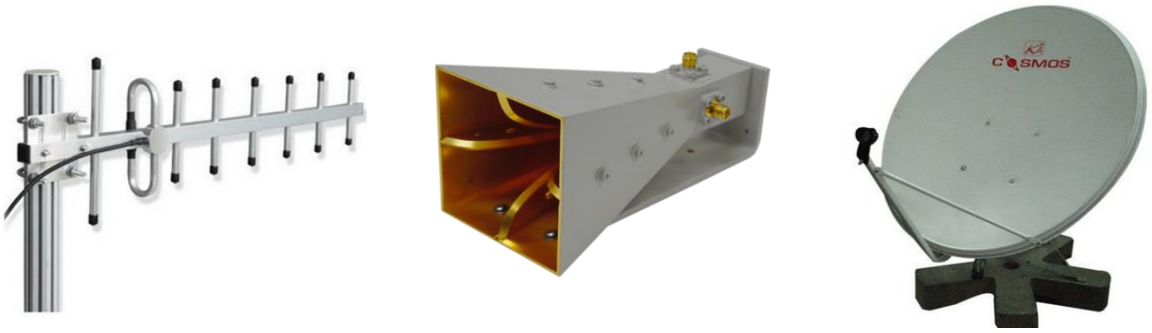

(a) (b) (c)

Fig.1.6. Antennas(a) Yagi-uda antenna[83] (b) Horn antenna[84] (c) Parabolic antenna[85]

The performance of antennas can be analyzed by using the parameters such as impedance bandwidth, gain, axial ratio, radiation pattern and polarization. Impedance bandwidth mentions the range of frequencies radiated due to proper coupling from the feed to the antenna and it is also expressed as fractional bandwidth. It can be calculated by indicating the reference level of the reflection coefficient is -10dB, or VSWR is 2, or return loss is 10dB. The lowest indicated value is f_{min} and the highest indicated value is f_{max}. The impedance bandwidth is the ratio of absolute bandwidth (difference between f_{max} and f_{min}) to center frequency.

Gain is another important parameter that decides the distance of transmission. It is the ratio of radiation intensity in a particular direction to an isotropic antenna. If the gain of the antenna is less, the signal covers a short distance only. If the gain of the antenna is more, the signal covers longer distances. It is always calculated with respect to the reference antenna.

A radiation pattern is a graphical representation of antenna far-field radiation characteristics as a function of direction. Gain, directivity and radiation vector are all different types of parameters that can be represented by the radiation pattern. They are termed gain patterns, directivity patterns and radiation vector patterns. Antennas are categorized based on the radiation pattern.

Omnidirectional antennas radiate uniformly the radio signal in all directions in one plane as shown in fig. 1.7. Omnidirectional antennas are best suitable for network hubs because they provide coverage in all directions. But, the gain of the antenna is limited. Some examples of the omnidirectional antennas are dipole antennas, slot antennas and monopole antennas.

Directional antennas radiate in a particular direction with increased gain compared to omnidirectional antennas as shown in fig. 1.7. Therefore, directional antennas are used to send and receive the enhanced signals in a particular direction. The major advantage of these directional antennas is that they have improved gain. Some examples of directional antennas are yagi-uda antennas, panel antennas, horn antennas and parabolic antennas.

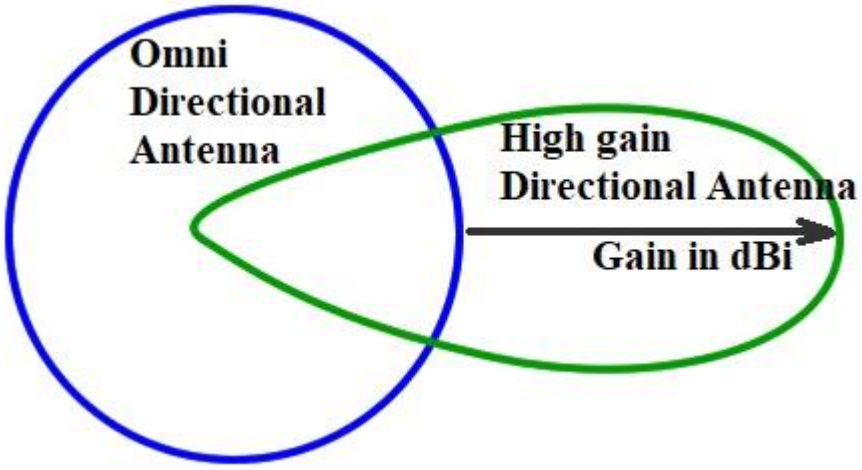

Fig.1.7. Omni-directional and directionl radiation pattern[86].

The alignment of an electric field in the electromagnetic wave radiated by the antenna decides the polarization of the antenna as shown in fig. 1.8. For a linearly polarized antenna, the electric field varies over a straight line and for circular polarization, the tip of the electric field forms the circle. If the wave coming out of a plane and electric field rotates in the clockwise direction, it is left-hand circularly polarized. If the electric field rotates in the anti-

clockwise direction, it is right-hand circularly polarized. Similarly for elliptical polarization, the tip of the electric field forms the elliptical pattern and there are left-hand elliptical polarization and right-hand elliptical polarization depending on the rotation of the direction of electric field. In the case of co-polarization, both the transmitter and receiver are oriented in the same polarization. In the case of cross-polarization, both the transmitter and receiver are oriented in different polarization.

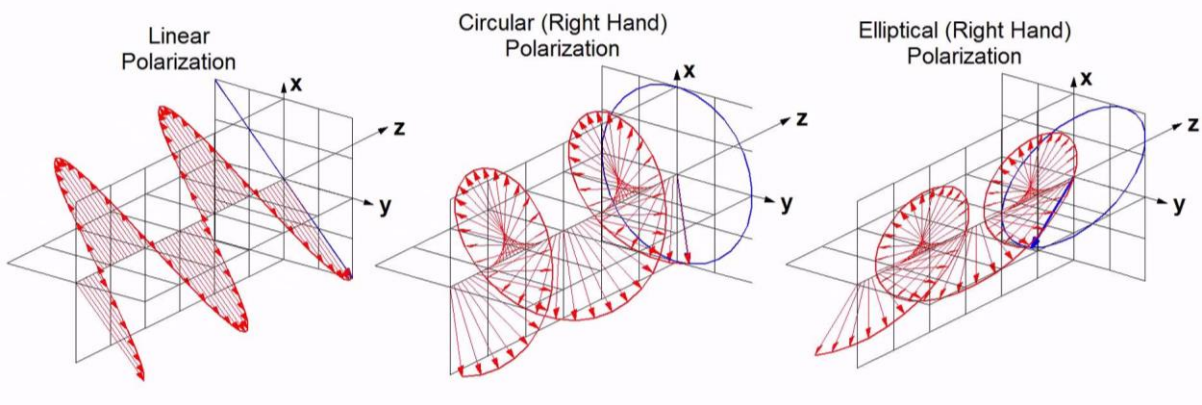

Fig.1.8. Different types of polarizations[87].

The polarization of the antenna will be decided by the current distributions on the conducting surfaces of the antenna which intern depends on the geometry and feed location. Polarization is an important parameter of the antenna which depends on the application. Linear polarization is preferred for fixed terminals, whereas circular polarization is suitable for mobile terminals. In circular polarization, the receiving antenna need not be aligned with respect to the transmitting antenna. But the generation of circular polarization is a complex phenomenon where the electric field has to be generated with two components in an orthogonal direction and 90^{o} phase delay[5]. Now a day's circular polarization is preferred for wireless mobile devices.

The type of polarization is decided by the axial ratio (AR). The axial ratio is calculated as the ratio of the major axis to the minor axis. In terms of decibels, it is a difference in power level between the maximum and minimum power radiated in one plane perpendicular to the direction of propagation. For circular polarization, the axial ratio lies between 0 to 3dB, for elliptical polarization, it varies from 3 to 20dB and for linear polarization, it is above 20dB.

Nowadays, the internet is the primary medium of information and people communicate from anywhere with an internet connection. Usually, the internet is provided through a local area network (LAN) cable. Now people are connected to the internet through wireless, without any cable which is possible by Wi-Fi (Wireless Fidelity) (IEEE 802.11). Wi-Fi is playing a major role in everyone's life. It is used by a wide range of devices, including smartphones, laptops and tablets, as well as remote sensors, actuators, televisions and many others. All the

wireless devices will be connected to the Wi-Fi router. For this, antennas are required at both the router and wireless devices to have continuous communication. Wi-Fi is continuously progressed as 802.11, 802.11b/a/g/n/ac/ax. The 802.11 (first version) is released in 1997. 802.11 ax (Wi-Fi 6) is released in 2019. Wi-Fi has advanced over the past 20 years from 2 Mbps to 10Gbps, with over 1000-fold improvement in speed and throughput. In the evolution of Wi-Fi technology, two frequencies are allotted as shown in fig. 1.9. One is the 2.4GHz frequency band (2.402GHz-2.483GHz) and the other is the 5GHz frequency band (5.150GHz-5.850GHz).

Fig.1.9. Wi-Fi frequencies [88]

Table 1.1: IEEE 802.11 Wi-Fi protocol summary

Protocol	**Frequency**	**Channel Width**	**MIMO**	**Maximum data rate (theoretical)**
802.11ax	2.4 or 5GHz	20, 40, 80, 160MHz	Multi User (MU-MIMO)	2.4 Gbps, 1024 QAM
802.11ac wave2	5 GHz	20, 40, 80, 160MHz	Multi User (MU-MIMO)	1.73 Gbps, 256 QAM
802.11ac wave1	5 GHz	20, 40, 80MHz	Single User (SU-MIMO)	866.7 Mbps, 256 QAM
802.11n	2.4 or 5 GHz	20, 40MHz	Single User (SU-MIMO)	450 Mbps, 64 QAM
802.11g	2.4 GHz	20 MHz	N/A	54 Mbps
802.11a	5 GHz	20 MHz	N/A	54 Mbps
802.11b	2.4 GHz	20 MHz	N/A	11 Mbps
Legacy 802.11	2.4 GHz	20 MHz	N/A	2 Mbps

In the 802.11b, 802.11g operate only in the 2.4GHz band whereas 802.11a, and 80211ac operate in the 5GHz band as shown in Table 1.1. 802.11 n and 802.11 ax use both 2.4GHz and 5GHz frequency bands. In the allotted bandwidth at 2.4 GHz, 20MHz and 40MHz channel bandwidths with overlapping channels are provided. And at 5GHz band 20MHz, 40 MHz, 80 MHz and 160

MHZ with non-overlapping channels are provided. When compared with 2.4GHz, 5GHz Wi-Fi has better data rates and increased channel capacity. In addition, 2.4 GHz Wi-Fi has interference with other wireless devices like Bluetooth devices and microwave ovens.

Many Wi-Fi antennas are available in the market such as 2.4GHz ceiling monopole antenna model No.CA-24-04 working at 2.4GHz (2.402GHz-2.483GHz) and TP-Link CPE610 5GHz Wi-Fi directional antenna working at 5GHz (5.150GHz-5.850GHz). Some of them are designed to work at both frequencies such as 2.4/5GHz Wi-Fi Ceiling monopole type antenna model No. CA-2458-02 working at 2.4GHz (2.402GHz-2.483GHz) and 5GHz (5.150GHz-5.850GHz).

Different types of antennas are available such as dipole antennas, ceiling dome monopole antennas, yagi-uda antennas, panel antennas and grid parabolic antennas for Wi-Fi applications.

2.4GHz Wi-Fi Antennas:

Yagi-Uda antenna: The model number Cyberbajt / YAGI 24-12 is displayed fig. 1.10 a. It has yagi beam-type radiation which operates in the frequency range 2400 - 2485 MHz following IEEE 802.11 b/g/n. The gain of the antenna is 12dBi and has linear polarization (horizontal or vertical polarization).

Directional Grid Antenna: The model number ALFA Networks / AGA-2424T is displayed in fig. 1.10 b and has a directional pattern for IEEE 802.11 b/g/n. The antenna is used in the frequency range 2400 - 2500 MHz with 24dBi gain with linear polarization (horizontal or vertical polarization).

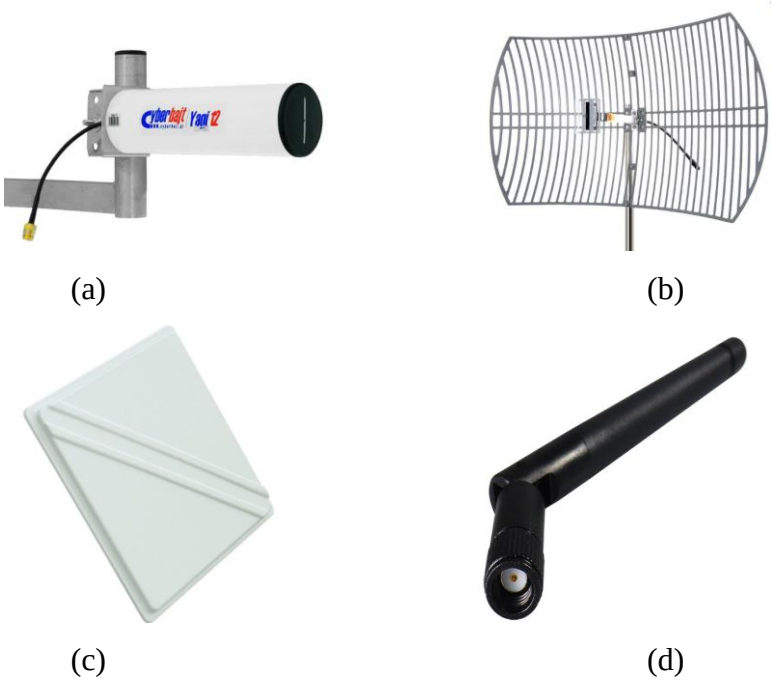

(a) (b)

(c) (d)

Fig.1.10. 2.4GHz Wi-Fi antennas (a)Yagi-uda antenna [89] (b) Directional Grid Antenna[90] (c) Directional Panel Antenna[91] (d) Omni directional antenna[92]

Directional Panel Antenna: The model number Interline / IP-G08-F2425-HV is displayed in fig. 1.10 c. It has a directional pattern. It is also operating in the frequency range 2400 - 2500 MHz. It can be useful for IEEE 802.11 b/g/n. The gain of the antenna is 8 dBi and It supports linear polarization (horizontal or vertical polarization).

Dipole antenna: The model number DA-24-04 is displayed in fig. 1.10 d. It has an omni-directional radiation pattern with linear polarization. The Antenna is useful for IEEE 802.11 b/g/n in the frequency range 2400 - 2500 MHz. The gain of the antenna is 2 dBi.

5GHz Wi-Fi Antennas:

Dipole antenna: The model number Interline HORIZON 12 (IH-G12-F5458-V) is displayed in fig. 1.11 a with omni directional radiation pattern. It is useful for IEEE 802.11 a/n in the frequency range 5.4 - 5.8 GHz. It supports linear polarization (horizontal or vertical polarization) with a gain of 12dBi.

Directional Panel Antenna: The model number Interline IP-G23-F5258-HV is useful for IEEE802.11a/n/ac in the frequency ranges 5.0 – 5.85 GHz as displayed in fig. 1.11 b. It has directional radiation with a gain of 23dBi and It supports linear polarization.

Directional Parabolic Antenna: The model number TP-Link CPE610 is operating at the frequency of 5.85 GHz displayed in fig. 1.11c. It can be useful for IEEE802.11a/n. The gain of 23dBi with directional radiation pattern. It shows linear polarization (horizontal or vertical polarization)

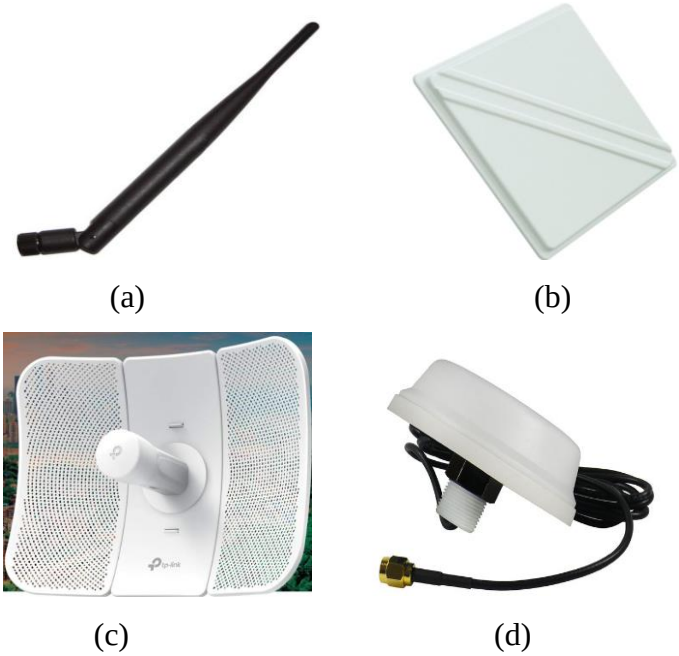

(a) (b)

(c) (d)

Fig.1.11. 5 GHz Wi-Fi antennas (a) Omni directional antennas[93] (b) Directional Panel Antenna[94] (c) Directional Parabolic Antenna[95] (d) Ceiling dome antenna[96]

Ceiling/Roof monopole Antenna: These antennas have the advantage to fix into ceiling/roof. The model number CA-2458-02 has an omnidirectional radiation pattern as displayed in fig.

1.11 d. It is operating in the frequency ranges 2.4 - 2.5 GHz, 5.1 - 5.9 GHz and It can be useful for IEEE802.11 b/g/n, IEEE802.11 a/n. The gain of 3dBi at 2.4GHz and 5dBi at 5GHz. It supports linear polarization (horizontal or vertical polarization).

The 5GHz Wi-Fi with the advantage of more channel bandwidth support data rate up to Gbps. Some of the antennas designed at 5GHz have more gain to provide a signal to longer distances. Omnidirectional coverage can be obtained by using point to multi-point high gain directional antennas where the number of directional antennas can be used to provide the signal to multiple directions as shown in fig. 1.12. The signal can be provided to a particular location by using point to point high gain directional antenna where the single directional antenna is used as shown in fig. 1.12a.

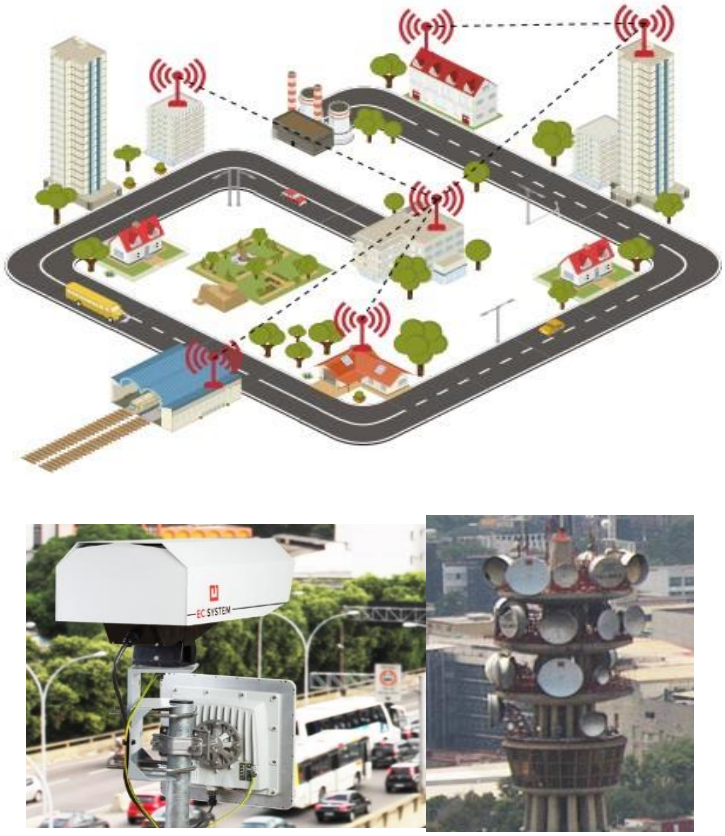

(a) . (b)

Fig.1.12. Wi-Fi coverage to the entire area [97] (a) Point to point equipment [98] (b) Point to multipoint equipment[99]

Although many types of antennas are designed at Wi-Fi frequency. The compact antenna design with less cost is a challenging problem. Antennas are developed for present and future applications using microstrip technology which is a planar antenna. Microstrip patch antenna has a ground plane and radiating patch separated by the dielectric material of small

thickness usually 0.8mm to 3.2mm. Microstrip patch antennas have the advantages of low profile, low cost and are easily integrated into planar antennas. But, they also have a few disadvantages of narrow bandwidth and low gain.

It can be observed that the 5GHz Wi-Fi has more spectrum (i.e. 5.150GHz-5.850GHz) with more number of channels and its frequency is not used by other wireless devices and also this spectrum has less interference with other wireless devices. Hence 5GHz Wi-Fi has become more popular when compared with 2.4GHz Wi-Fi in present and future applications. As the antenna is a major component of any wireless system, antennas for 5GHz are to be designed with better performance.

The major problem of wireless devices is a weak signal due to the low gain of an antenna. Weak signal and bad coverage problems can be solved by using high gain directional antennas. Due to the above-mentioned reasons, high gain directional antennas may be preferred at 5 GHz Wi-Fi.

In the case of linear polarization, the polarization of the signal is changed due to faradays rotation in the atmosphere or multipath propagation. The signal is not received by the receiver antenna due to a change in polarization whereas the circular polarization still maintains the same polarization. So there is no polarization loss in circular polarization. Circular polarization can be attained by using a helical antenna. But these structures are very large, and not suitable for a compact device. The microstrip patch antenna is generating circular polarization with dual feeding techniques but it is difficult to give dual feeding. So the antenna designers are focusing to design circularly polarized antennas using single feeding techniques. Antennas for 5GHz Wi-Fi band are to be explored further to meet all the future demands.

1.2. Motivation

The antenna is a major element of the 5GHz Wi-Fi system which is used in many applications. To meet the demands of the 5GHz Wi-Fi system, an antenna has to be designed to operate in the 5.15GHz to 5.85GHz frequency band. To meet the requirements of the size constraints, the designed antenna at 5GHz Wi-Fi is to be as compact as possible. It is well known that microstrip technology gives planar and compact designs. Basically, the microstrip patch antenna has a narrow bandwidth. It is required to improve the bandwidth of the microstrip patch antenna to operate with fractional bandwidth of 12.7%. The bandwidth of the antenna can be improved by applying various available techniques. To maintain low transmitted power an

omnidirectional antenna can be replaced with multiple directional antennas to further enhance the gain. Existing and novel gain enhancement techniques can be applied to the 5GHz Wi-Fi antenna. The novel combination of gain and bandwidth enhancement techniques together can be incorporated to achieve novel designs.

There is a requirement for circularly polarized antennas to overcome the drawbacks of linearly polarized antennas. Polarization of EM wave change due to faraday's rotation in the atmosphere or due to multipath propagation. Hence, the signal is not received by the linearly polarized receiver antenna due to polarization mismatch. So, the circularly polarized antenna is preferred at 5GHz Wi-Fi frequency. Circular polarization is becoming the major requirement of mobile devices. So, the 5GHz antenna should have broadband, high gain and also has to generate circular polarization. In general, two feeds are suggested for generating circular polarization. Novel techniques like slots, truncation and structural modifications can be applied to achieve circular polarization with a single feed.

There is a demand to integrate many services into one device which makes the antenna have a compact size and the antennas used at 5 GHz Wi-Fi is to have a directional pattern with high gain and broadband bandwidth. Meeting the 5GHz Wi-Fi requirements is a great challenge for antenna designers. The design of such antennas with optimal characteristics is difficult to attain using conventional methods. Hence, novel techniques have to be applied for the realization of a 5GHz Wi-Fi antenna.

1.3. Literature Review

Various techniques are published to improve the bandwidth of the microstrip patch antenna. One such technique is the application of reactive impedance surfaces (RIS). Hossein Mosalleai (2004) et al investigated a reactive impedance surface (RIS) to increase the impedance bandwidth. The RIS is designed with an array of square patches which are placed below the radiating square patch. The antenna achieved an impedance bandwidth of 6.7% with a gain of 4.5dBi at 1.85GHz. But the gain of the antenna is not enough for present applications [6]. D. Qu. Shafai (2006) et al proposed a high impedance surface as a ground plane to the microstrip patch antenna to improve the impedance bandwidth. The antenna achieves a bandwidth of 25% (10.44GHz-13.38GHz) and the gain is 8.02dBi [7]. Shyam sundar jash (2019) et al presented a complementary C shaped slot loaded patch with RIS structure as a ground plane to design broadband circularly polarized antennas [8]. The above-mentioned techniques improved the impedance bandwidth only.

Antenna gain can be improved by using different techniques as mentioned in the published literature. Recently, the Fabry Perot resonator is applied along the radiation direction to the antenna for gain enhancement. In the Fabry Perot resonator principle, a superstrate is placed approximately half wavelength above the antenna. A cavity is created between the superstrate and the antenna ground plane. The rays emitted by the antenna bounce back and forth between the superstrate and ground plane. Finally, coherent addition of rays is emitted in the direction of normal to the superstrate. Hence, the gain of the antenna can be improved. Superstrates can be designed with a partially reflecting sheet, frequency selective surface, non uniform superstrate and dielectric slab.

Zahra Mousavi Razi (2015) et al discussed the superstrates with 4 different types of elements such as S-shaped elements, square patches, omega-shaped elements and SRR cells. It is observed that the superstrate designed with S-shaped elements has shown good improvement in impedance bandwidth and the gain of the antenna [9]. Yuejun Zheng (2017) et al proposed a superstrate with two types of FSS elements in the chessboard manner to improve the gain of the antenna at 10.8GHz [10]. Swati vaid (2016) et al designed a double-sided PRS with complimentary square loops. The PRS is showing a positive phase gradient property over desired frequency ranges for the enhancement of gain of the patch antenna. The PRS helps to get dual-band operation 3.3 %(8.75-9.04) and 1.9 %(9.34-9.52) with a gain of 10.2 dBi and 8.5dBi respectively [11]. Mohamed Lamine Abdelghani (2017) et al proposed a dual-band antenna at 2.4 GHz and 5GHz with dual slots. The Fabry Perot effect is created with a double-layered PRS surface to provide a positive reflection phase with high reflectivity over a dual-frequency range. The superstrate has improved the peak gains of antennas to 14.9dBi and 14.2 dBi at 2.4 GHz and 5GHz [12]. Zhen Guo Liu proposed an FSS superstrate with dissimilar patches above the U-slotted patch antenna. The antenna achievese an impedance bandwidth of 12.2% and directivity of 18.53dBi [13]. Pan Feng (2017) et al proposed a non-uniform superstrate above the patch antenna at 10GHz to improve the gain of antenna to 20.55dBi and impedance bandwidth to 6.1% [14]. Peng Xie (2017) et al presented a Fabry Perot resonator antenna by keeping reflective metasurface as a ground plane to the dual-band antenna with different polarization in different bands and PRS is used as a superstrate to improve gain of antenna to 17.6dB at 8.75GHz and 19dB at 9.8GHz respectively[15]. M.A Meriche (2019) et al presented a single layer partially reflecting surface superstrate with a 7×7 array of complementary square rings on both sides of a dielectric substrate. This superstrate is showing positive reflection phase gradient property over the desired frequency range to improve the gain

of an antenna to 8.2dB [16]. In the published literature [9-16], gain enhancement techniques are applied for linearly polarized antennas.

In some published literature, the Fabry Perot resonator principle is applied for the circularly polarized antenna which is listed below. Circular polarization can be generated with self-polarizing FSS, the truncated corner square patches and 45^{o} tilted square patches with crossed slots in the following publication [17-21]. S.A. Muhammad (2011) et al proposed a circularly polarized Fabry Perot antenna with a cylindrical waveguide as a feeding element along with a corrugated ground plane to generate linearly polarized waves at 45^{o}. The self-polarizing FSS is placed above the antenna to get a circularly polarized high gain Fabry Perot cavity antenna. The structure achieves a higher gain of 13.5dB at 2.5GHz and axial ratio bandwidth of 1.8 %(2.475-2.520). The impedance bandwidth is 1.12 %(2.49-2.52GHz)[17]. S.A Muhammad (2013) et al presented a Fabry Perot antenna with a self-polarizing property to convert linear polarization into a high gain circular polarized antenna. The source feed is placed in the middle of two FSS and polarization twisting ground plane at one side. The prototype shows a combined bandwidth of 3% at 3.9GHz with realized gain of 18dB [18]. M. Akbari (2016) et al presented a circularly polarized dielectric resonator antenna which is coupled through a cross slot in the ground plane. Superstrate is designed with FSS unit cells to increase the gain of antenna to 15.2dB at 30GHz [19]. Lei Zhang (2017) et al proposed a metasurface of shared aperture to enhance the gain of CP micro strip patch antenna [20]. Ankit Sharma (2019) et al presented a partially reflecting surface and absorbing metasurface to enhance the gain of an antenna that is circularly polarized and reduce the RCS reduction. Top layers of substrates act as absorbing metasurface and bottom layers of substrates act as partially reflecting surfaces to improve gain of antenna [21].

The metamaterial superstrates are designed with negative permittivity and negative permeability simultaneously. Hence, they exhibit negative refractive index(NRI) properties. Furthermore, the propagation vector, electric and magnetic field vector of these materials form a left handed materials(LHM) or negative refractive index materials. The metamaterial with negative refractive index property act like LHM perfect lens to enhance the gain of antennas [22-28].

In the above-discussed papers [9-28], the superstrate is placed at a height of either half-wavelength or quarter wavelength. The metasurface is used in the next section in which the metasurface can be placed at a height of less than a quarter wavelength for gain improvement. The gain of the antenna can be improved by using a metasurface or superstrate at a height less

than the quarter wavelength in the published literature as listed below. Long li et al proposed a partially reflecting surface superstrate with a fishnet structure and mushroom-loaded patches are placed around the patch to reduce the height of superstrate to λ/125 to improve the gain of square patch antenna [29]. Prakash Kumar Panda (2018) et al proposed a metamaterial superstrate at a height λ/12 with Ɛ and μ near-zero property. The metamaterial superstrate has the property of Near Zero Refractive Index(NZRI) Property to enhance the gain of the antenna by 3.4dBi at 2.6GHz [30]. Priyanka Usha proposed a metasurface at a height less than λ/4 with epsilon near zero and negative refractive property to focus the EM wave in the normal direction of superstrate [31]. Hence the gain of ultra-wideband antenna is improved. In the above-discussed structures [29-31], the superstrate is placed at a height of less than a quarter wavelength above the antenna. In the next section, the superstrate is placed above the radiating element without any air gap.

For gain and bandwidth enhancement, the metasurface is placed above the radiating slot without an air gap in the published literature listed below. The metasurface is a two-dimensional structure which helps to improve the gain and bandwidth of antennas. The metasurface discussed here has a dual-layer where one layer consist of metasurface and the feed is placed on another layer. It can be called as a dual-layer metasurface. Initially, linearly polarized antennas with dual-layer metasurface are discussed followed by circularly polarized antennas with dual-layer metasurface.

Feng Han Lin (2017) et al proposed diamond-shaped patches as a metasurface. These patches are excited by a uniform slot in the ground plane. The slot is excited by a micro strip line. The micro strip line is placed in the bottom plane which is orthogonal to the slot. The antenna has achieved an impedance bandwidth of 31% with a gain of 13-14.5dBi at 5GHz - 6GHz [32]. Hao Bai(2019) et al presented high gain metasurface antenna. The antenna made up of two stacking layers with 4×4 array of square patches with same size. The antenna achieved impedance bandwidth of 7.8% at 4.36GHz, 3.6% at 5.02GHz and 41.1%at 6.81GHz. The peak gains are 10.1dBi, 6.9dBi, 10.5dBi respectively [33]. No circular polarization is reported in the above-discussed papers.

Some papers have designed high gain and broadband circularly polarized antenna by placing truncated corner square patches in the middle of the ground plane and metasurface in [34]. Ankit Sharma proposed a circularly polarized antenna with a square ring slot in the ground plane and dual SRR with a microstrip feed line on the opposite side. The metasurface is designed with two similar artificial magnetic conductors orthogonal to each other to improve

the gain of the antenna [35]. But these structures [32]-[35] have used dual layer substrates or multiple layer substrates to design the above-mentioned antennas.

The metasurface is designed using aperture CPW feed in single layer substrate for linearly polarized antennas in the published literature listed below. Hsiu Ping Liao (2019) et al proposed a metasurface on the top face of the substrate with a 3×3 array of two-step dipoles in a tapered manner. The bottom of the substrate is designed with an aperture coplanar waveguide (CPW) feed with a stepped slot. The antenna designed with the above specifications attains an impedance bandwidth of 22.11% with a broadside gain of 7.5dBi [36]. Jun fang Wang (2019) et al proposed a metasurface with a 3×3 array of square patches and the bottom of the substrate is designed with an aperture CPW feed with stair shaped slot. The size of patches in the middle row patches is increased. The antenna designed with the above specifications attains an impedance bandwidth of 67.3% with a peak gain of 9.18dBi [37]. In the published literature, single-layer metasurface antennas with circular polarization are not explored.

In the published literature, reactive impedance surface is applied for bandwidth enhancement and the Fabry Perot resonator principle is attempted to gain improvement. In addition, most of the antennas are generating linear polarization. And also very few papers are presented for gain and bandwidth improvement simultaneously. For a system, the gain and bandwidth product is constant. An improvement in gain decreases the impedance bandwidth and vice versa. No authors have attempted gain and bandwidth enhancement techniques together. In the proposed work, it is attempted to improve gain and bandwidth together with RIS and superstrate. In addition, circular polarization is also realized in most of the proposed antennas in the thesis work. These novel techniques are applied to design a 5 GHz Wi-Fi antenna, which is not available in the published literature. In designing the proposed antenna, the RIS surface is placed for bandwidth enhancement together with the Fabry Perot principle and metasurface for gain enhancement. In most of the proposed antennas, the generation of circular polarization is realized by applying truncation to radiating patches and metasurface unit cells.

The conventional patches like the pentagonal patch and square patch are truncated to get circular polarization. These structures are combined with RIS structure and highly reflective FSS superstrate or dielectric superstrate to design high gain and broadband antennas for 5 GHz Wi-Fi applications. Moreover, the unconventional patch structures like H, C, E and S with RIS structures are designed to get broadband circularly polarized antennas. It is observed that the S-shaped patch is giving good impedance matching compared with other structures. The positive

phase gradient superstrate is placed above the S-shaped patch with RIS structure to design high gain and broadband circularly polarized antenna for 5 GHz Wi-Fi applications.

In order to design antenna in a compact size, metasurface with aperture CPW feed techniques are opted to design high gain and broadband circularly polarized antenna in single layer substrate. Initially, the L-shaped aperture CPW feed is designed on the bottom face and an array of circle patches as a metasurface are designed on the top face of the substrate to get high gain and broadband circular polarization at 5 GHz Wi-Fi applications. Later the array of truncated corner square patches or 45^{o} rotated slot-loaded square patches are used as metasurface with uniform aperture CPW feed to design high gain and broadband circularly polarized antennas in single layer substrate at 5GHz Wi-Fi applications.

The antennas are fabricated and the reflection coefficient is measured using a network analyzer. The radiation pattern measurements are done in an anechoic chamber. The gain and axial ratio are calculated from the measured results. The measured results are compared with simulation results.

1.4. Research Objective

The research primarily focuses on achieving the following objectives:

- To design, simulate, fabricate and test various high gain and broadband circularly polarized antennas for 5 GHz Wi-Fi applications.
- To improve the bandwidth of antenna using reactive impedance surfaces (RIS) structure as a ground plane.
- To improve the gain of the antenna using superstrates above the antenna.
- To improve the gain and bandwidth simultaneously by combining RIS structure as a ground plane and placing superstrates above the antenna.
- To achieve broadband circular polarization while getting high gain and broadband impedance bandwidth.
- To design a compact antenna while getting above performance characteristics.
- To validate the above antenna designs experimentally and compare them with simulation results.

1.5. Contributions of Research Work

The key contributions are summarized as follows:

(1) The Wi-Fi antennas are discussed and the importance of 5 GHz Wi-Fi antennas is reported. Later the need for a 5 GHz Wi-Fi antenna to have broadband and high gain circular polarization and their significance for future Wi-Fi applications are discussed.

(2) A high gain and broadband antenna is designed using a micro strip square patch with RIS structure as a ground plane and dielectric sheets vertically above the antenna. The antenna achieved an impedance bandwidth of 6.9 %(5.13 GHz - 5.50GHz) with an average gain of 9.5 -10.23 dBi.

(3) A microstrip square patch with RIS structure as ground plane and FSS superstrate above the antenna achieved the impedance bandwidth of 5.85%(5.11GHz-5.42GHz) with a peak gain of 8.5dBi.

(4) A pentagonal patch with RIS structure as ground plane and highly reflective FSS superstrate is designed above the antenna to obtain an impedance bandwidth of 17.72% (4.93-5.89GHz) with a peak gain of 12.48dBi. In addition to that, an axial ratio bandwidth of 2.4% (5.01-5.14GHz) is obtained.

(5) A truncated corner square patch with RIS structure as ground plane and dielectric superstrate above the antenna is developed to attain impedance bandwidth of 18% (4.97-5.95GHz) with a peak gain of 9.75dBi. In addition to that the axial ratio bandwidth of 2.9% (5.15-5.30GHz).

(6) A broadband circularly polarized antenna is designed with H shaped patch with a RIS structure as a ground plane. The antenna shows an impedance bandwidth of 23.9% (5.04GHz-6.41GHz) and axial ratio bandwidth of 16.2 % (4.92GHz-5.79GHz).

(7) A broadband circularly polarized antenna is designed with E shaped patch with a RIS structure as a ground plane. The antenna shows an impedance bandwidth of 27.7% (4.82GHz-6.37GHz) and axial ratio bandwidth of 12.4 %(5.11GHz-5.79GHz).

(8) A broadband circularly polarized antenna is designed with C shaped patch with a RIS structure as a ground plane. The antenna shows an impedance bandwidth of 24.9% (4.81GHz-6.18GHz) and axial ratio bandwidth of 12.9 %(5.18GHz-5.90GHz).

(9) S-shaped patch antenna with RIS structure as ground plane and positive phase gradient superstrate to achieve impedance bandwidth of 31.8% (4.81GHz-6.63GHz) with a peak gain of 10dBi. In addition to that the axial ratio bandwidth of 18.9% (4.99GHz-6.03GHz).

(10) H shaped patch with meta patches and CPW fed uniform aperture in single layer substrate is designed to get impedance bandwidth of 34.8% (4.57-6.50GHz) with a gain of 10-11dBi.

(11) Metasurface with circle-shaped patches and L-shaped aperture CPW feed in single layer substrate is designed to get impedance bandwidth of 20.18 (4.9-6GHz) with a peak gain of 10.43dBic. In addition to that the axial ratio bandwidth of 16.21% (5.1-6GHz).

(12) Truncated corner square patch metasurface antenna is designed with uniform aperture CPW feed in single layer substrate to get impedance bandwidth of 38.2% (4.5GHz-6.63GHz) with a peak gain of 10.37dBic.In addition to that the axial ratio bandwidth of 13 %(5.0GHz-5.7GHz).

(13) A 45^{o} slot-loaded square patch metasurface antenna is designed with uniform aperture CPW feed in single layer substrate to get impedance bandwidth of 30% (4.56GHz-6.21GHz) with a peak gain of 10.21dBic.In addition to that the axial ratio bandwidth of 8.6 %(5.23GHz-5.7GHz)

1.6. Chapter Organization

Chapter 1: Introduction

This chapter gives a brief idea about Wi-Fi standards and its techniques to improve the data rates in advanced versions. The benefits of 5 GHz Wi-Fi over 2.4GHz Wi-Fi are discussed. The advantages of directional antennas over omnidirectional antennas are given. Later the need for high gain and broadband circularly polarized antennas at 5GHz Wi-Fi are discussed. The literature review is studied and the research objective is framed for 5GHz Wi-Fi. Then the contributions are listed accordingly.

Chapter 2: Conventional patches with RIS and superstrate for high gain and broadband antenna

This chapter explains the designs of conventional microstrip patch antennas. The techniques to improve the gain and bandwidth simultaneously are discussed. Later circular polarization is generated using conventional patches. The unit cell characteristics are studied and the superstrate is designed with the array of unit cells. The designed superstrate is used to improve the gain of the CP antenna and bandwidth is improved by using the RIS structure.

Chapter 3: Unconventional patches with RIS and superstrate for high gain and broadband circularly polarized antennas

This chapter discusses the design of unconventional patches and reactive impedance surfaces are placed below the patches for designing broadband circularly polarized antennas. The superstrate is designed with positive phase gradient unit cells. The designed superstrate is placed above the unconventional patch with RIS to improve the gain of the antenna.

Chapter 4: Metasurface with CPW fed L-shaped aperture for high gain and broadband circularly polarized antennas

This chapter explains the high gain broadband circularly polarized antenna in single layer substrate. Initially, the technique of metasurface with uniform aperture CPW feed for designing high gain and broadband antenna. Later the circular polarization is generated by using L shaped aperture CPW with a metasurface. Then the techniques of stubs in the slots and non-uniform patches in the metasurface are discussed to further improve impedance bandwidth and axial ratio bandwidth.

Chapter 5: Metasurface with CPW fed uniform aperture for high gain and broadband circularly polarized antennas

This chapter discussed the design of high gain and broadband circularly polarized antennas in single-layer substrates using truncated corner square patches and 45^{o} rotated slot-loaded square patches. The array of patches is used as a metasurface on one side of the substrate and they are excited uniform aperture CPW in the bottom plane. Then changes are made in the metasurface to improve the impedance bandwidth and axial ratio bandwidth.

Chapter 6: Conclusion and Future Scope:

All the results are concluded and the validation of the results is given in this section. The antennas can be designed with a reflector and parasitic patches for further gain and bandwidth enhancement. Compact antennas can be designed for future Wi-Fi applications at higher frequencies (6GHz).

1.7. Conclusion

The significance of antennas in wireless communication is discussed. Later the need of Wi-Fi antennas for internet connectivity and communication is reported. In addition to that the Wi-Fi standards, techniques and maximum data rates are reported. Then the need for broadband antennas and high gain directional antennas for 5GHz Wi-Fi applications are analyzed. The motivation for the design of high gain and broadband circularly polarized antenna at 5 GHz Wi-Fi applications is explained. The literature survey for the improvement of gain, impedance bandwidth and axial ratio bandwidth is studied. The research objective to design a high gain and broadband circularly polarized antenna at 5 GHz Wi-Fi is framed. The chapters are organized for the achievement of the objective and contributions are listed accordingly.

Chapter 2

Conventional Patch Antennas with Reactive Impedance Surface and Superstrates

2.1 Introduction

Novel antennas are required for 5GHz Wi-Fi applications to meet future demands. In Wi-Fi technology, 5GHz band is used for high data rates. It is required to design a broadband antenna for 5GHz Wi-Fi application. The distances to be covered by the Wi-Fi system are specified. The performance of the system can be improved by selecting an antenna with a high gain to transmit up to the specified distance. Hence to meet the demands of high data rate and longer distance transmission, for Wi-Fi systems in particular at 5GHz, the designed antenna must have broad bandwidth with high gain which is a challenge to design for engineers. In addition to that, circular polarization is desirable to overcome the alignment issues of the transmitter and receiver antenna. Hence, there is a requirement to design high gain and broadband circular polarized antennas for 5GHz Wi-Fi applications.

The impedance bandwidth of the antenna is enhanced by using a reactive impedance surface and the gain of the antenna is improved by using a superstrate. In order to achieve circular polarization, the basic conventional patches like pentagonal patches, and square patches are truncated and the probe feed position is optimized. To design a high gain and broadband circularly polarized antenna for 5GHz Wi-Fi, the conventional patches are combined with RIS structure and superstrates simultaneously. Mostly known technique to improve the gain of the antenna is the antenna array [1-2]. Techniques are given for improving bandwidth and gain separately in published literature. Few papers are also available, where gain and bandwidth are improved simultaneously.

In the published literature, circular polarization is generated using slot-loading and truncation of corners of radiating patches. Impedance bandwidth and axial ratio bandwidth of antennas are improved by using reactive impedance surface structures below the radiating element as listed below. L Bernard (2011) et al proposed a slot-loaded patch antenna to get circular polarization. The reactive impedance surface is made up of 45^{o} rotated square patches to improve the impedance bandwidth and circular polarization at 2300MHz [38]. Teruhisa Nakamura (2011) et al proposed a truncated corner square patch to get circular polarization. The Reactive impedance surface is designed with an array of rectangular patches to achieve an impedance bandwidth of 48.6% and axial ratio bandwidth of 20.4% in the 5GHz region [39].

N Nasimuddin (2016) et al proposed a circular ring slot-loaded rectangular patch to design a circularly polarized antenna at 4GHz. The reactive impedance surface is designed with a 7×7 array of rectangular ring unit cells to achieve an impedance bandwidth of 36% at the 4GHz region [40]. The above-mentioned techniques have improved the impedance and axial ratio bandwidth only. But there is no improvement in gain in the above-mentioned antennas [38-40].

In the published literature, the gain of antennas is improved using the Fabry Perot principle where the partially reflecting surface is used as a superstrate. The superstrate is placed at a height of half-wavelength or quarter wavelength above the antenna. The partially reflecting surface is made up of a dielectric sheet or it can be designed as a frequency selective surface or metamaterial surface. These superstrates are used for the gain improvement of linearly polarized antennas as listed below. Q. L. Li (2017) et al placed 13 dielectric sheets vertically above the patch antenna to improve the gain of the antenna by 11dB at 8.5GHz [41]. GV Trenteni (1956) investigated the increase in directivity when the partially reflecting sheet is placed at half-wavelength above the antenna [42]. B.A. Zeb (2015) et al placed a thick dielectric unprinted slab at a quarter wavelength horizontally above the slot antenna to improve the directivity of an antenna at 11.5 GHz [43]. Ayan Chatterjee (2015) et al presented a superstrate with a 6×6 array of unit cells. The gain is improved from 5-8GHz [44]. Hussain Attia (2017) et al presented a dual-layer partially reflective surface superstrate with positive reflection phase gradient property above the slot antenna resonating at 60GHz. The antenna achieved a gain improvement of 12.2dBi over a slot antenna [45]. Muftah Asaadi (2018) et al proposed a high -dense dielectric patch antenna at 28GHz with two types of superstrates for gain improvement. The first antenna with a highly reflective superstrate has a maximum gain of 17.78dBi and the next antenna with a positive phase gradient superstrate has a maximum gain of 15.4dBi [46]. In the above-discussed papers, the gain of an antenna is improved by using a Fabry Perot resonator principle. But the circular polarization is not reported in the above-mentioned papers [41-46].

In the following published literature, Fabry Perot resonator principle is used for gain enhancement for circularly polarized antennas. Circular polarization is realized by applying corner truncations and slot-loading techniques. Kamil pitra (2015) et al presented a circularly polarized square patch antenna with a cross-slot. The gain of the antenna is improved by using the FSS superstrate which consists of square patches on the top face of the substrate and a fish net on the bottom face of the substrate [47]. Robert Orr (2014) et al published a 45^{o} tilted patch with HIS surface and a partially reflecting surface. The partially reflecting surface has

independent control on magnitude and phase of reflection coefficients to enhance the gain of the antenna to 21dB at 15GHz[48]. S. X. Ta (2017) et al proposed a circularly polarized antenna with a truncated corner square patch. The superstrate is designed with high permittivity dielectric substrate to have high refractive index property to improve the gain of the antenna to 13.17dBic and improve the AR bandwidth to 13.6% [49]. TK Nguyen (2019) et al designed a stacked truncated corner patch antenna to get circular polarization. The superstrate is used to enhance the axial ratio bandwidth and broadside gain [50]. Wanquan Cao (2019) et al presented a circularly polarized magneto-electric dipole antenna. The antenna gain is improved by using a partially reflecting surface [51]. The above-mentioned techniques have improved the gain of the circularly polarized antenna only [47-51].

In the published literature, the impedance bandwidth of the antenna is improved by using a reactive impedance surface and the gain of the antenna is improved by using Fabry Perot resonator antennas. Even though the gain-bandwidth product is constant. Both the gain and bandwidth improvements can be simultaneously improved by combining the novel techniques such as the Fabry Perot resonator and reactive impedance surface. Conventional structures are truncated to get circular polarization and they are combined with RIS structure and superstrates to design a high gain and broadband circularly polarized antennas.

The conventional structures like the equilateral pentagonal patch and square patches could not generate circular polarization. These structures are truncated and the probe feed position is optimized to get circular polarization. There are different ways to get circular polarization with regular structures such as a small portion of the right side edge is truncated to the pentagonal patch, two diagonal corners are truncated to the square patch and a 45^{o} inclined slot is loaded to the square patch as shown in fig. 2.1.

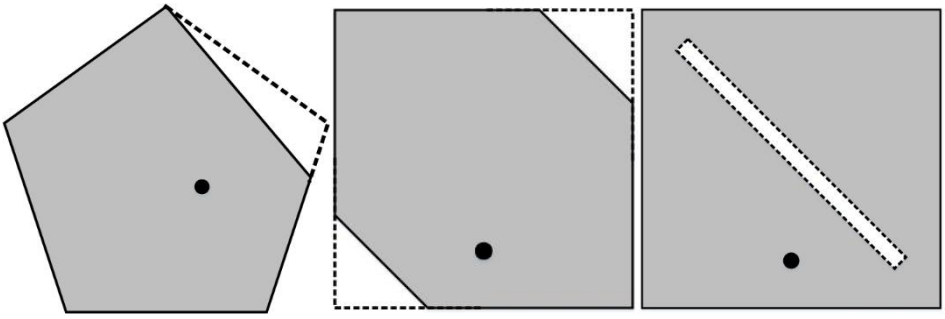

Fig.2.1. Truncated conventional structures

In this chapter impedance bandwidth of the antenna is improved by using a reactive impedance surface and the gain of the antenna is improved by using dielectric sheets vertically above the antenna. The gain and bandwidth of the antenna are improved simultaneously by combining both techniques. The dielectric sheets are replaced with resonant cavity superstrates

to simplify the fabrication. Circularly polarized antennas are realized. Gain improvement is obtained using highly reflective FSS superstrate and also dielectric superstrate separately.

In the next section, a brief introduction about the reactive impedance surface and different types of superstrates as partially reflecting surfaces are discussed.

2.1.1 Reactive Impedance Surface

A microstrip patch antenna consists of a radiating patch and ground plane separated by a dielectric material of height 'h' which is called as a substrate. Ground plane act as a perfect electric conductor (PEC) and an image of the radiating patch is formed at a distance 'h' from the PEC. The signal from the source (radiating patch) and image are added up in the forward

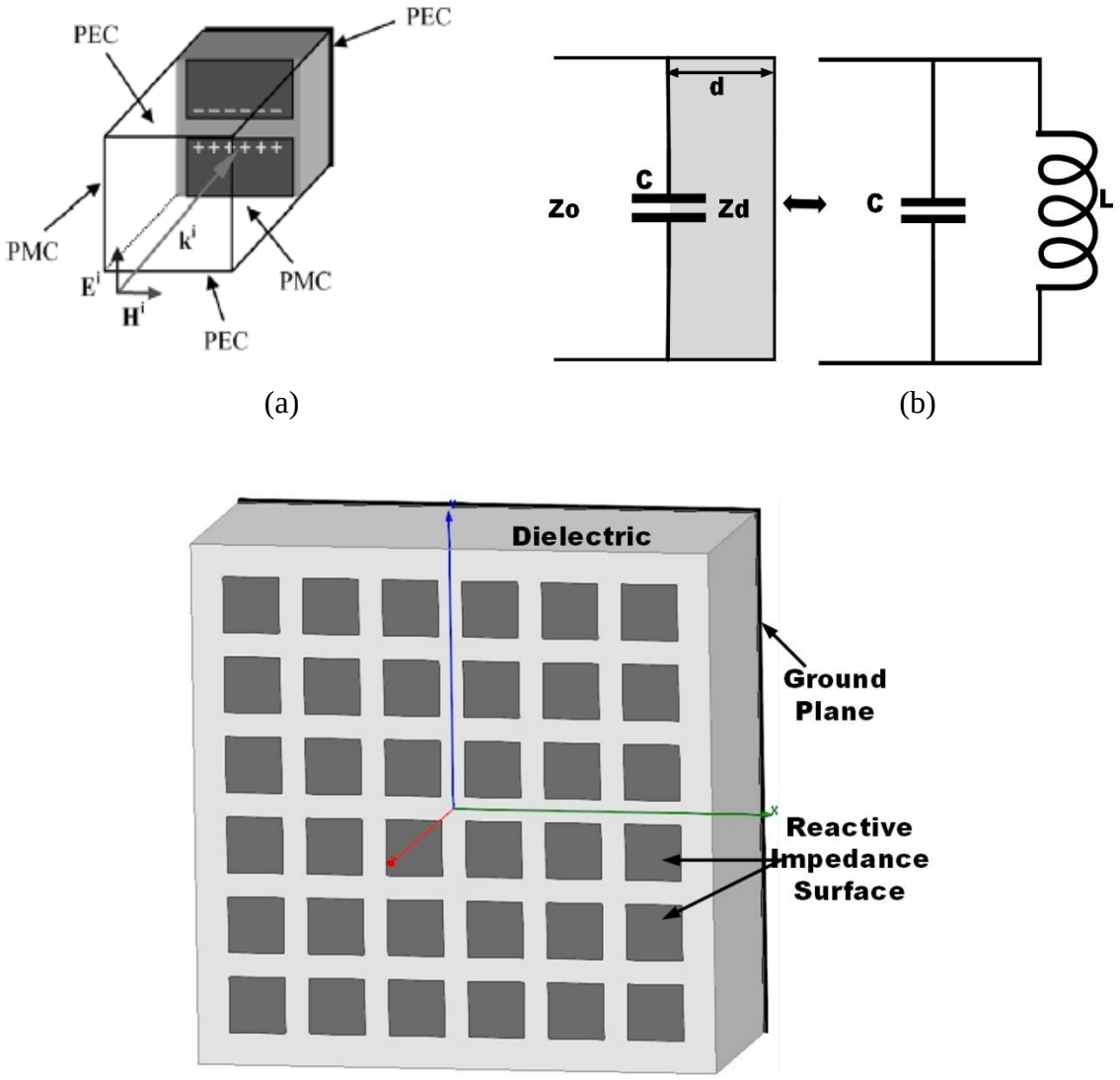

(a) (b)

(c)

Fig.2.2. Reactive impedance surface (a) Unitcell (b) Equivalent circuit (c) 3D view of RIS structure

direction. PEC reflects the electric field at the 180^{o} phase shift. In the forward direction, the signal from the source and signal from the image must add in phase for proper radiation. This will happen only for a narrow range of frequencies. Hence, microstrip antennas in general have narrow impedance bandwidth. To reduce the coupling between the signal from the source and the signal from the image, a periodic array of patches is incorporated between the patch and ground plane[6] as shown in fig. 2.2(c). These radiating patches store the energy either electric or magnetic and improve the decoupling between two signals. In turn, the bandwidth of the antenna is improved. Energy stored in the substrate behaves like a reactive impedance. Hence, these surfaces are called as reactive impedance surfaces.

This structure is modelled by a transmission line. The gap between the patches acts like a shunt capacitor. It is placed at a distance from a PEC-backed (short-circuited) dielectric substrate. This short-circuited dielectric substrate is modelled by a lumped shunt inductor parallel to the capacitor as shown in fig. 2.2(b). The parallel LC circuit is inductive at frequencies below resonance, an open circuit at the resonance (behaving like a perfect magnetic conducting surface) and capacitive above the resonant frequency. At frequencies much lower than the resonant frequency, the surface impedance approaches zero and the structure behaves as a PEC surface. The reactance of the RIS structure provides impedance matching over a wide range of frequencies. Therefore the impedance bandwidth of the antenna is improved.

2.1.2 Fabry Perot Resonator Antennas

A Fabry-Perot Resonator (FPR) antenna is designed with radiating elements backed by a ground plane and a partially reflecting surface superstrate above the radiating element as shown in fig. 2.3. The waves emitted by the radiating element are incident on the superstrate and some of the rays are reflected back, the reflected rays are once again reflected by the ground plane. When the distance between the antenna ground plane and superstrate is integer multiples of half wavelength, the coherent addition of waves is formed in the normal direction of the superstrate. Hence, the gain of an antenna is increased remarkably.

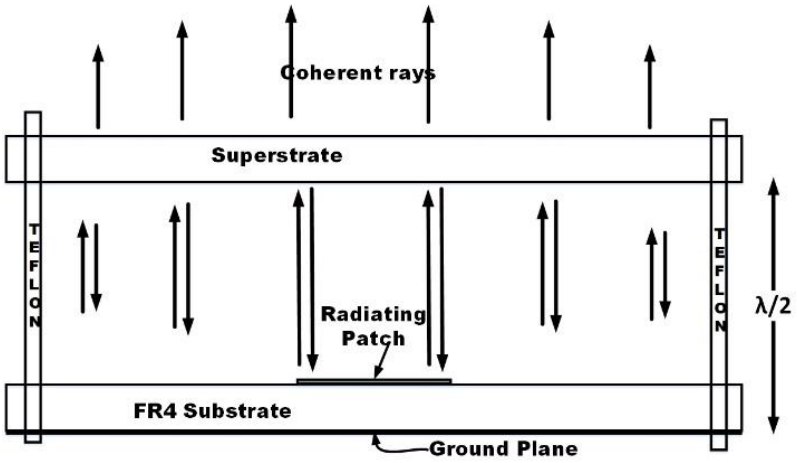

Fig.2.3. Fabry Perot resonator principle

Different types of partially reflecting surface superstrates are available

2.1.3 Frequency Selective Surface(FSS) Superstrate

FSS is one type of partially reflecting surface which is designed with an array of unit cells. The dimensions of the unit cell decide the frequency range of operation. The gain of an antenna can be enhanced by placing a superstrate above the antenna.

There are 2 types of FSS superstrates

2.1.3.1 Positive Phase Gradient FSS Superstrate: In this type of superstrate, the unit cell is designed to get a positive phase gradient property over the selected range of frequencies by selecting the suitable dimensions of the unit cell. The superstrate is placed approximately half-wavelength height above the ground plane.

$$h = \frac{\lambda}{2}\left(\frac{\phi}{2\pi} + 0.5\right) + N\frac{\lambda}{2} \qquad (1)$$

Where ϕ is the phase of the reflection coefficient of the FSS superstrate, and λ is the free-space wavelength. N is the order of resonant mode and equal to 0,1,2,3… N. The equation of phase can be written from the equation [46].

$$\phi = \frac{4\pi h}{c} f - (2N - 1)\pi \qquad (2)$$

Equation (2) shows the condition to get maximum gain in the broadside direction in terms of positive phase gradient property over the selected frequency range.

2.1.3.2 Highly Reflective FSS Superstrate: In this type of superstrate, the unit cell is designed to get a highly reflective phase in the selected frequency range by choosing the suitable dimensions of the patch.

When the FSS superstrate is placed at an approximately half-wavelength height from the antenna, it creates an air-filled cavity between the ground plane and the superstrate. The electromagnetic rays are focussed along the transmit direction and form concentrated rays in the broadside direction, thus, the gain of an antenna is improved, when a highly reflective superstrate is placed at an optimum height from the antenna.

$$D = 10 \log \frac{1+|\Gamma_{fss}|}{1-|\Gamma_{fss}|} \quad (3)$$

Where Γ_{fss} is magnitude of reflection coefficient

Equation (3) shows that the directivity can be enhanced as the magnitude of the reflection coefficient increases to unity (0dB) [46].

2.1.4 High Dense Dielectric Sheet

The dielectric substrate with high permittivity has a property of high refractivity when it is placed at an approximately half-wavelength height above the ground plane [43]. The rays emanating from the antenna incident upon the interface of different media will bend according to Snell's law. The high gain resonance condition is obtained by properly choosing the position and thickness of the high dielectric constant materials. Hence, the gain of an antenna is improved.

2.1.5 Non Uniform Metallic Superstrate

The superstrate is designed with different sizes of patches[13-14]. When the size of the patch increases, the maximum gain of antenna shifts to lower frequencies and vice versa. When the superstrate is designed with different sizes of patches, the maximum gain is achieved over broad frequency ranges. Non-uniform superstrate is also used to improve the axial ratio bandwidth of the antenna.

2.1.6 Metamaterial Superstrate

It is designed with an array of metamaterial unit cells [22-28]. These metamaterials consist of negative permittivity and negative permeability simultaneously i.e. negative refractive index. Furthermore, the propagation vector, electric and magnetic field vector of these materials form left-handed materials or negative refractive index materials. The metamaterial with negative refractive index (NRI) property acts like LHM perfect lens. The radiated electromagnetic energy in the cavity is gathered and focused in the normal direction of the superstrate. Hence, the gain of the antenna is increased in the broadside direction.

2.2 Micro Strip Square Patch Antenna with RIS Structure and Dielectric sheets

In this work, the microstrip patch antenna is designed. Its bandwidth is improved by using RIS structure as a ground plane and the gain of the antenna can be improved by placing dielectric sheets placed vertically above the antenna. The gain and bandwidth of the patch antenna are improved simultaneously by combining both techniques for 5 GHz Wi-Fi applications.

2.2.1 Micro Strip Square Patch Antenna

The square patch is designed on grounded FR4 substrate (ε_r=4.4, loss tangent tanδ= 0.02 and thickness h=1.6mm) with a dimension of 62mm×62mm as shown in fig. 2.4. The inner conductor of the SMA connector is connected to a square patch after inserting through the substrate and the outer conductor of the SMA connector is connected to a ground plane.

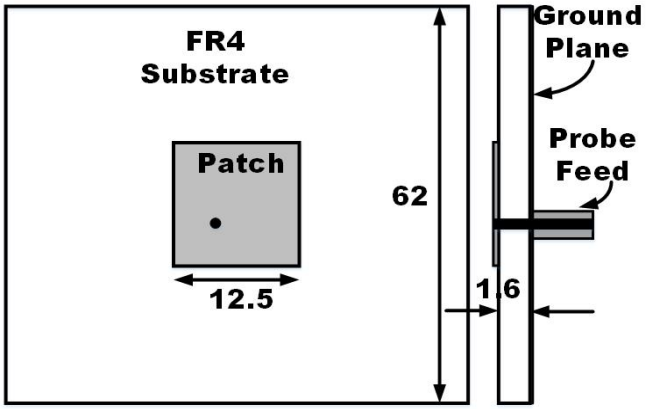

Fig.2.4. Microstrip square patch antenna top view and side view

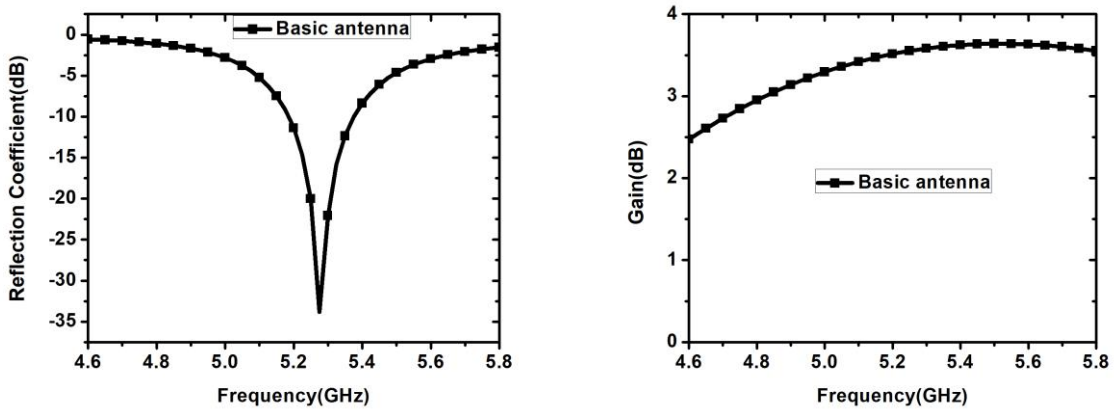

Fig .2.5. Simulation results of square patch antenna (a) Reflection coefficient (b) Gain

The antenna is simulated using HFSS 13 and the simulation results are shown in fig. 2.5. It can be observed that the impedance bandwidth is 3.6% (5.18 GHz - 5.37GHz) and the gain of an antenna is 3.5-3.63 dBi over the resonant frequency range.

2.2.2 Micro Strip Square Patch Antenna with Reactive Impedance Surface

The reactive impedance surface is made up of a 6×6 array of square patches. The RIS structure is placed in the middle of the square patch and ground plane [6] as shown in fig. 2.6. The size of square patches in the RIS structure is selected as 3.3mm, the substrate height above the RIS structure is 0.8mm, the substrate height below the RIS structure is 1.6mm, and the size of the square patch is selected as 11.75mm to resonant in the same frequency band. The square patch with RIS structure is simulated using HFSS 13 and the simulation results are compared with the square patch antenna alone as shown in fig. 2.7. The impedance bandwidth is improved by 2.46%. The gain of the antenna is almost the same i.e. 3.6dB – 3.79dB.

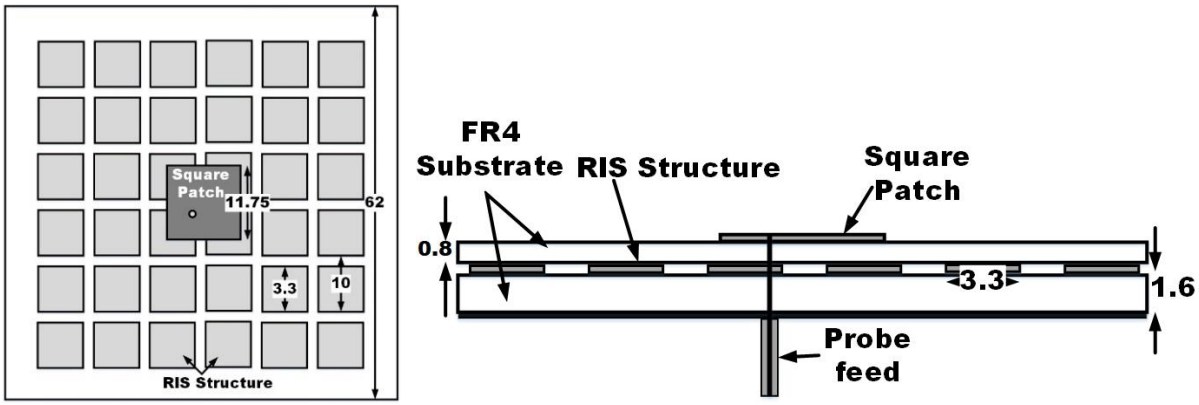

Fig.2.6. Square patch antenna with RIS structure (a) Top view (b) Side view

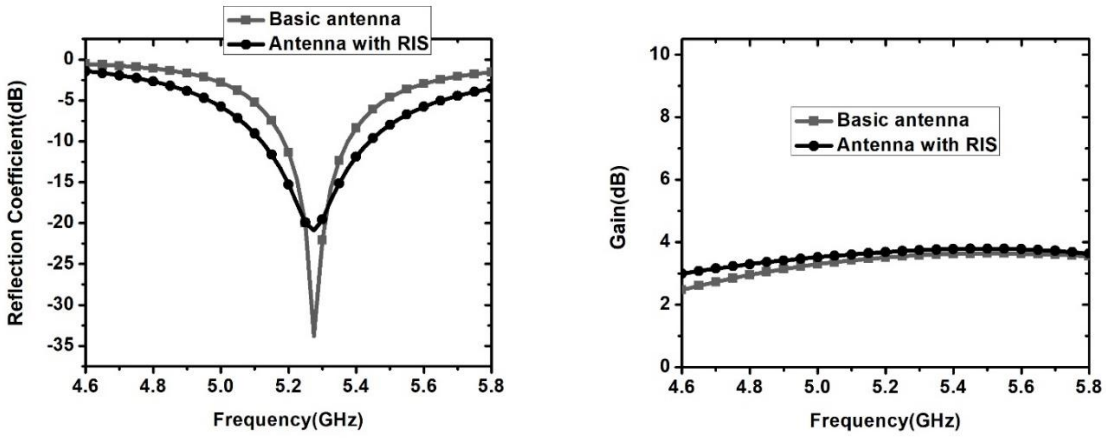

Fig.2.7. Comparison of simulation results of a square patch antenna, square patch antenna with RIS (a) Reflection Coefficient (b) Gain

2.2.3 Micro Strip Square Patch Antenna with RIS Structure and Dielectric Sheets

In order to improve the gain of the antenna, 13 dielectric sheets are placed vertically above the antenna with RIS structure as shown in fig. 2.8**.** The dielectric sheets are acting as a lens [41]. They focus the waves in the normal direction of the antenna. Hence, the gain of an antenna is improved heavily. The gain and bandwidth are simultaneously improved by using RIS structure as a ground plane and dielectric sheets above the antenna as shown in fig. 2.8.

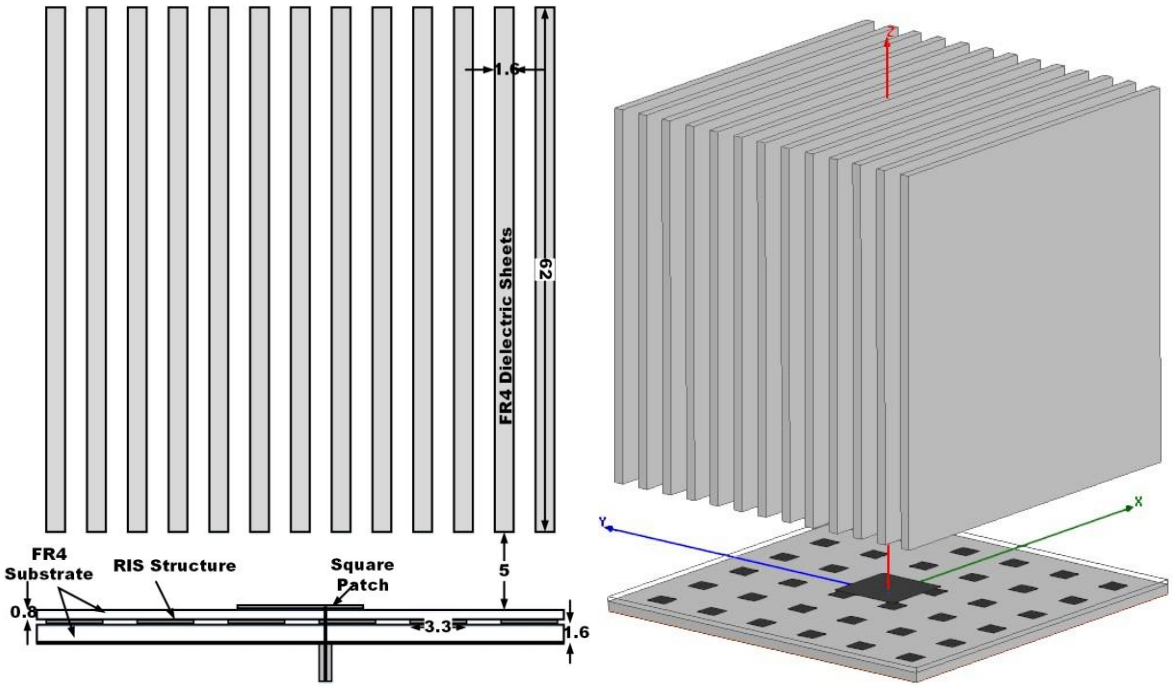

Fig.2.8. Square patch with RIS structure and Dielectric sheets (a) Front view (b) 3D view

The patch antenna with RIS structure as a ground plane and dielectric sheets vertically above the antenna is simulated using HFSS 13. The simulation results are compared with patch and patch with RIS as shown in fig. 2.9. It shows that the impedance bandwidth is 6.9% (5.13 GHz - 5.50GHz) i.e. improvement of 3.3% and the gain of an antenna is 9.5 -10.23 i.e. improvement of 6-6.5dB over a square patch antenna.

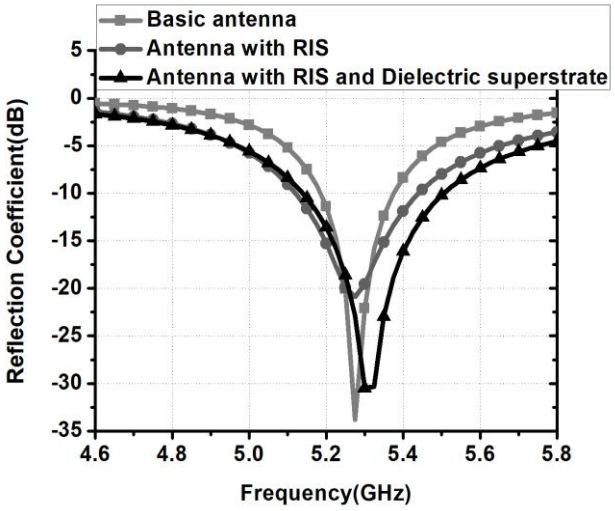

(a)

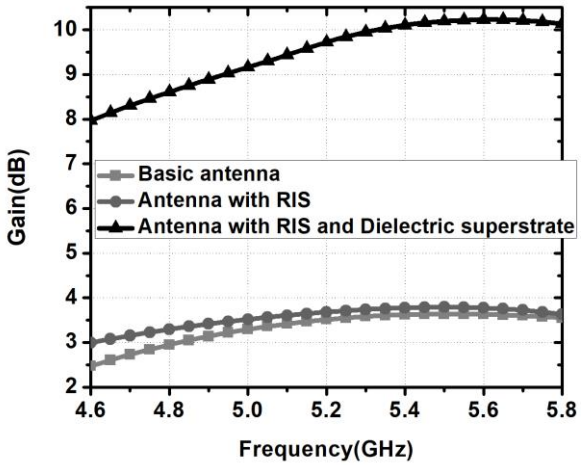

(b)

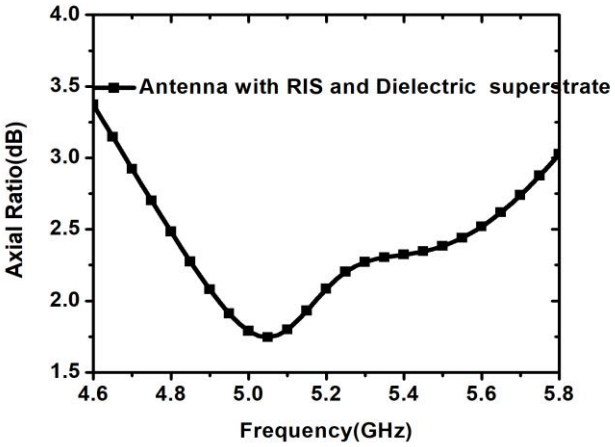

(c)

Fig.2.9. Simulation results of a square patch, square patch with RIS structure, square patch with RIS structure and Dielectric sheets (a) Reflection Coefficient (b) Gain (c) Axial ratio

2.3 Micro Strip Square Patch Antenna with RIS Structure and Frequency Selective Surface (FSS) Superstrate

The dielectric sheets are acting as a lens, but placing dielectric sheets vertically above the antenna is difficult and costly. The resonant cavity superstrates are simple to design and fabricate. So the FSS superstrate is used to improve the gain of an antenna. The square patch with RIS structure is taken from section 2.2 as shown in fig. 2.6. To this antenna, the FSS superstrate is applied for gain enhancement.

2.3.1 FSS Superstrate

The FSS superstrate is designed with a 6×6 array of unit cells [44] as shown in fig. 2.10. Each unit cell is designed with a square patch on the top and bottom plane, and a fishnet structure in the middle layer. A detailed analysis of unit cell characteristics is given in section 2.4.3. The top and bottom planes act as a capacitive layer whereas the fishnet structure act as an inductive layer. The resultant structure act as a frequency selective surface superstrate.

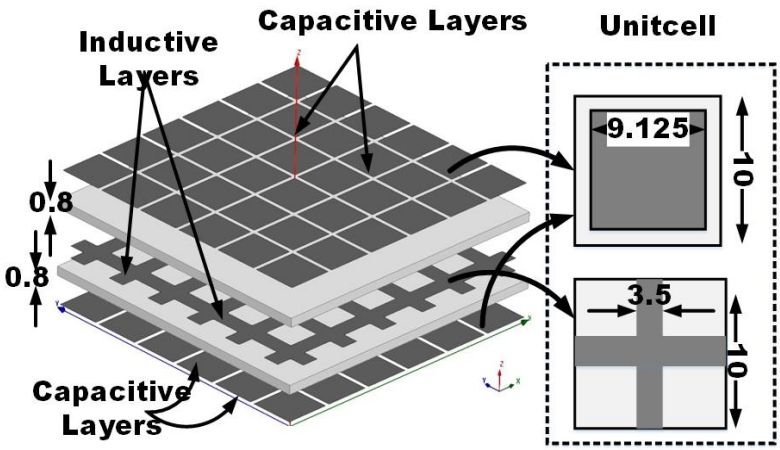

Fig.2.10. Three-dimensional view of FSS superstrate

2.3.2 Micro Strip Square Patch Antenna with RIS and FSS Configuration

The above-mentioned superstrate is placed at an approximately half-wavelength height above the antenna with RIS structure as shown in fig. 2.11. The resonant cavity is created between the superstrate and RIS structure. The waves trapped in the cavity bounce back and forth and finally, coherent addition of rays are emitted in the normal direction. The gain and bandwidth are simultaneously improved by adding an FSS superstrate above the antenna and RIS structure as a ground plane as shown in fig. 2.11.

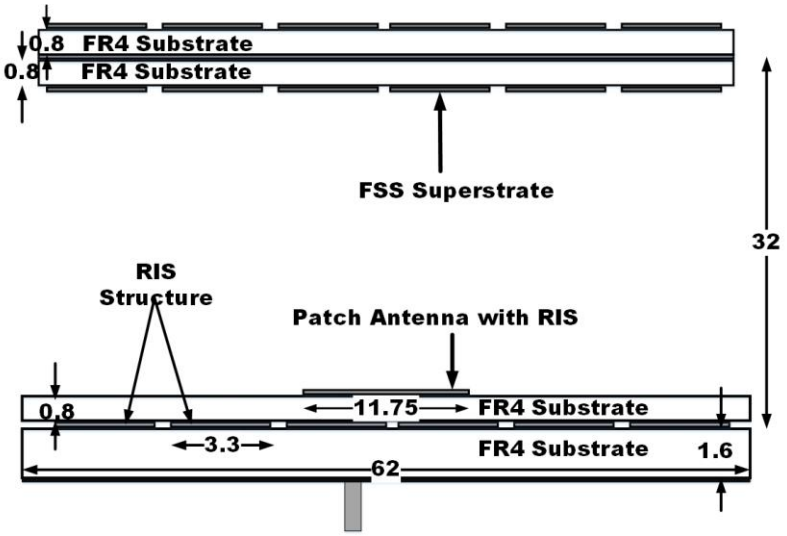

Fig.2.11. Microstrip square patch antenna with RIS structure and FSS superstrate

The patch antenna with RIS structure as a ground plane and FSS superstrate above the antenna is simulated using HFSS 13 and simulation results are shown in fig. 2.12. The simulation results show that the impedance bandwidth is 5.85 %(5.11GHz-5.42GHz) i.e. improvement is around 2.25% and the gain of the antenna is above 8.5dB i.e. improvement is around 5dB over a square patch antenna.

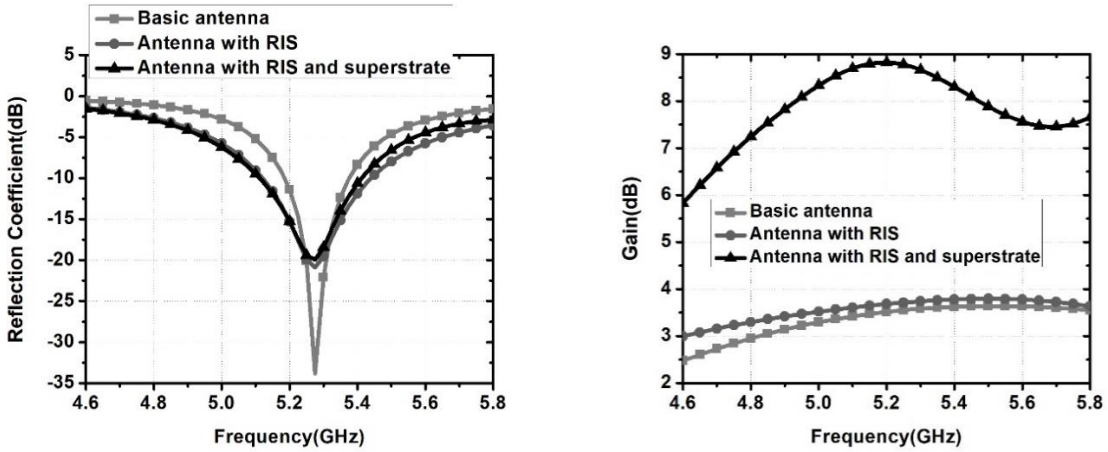

Fig.2.12. Comparison of simulation results of microstrip square patch, patch with RIS structure, patch with RIS structure and FSS superstrate (a) Reflection Coefficient (b) Gain.

2.4 Pentagonal Patch Antenna with RIS Structure and FSS Superstrate

The earlier discussed design has not produced any circular polarization. The conventional pentagonal patch antenna is designed and a small portion of the right side corner is truncated to generate circular polarization. It will lead to the design of high gain and broadband circularly polarized antennas for 5 GHz Wi-Fi applications.

2.4.1 Pentagon Shape Patch Antenna

Pentagon shape patch antenna provides better performance than other conventional structures like a circle and rectangular structures. Other conventional structures need multiple feeding to get circular polarization whereas pentagon shape patch antenna generates circular polarization with single feeding only. The equilateral pentagon shape patch antenna could not generate circular polarization. A small portion of the right side edge is removed from the equilateral pentagon shape patch antenna [52] as shown in fig. 2.13. The feed position of the antenna is optimized to generate two orthogonal fields with equal magnitude and perpendicular to each other i.e. circular polarization. The pentagon shape patch is printed above the FR4 substrate and the metal layer in the bottom plane act as a ground plane. The probe feeding is given by the SMA connector. The inner conductor of the SMA connector is connected to the pentagon patch and the outer part of the SMA is connected to the ground plane.

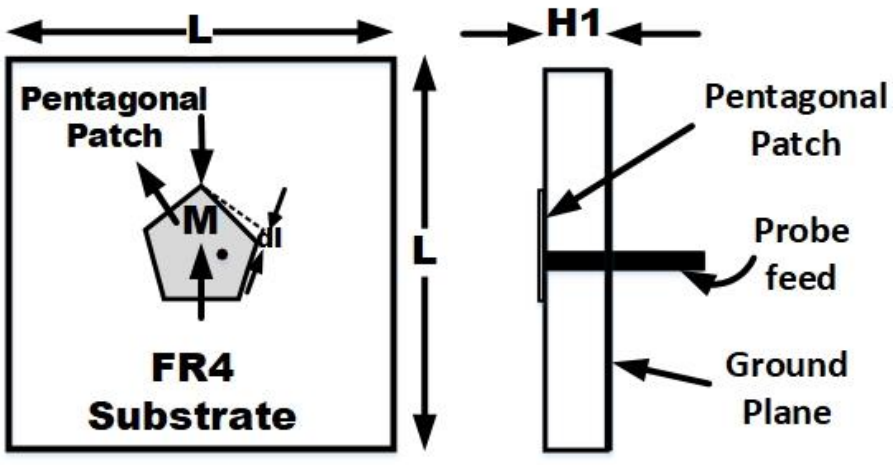

Fig.2.13. The conventional pentagon shape patch antenna a) Top view b) Side view

This antenna design is based on the finite element method in High-Frequency Structure Simulator software. The simulation results show that impedance bandwidth is 7.8% (5.11-

5.52GHz), Gain is 3.4-3.5dBi, and axial Ratio is 1.9% (5.27-5.37GHz) respectively as shown in fig. 2.15. The substrate is considered large enough to accommodate the modification done for gain and bandwidth.

2.4.2 Pentagonal Shape Patch Antenna on RIS Structure

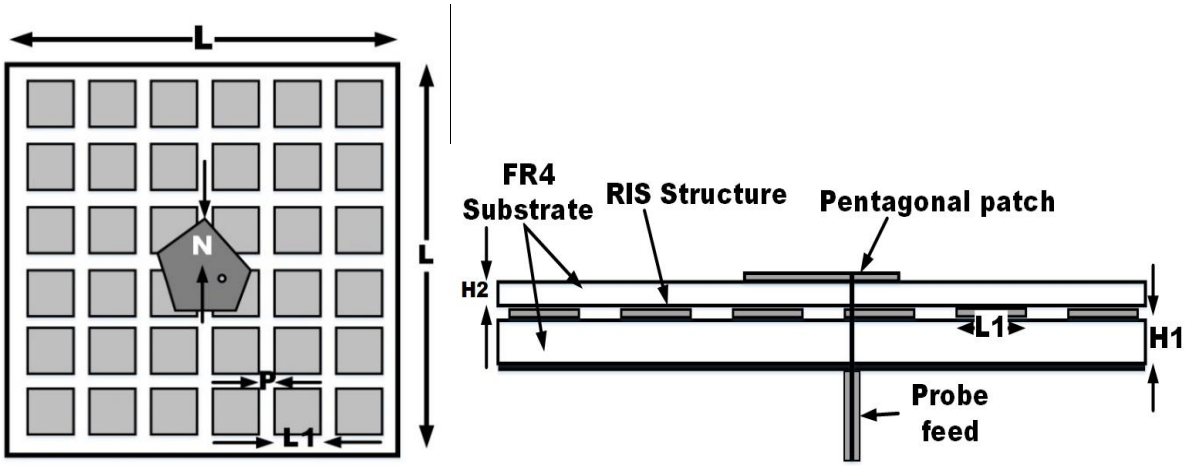

Fig.2.14. Pentagonal patch antenna with RIS structure (a) Top view (b) Side view

A reactive impedance surface is a structure that introduces additional reactance to improve impedance bandwidth. In the proposed antenna, the RIS structure is added in between the patch and ground plane to improve the impedance bandwidth of the antenna. An array of patches will be introduced between the patch and ground plane. The square patches are selected for the proposed design. The size of the patch and the number of patches are the parameters that control the impedance matching. After optimizing the patch size and array size, the array is made by a 6×6 array of square patches printed on the top side of the FR4 substrate. The parametric study is done on the dimension of the square patch (L1), its periodicity (L1+P), substrate height (H1) below the RIS surface, and substrate height (H2) above the RIS surface. The side of square patches (L1), the distance between the patches (P), the height H1, and the height H2 are optimized for wide bandwidth to 4.5mm, 5.5mm, 1.6mm, and 0.8mm respectively.

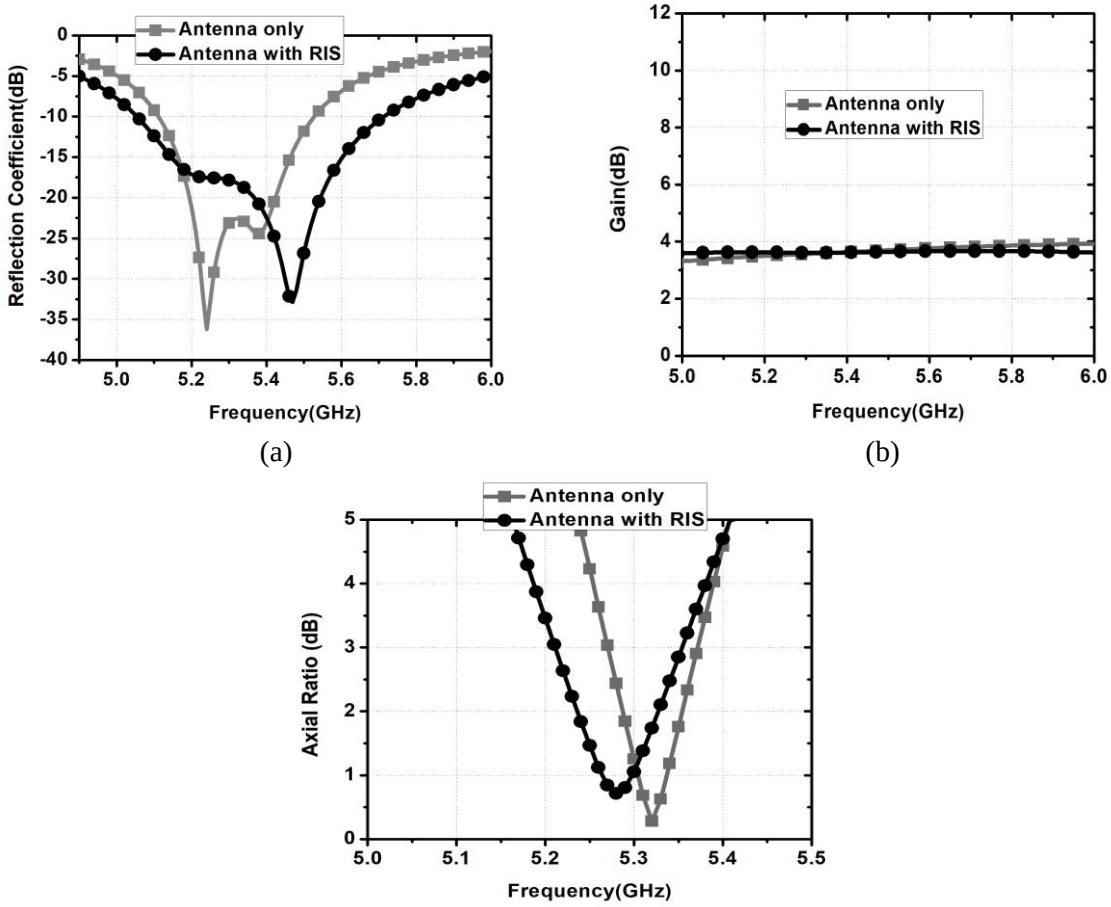

Fig.2.15. Comparison of simulation results for the pentagonal patch antenna, patch antenna with RIS structure (a) Reflection Coefficient (b) Gain (c) Axial ratio

After optimization of the RIS structure, an impedance bandwidth of 12.2% (5.05GHz - 5.71GHz) is achieved as shown in fig. 2.15(a), and also there is an increase in the 3dB axial ratio bandwidth. An axial ratio bandwidth of 2.7% (5.21GHz - 5.35GHz) is achieved as shown in fig. 2.15 (c). The RIS technique has improved the impedance bandwidth, but there is no considerable improvement in the antenna gain as shown in fig. 2.15 (b). In order to improve the gain of the antenna, the FSS superstrate is placed above the antenna.

2.4.3 Frequency Selective Surface (FSS) Superstrate

FSS is a surface in which the transmission and reflection characteristics vary with frequency. The transmission is varied by using an array of unit cells. The surface contains a periodic array of unit cells printed on one side or two sides of the substrate. To modify the wave propagation, the FSS is placed along the direction of wave propagation. The superstrate and RIS structure forms a resonant cavity and it will improve the gain of the antenna when constructive interference is created between the RIS structure and superstrate.

2.4.3.1 Highly Reflective Unit Cell Design: The design details of highly reflective unit cells are studied in this section. The circle-shaped patches are preferred in FSS superstrate due to their symmetry nature along the φ direction and improve the CP gain over the wide frequency range [51]. The highly reflective unit cell consists of circle-shaped patches on the top layer and bottom layer. In addition to that, a modified fishnet structure is used as a middle layer. These three layers are separated by the substrate in between them as shown in fig..2.16. The top and bottom layers act like the capacitive layer and the middle layers act as an inductive layer to form a superstrate.

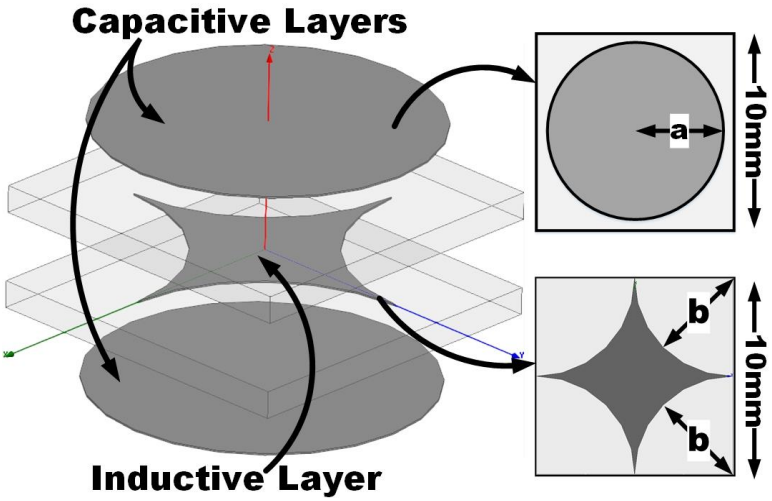

Fig.2.16. Three-dimensional view of highly reflective FSS unit cell.

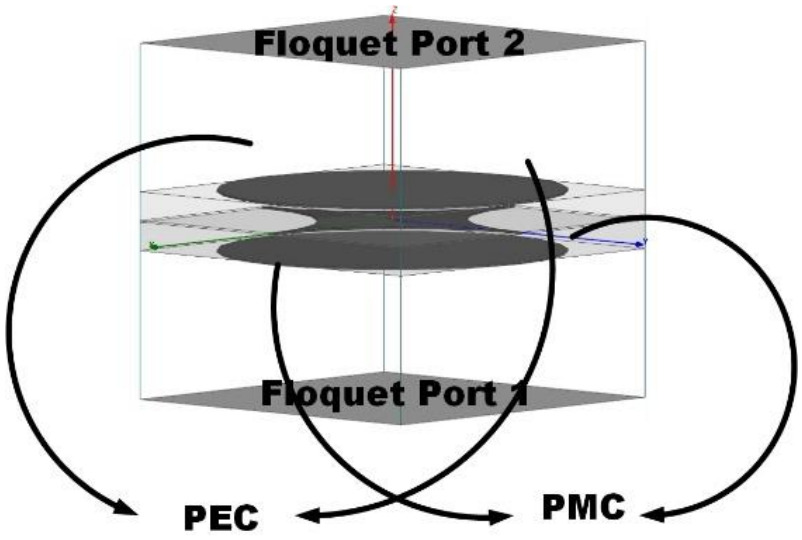

Fig.2.17. Boundary conditions of a highly reflective FSS unit cell.

The highly reflective frequency selective surface is designed as a 6 x 6 array of periodic unit cells printed on Rogers's RO 4003C substrate, which is used as a superstrate of the antenna. When the FSS superstrate is placed at an approximately half-wavelength height from the

antenna, it creates an air-filled cavity between the superstrate and the RIS structure. The electromagnetic rays are focussed along the transmit direction and form concentrated rays in the broadside direction, thus, the gain of an antenna is improved, when a highly reflective superstrate is placed at an optimum height from the antenna. It is well known that directivity can be enhanced as the magnitude of the reflection coefficient increases to unity (0dB) [46].

$$D = 10 \log \frac{1 + |\Gamma_{fss}|}{1 - |\Gamma_{fss}|}$$

The unit cell is designed in HFSS software and boundary conditions are applied as shown in fig. 2.17. The parametric study is done by changing a and b values where 'a' is the radius of the top side conductor and 'b' is the curvature radius of the middle conductor. These dimensions of the unit cell control the characteristics of FSS.

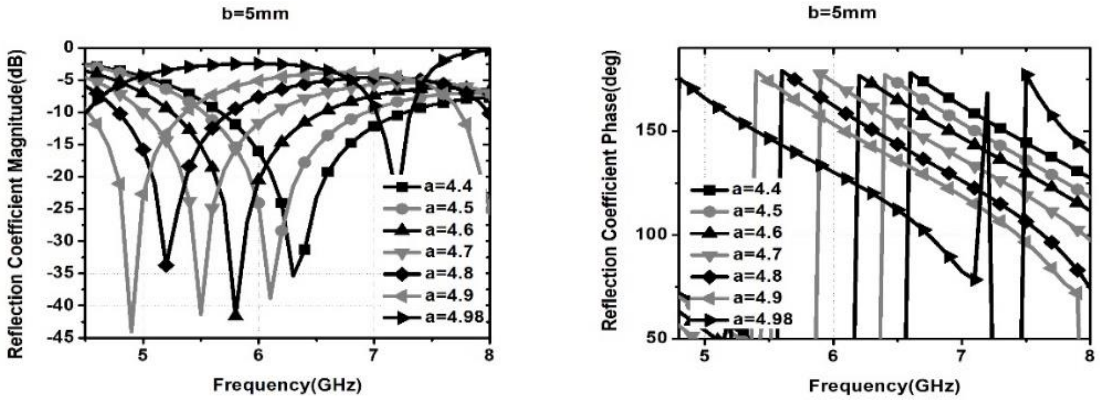

(a) (b)

Fig.2.18. Highly reflective FSS unitcell characteristics (a) Magnitude of reflection coefficient (b) Phase of reflection coefficient.

The magnitude and phase of the reflection coefficient are shifted to the lower frequencies with an increase in the radius 'a' as shown in fig. 2.18. The magnitude of the reflection coefficient increases towards 0dB i.e. unity in the selected frequency range(5.1GHz-5.7GHz) and the phase of the reflection coefficient is near 180^0 over the selected frequency range (5.1GHz-5.7 GHz) as dictated by the requirements of a highly reflective superstrate to improve gain. These conditions are achieved when 'a' is 4.98mm and 'b' is 5mm. The optimized dimensions of antenna and unit cell dimensions are given in Table 2.1.

2.4.4 Pentagonal Patch Antenna with RIS - FSS Configuration

The proposed antenna is composed of the pentagon shape patch antenna along with highly reflective FSS and RIS structures. RIS structure is attached beneath the pentagon shape patch antenna and highly reflective FSS is positioned above the antenna as shown in fig. 2.19 and fig. 2.20. The cavity created by the contribution of these layers acts like a Fabry Perot cavity

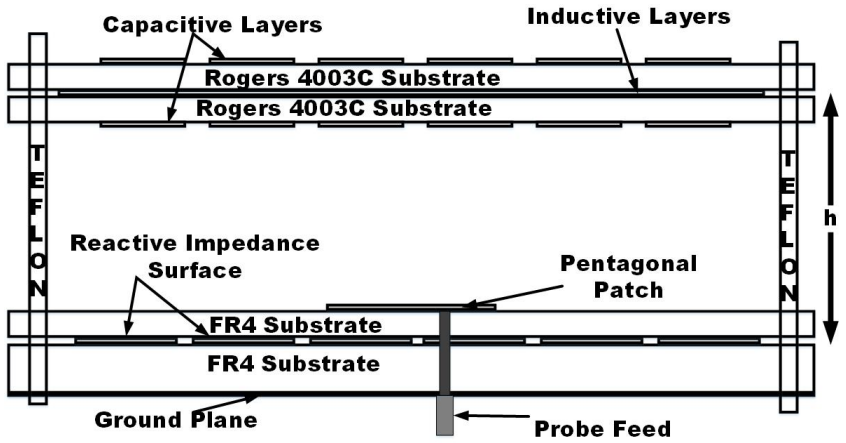

Fig.2.19. Geometry of composite structure of pentagonal patch with RIS and FSS (Front View)

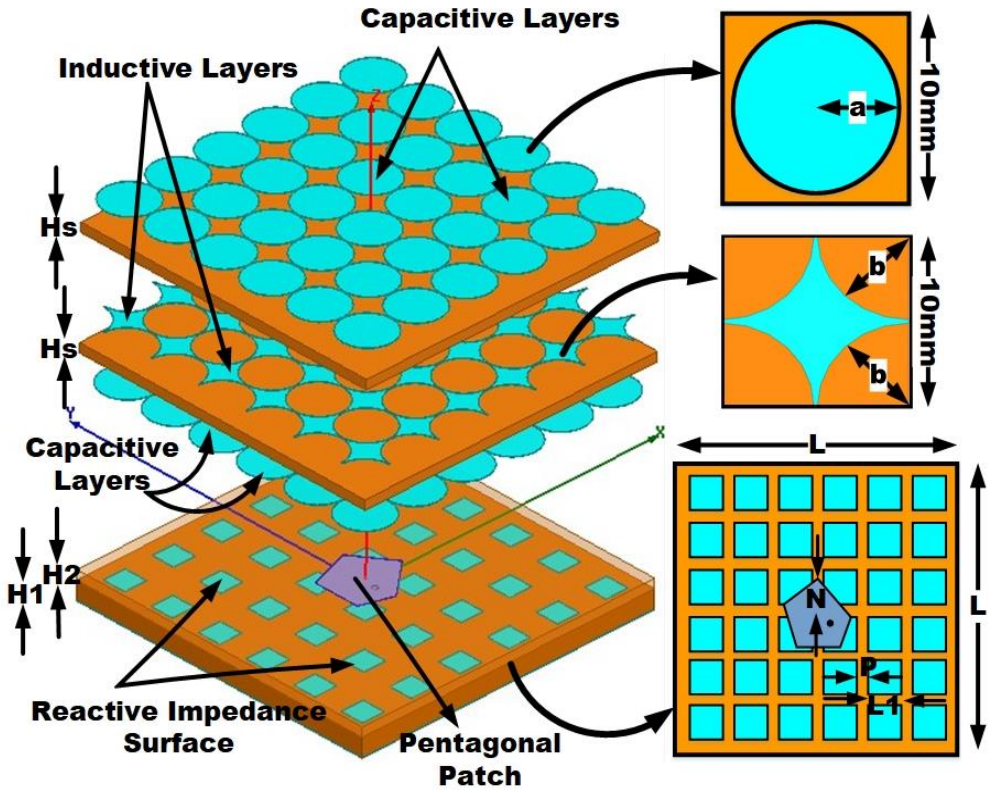

Fig.2.20. Three-dimensional view of a composite structure of pentagon patch antenna with RIS and FSS

resonator. Here, the directly transmitted rays from the antenna and reflected rays from the superstrate are trapped in the cavity. The coherent addition of trapped rays radiates along the broadside direction. Hence, the gain of the antenna improved remarkably.

Table 2.1: Optimized Parameter Values

Parameter	Value(mm)	Parameter	Value(mm)
L	70	dl	1.7
H1	1.6	L1	4.5
H2	0.8	p	5.5
Hs	0.813	a	4.98
M	8.4	b	5
N	7.5	h	32

The proposed antenna with RIS and FSS is simulated in HFSS software. The simulated results are shown in fig. 2.21. The impedance bandwidth is 17.72% as shown in fig. 2.21(a) and the improvement is around 10%. The antenna gain is around 12 dBi in the frequency range of 5.1GHz to 5.7GHz as shown in fig. 2.21(b) and the improvement in the gain is around 9 dBi. The axial ratio is 2.5% as shown in fig. 2.21(c). The proposed antenna results are compared with basic conventional antenna results as mentioned in Table 2.2.

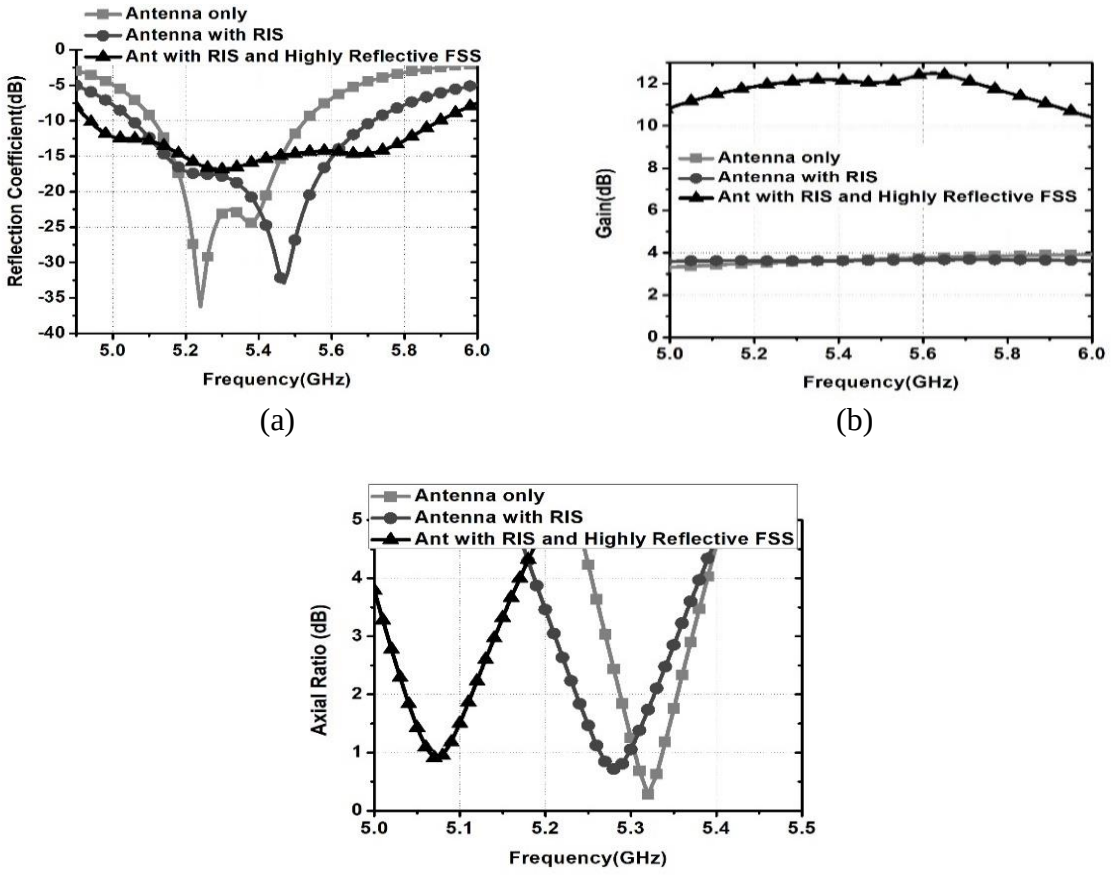

Fig.2.21. Comparison of simulation results for the antenna, antenna with RIS, and antenna with RIS and FSS at h=32mm (a) Reflection Coefficient (b) Gain (c) Axial Ratio

It is observed that the conventional antenna with RIS structure has considerable improvement in the impedance bandwidth as shown in fig. 2.21. But there are no considerable improvements in the antenna gain. The conventional antenna with RIS structure and FSS superstrate has improvement in both gain and impedance bandwidth simultaneously as shown in fig. 2.21. Besides, the antenna has a 3dB axial ratio bandwidth of 2.4%.

Tabel. 2.2. Comparison of antenna, antenna with RIS, and antenna with RIS and FSS at h=32mm.

S. No.	Antenna	Impedance Bandwidth	Gain (dBi)	Axial Ratio
1	Pentagon Shape Patch Antenna	7.8% (5.11-5.52GHz)	3.4-3.7	1.90% (5.27-5.37GHz)
2	Antenna with RIS	12.24% (5.05-5.71GHz)	3-4	2.7% (5.21-5.35GHz)
3	Antenna with RIS and highly reflective FSS	17.72% (4.93-5.89GHz)	12.48	2.4% (5.01-5.14GHz)

It is observed that the proposed antenna surface current density vector on the patch is rotating clockwise direction as the phase increases i.e the antenna is left-hand circularly polarized (LHCP) as the direction of propagation (Z) is topside antenna as shown in fig. 2.22.

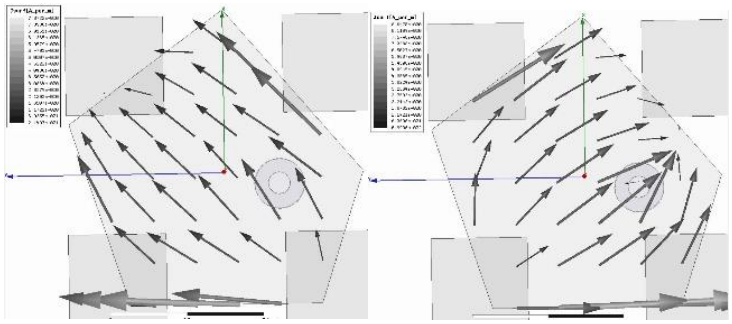

a. Phase = 0^o **b.** Phase = 90^o

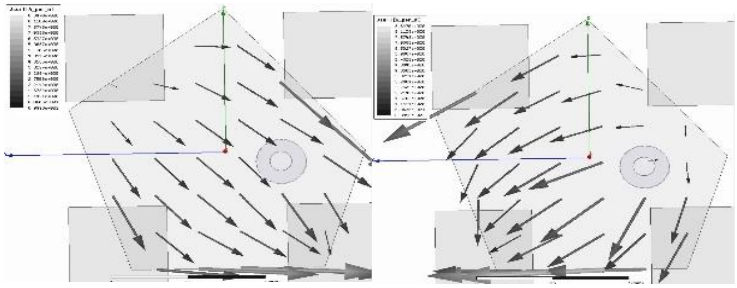

c. Phase = 180^o **d.** Phase = 270^o

Fig.2.22. Antenna with RIS and FSS surface current density vector on pentagon patch at 5.1GHz.

The surface current density vector is towards 135^o for the phase 0^o as shown in fig. 2.22 a, it is towards 45^o degrees for the phase 90^o as shown in fig. 2.22 b, it is towards -45^o for the

phase 180^o as shown in fig. 2.22 c, it is towards -135^o for the phase 270^o as shown in fig. 2.22 d.

The LHCP gain is high over the entire bandwidth as shown in fig. 2.23. The right-hand circularly polarized (RHCP) gain is -15dB at 5.1GHz frequency where the antenna is maintaining circular polarization and the RHCP gain is increasing in other frequencies.

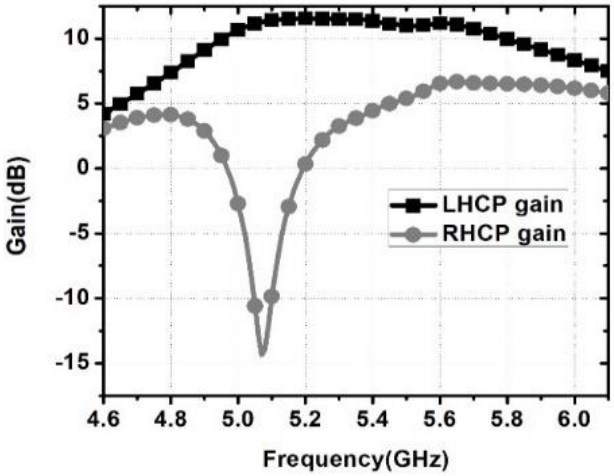

Fig.2.23. Simulated LHCP and RHCP gain plot for the antenna with RIS and FSS

The proposed antenna results are compared with published literature as shown in Table 2.5. It is observed that the proposed antenna planar size is very less (1 λo× 1 λo) and the superstrate is placed at approximately half-wavelength height (λo/2) as mentioned in published literature.

2.4.5 Fabrication and Measured Results

The fabrication of the pentagon shape patch antenna with the RIS surface is done on the FR4 substrate and the fabrication of the superstrate is done on the Rogers RO 4003C substrate by using LPKF milling machine S100. The superstrate is placed approximately half wavelength above the antenna using Teflon rods as shown in fig. 2.24. Teflon rods are used which has no impact on radiation characteristics. The female type rounded four-hole coaxial RF SMA connector is inserted through FR4 substrates and it is soldered to the pentagon shape patch and the outer part is soldered to the ground layer. The reflection coefficient of the antenna is measured using a network analyzer in the frequency range of 4.5GHz to 6.5GHz as shown in fig. 2.25a. The gain of the antenna is measured by using the gain transfer method in which the gain of a standard antenna is known.

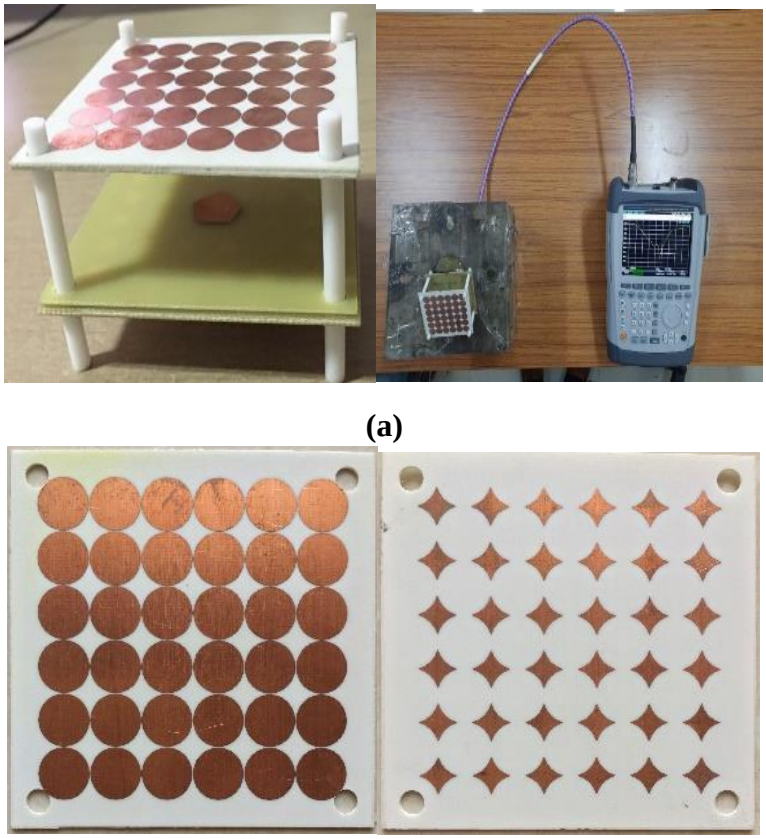

(a)

(b)

Fig. 2.24 . Prototype of fabricated antenna with RIS and FSS layers. a) Composite structure and its setup b) Capacitive layers and inductive layers

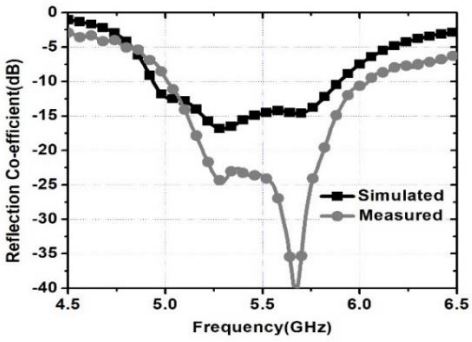

(a)

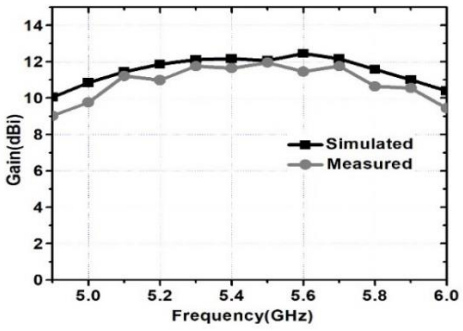

(b)

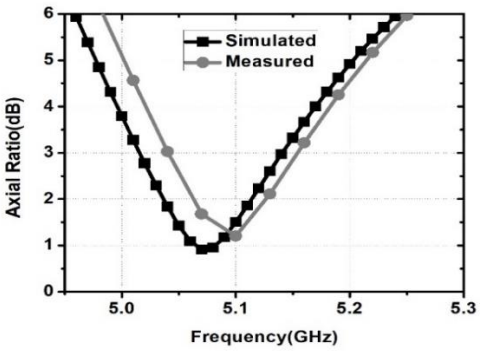

(c)

Fig.2.25. Simulated and measured results of antenna with RIS and FSS at h=32mm

(a) Reflection Coefficient (b) Gain (c) Axial Ratio

In the setup, the standard horn antenna is used as a transmitting antenna, whose gain values are already known. The fabricated antenna is used as a receiving antenna and it is rotated around its axis. The measured gain is similar to the simulated gain as shown in fig. 2.25b. The axial ratio measurement is done and it is plotted in fig. 2.25c. There is a slight change in the results due to fabrication errors. The radiation pattern of the fabricated antenna and simulated antenna are compared at 5.1GHz, 5.5GHz, and 5.8 GHz as shown in fig. 2.26.

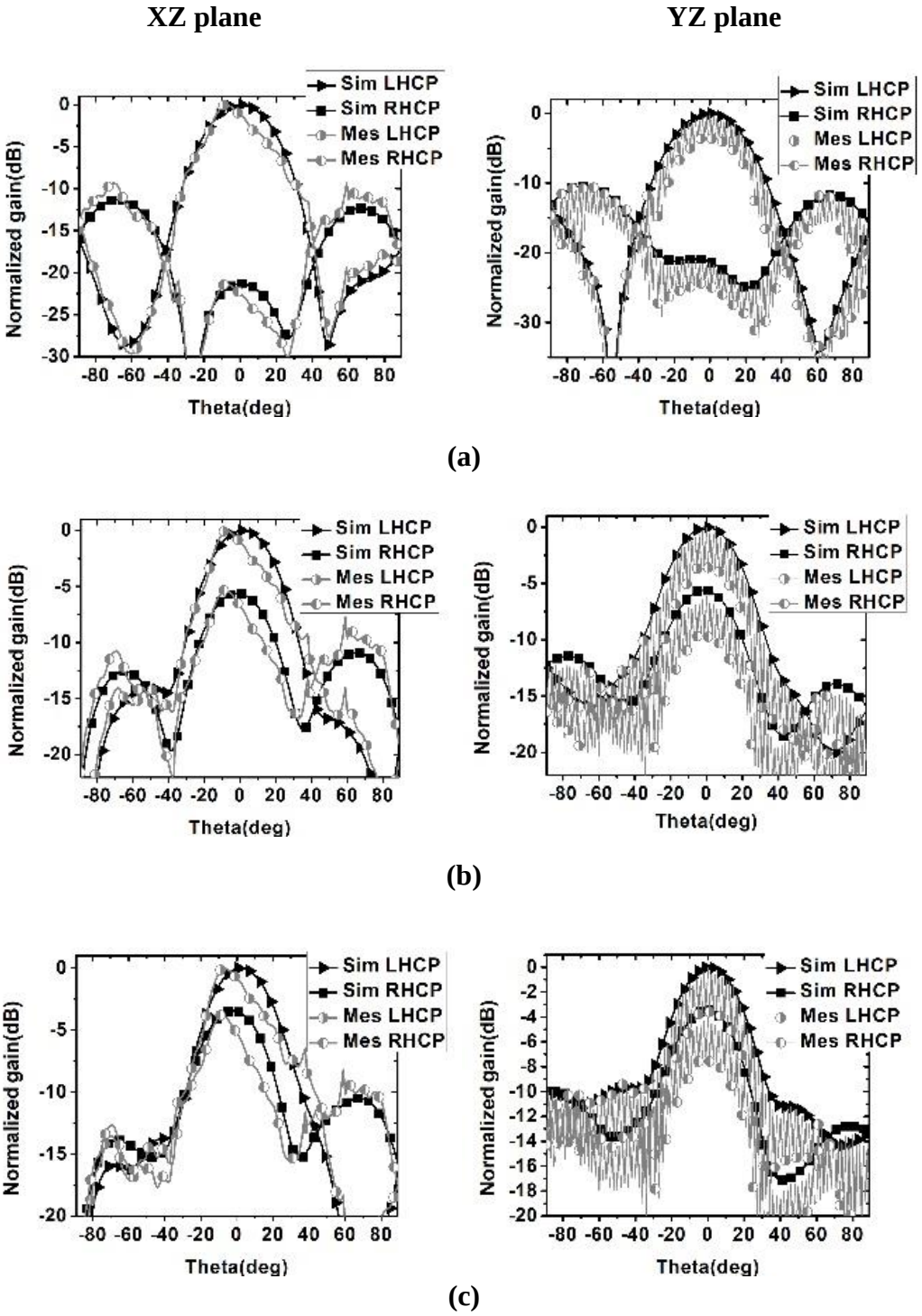

Fig. 2.26. Simulated and measured radiation patterns of antenna with RIS and FSS (a) 5.1 GHz (b) 5.5 GHz (c) 5.8 GHz.

2.5 Truncated Corner Square Patch Antenna with RIS and Dielectric Superstrate

2.5.1 Square Patch with Corner Truncated Antenna

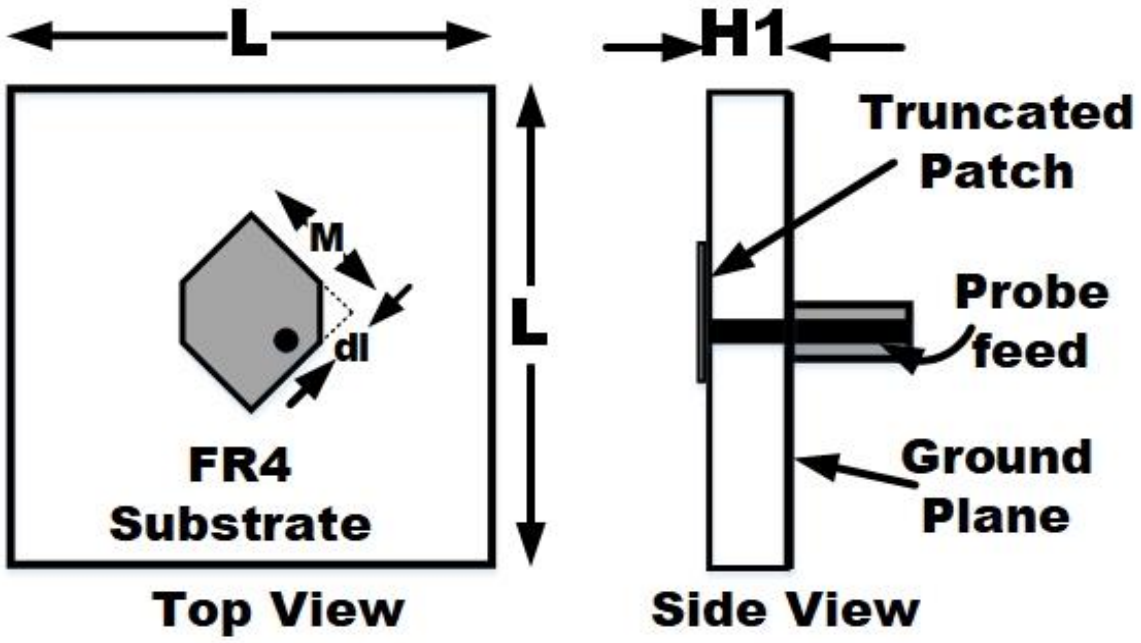

Fig.2.27. The geometry of a square patch with a corner truncated antenna

The corners of the square patch are trimmed on their two diagonal corners and it is printed on grounded FR4 dielectric substrate (Ɛr=4.4, tanδ=0.02, h= 1.6mm) as displayed in fig. 2.27. The dimensions of the patch are selected as 'M' is 12.8mm and 'dl' is 2mm. The patch is excited by probe feed and its feed position is optimized to resonate at 5.3GHz. The probe is inserted through a ground plane and substrate. The probe is connected to the truncated corner square patch.

The antenna is simulated using HFSS 13 software and simulation results are shown in fig. 2.28. The antenna has shown an impedance bandwidth of 6.4% (5.13-5.47GHz.). The gain of the antenna is 3-4 dBi. The antenna is achieved an axial ratio bandwidth of 1.7% (5.23GHz-5.32GHz).

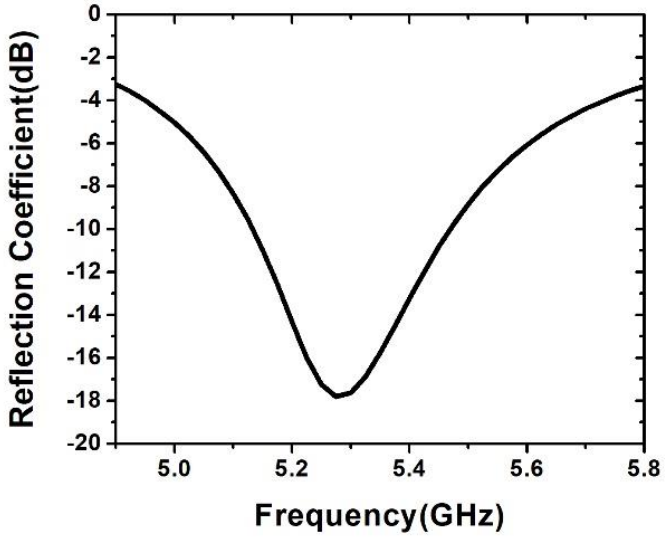

(a)

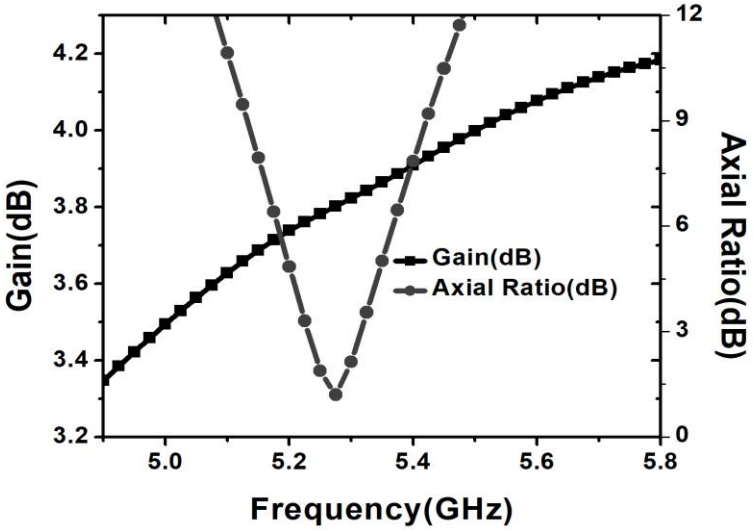

(b)

Fig. 2.28. Simulated results for the square patch with truncated corner antenna (a) Reflection Coefficient (b) Gain and Axial ratio

2.5.2 Antenna with RIS and dielectric superstrate

The RIS structure is designed as a 6×6 array of square patches and it is used as a ground plane to the truncated corner square patch antenna [6] as displayed in fig. 2.29. The Fabry Perot resonator antenna is designed by placing an FR4 dielectric substrate (Ɛr=4.4, tanδ=0.02, h= 3.2mm) approximately half-wavelength height above the ground plane [43] as shown in fig. 2.29. The cavity is formed in between the two parallel sheets i.e. RIS structure and the dielectric superstrate. The rays emanating from the antenna an incident upon the interface of different media. These waves bend according to Snell's law. The reflected rays from the superstrate are once again reflected by the ground plane. The trapped rays inside the cavity are bounced back

and forth and finally, a high gain resonance condition is obtained by properly choosing the position and thickness of the high Ɛr dielectric superstrate and coherent addition of rays emitted in the broadside direction. Hence the gain of the antenna is improved. The dimensions of patch (M, dl) are optimized to get the best results. The composite structure of square patch with

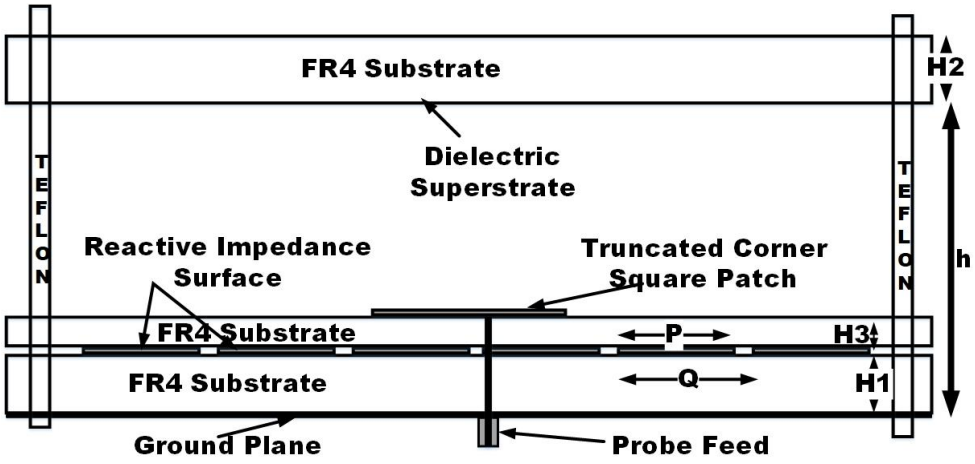

Fig. 2.29. The geometry of the composite structure of the patch with dielectric superstrate and RIS structure

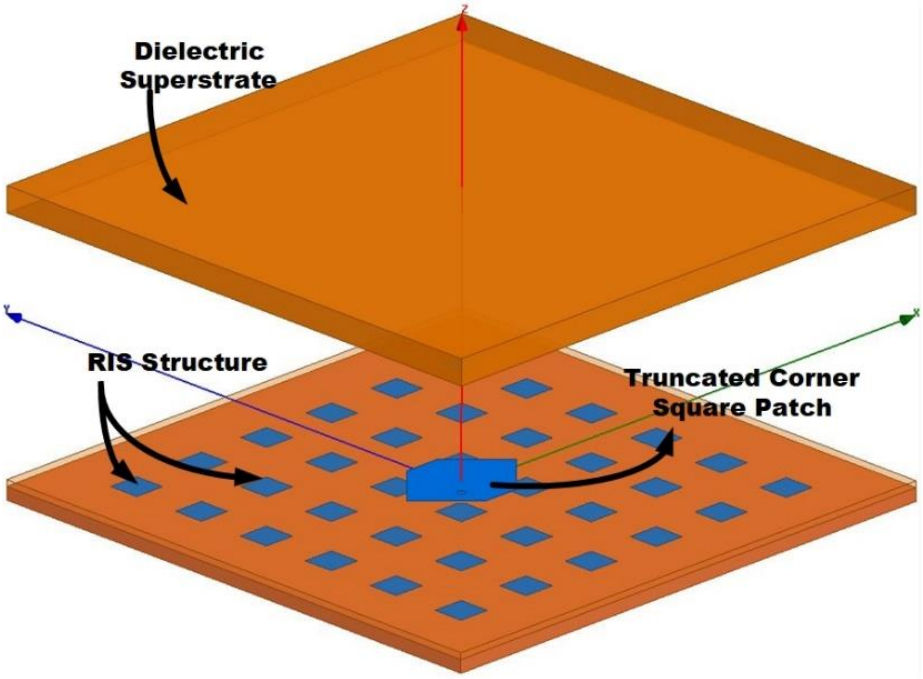

Fig. 2.30. A 3-D view of the composite structure of patch with dielectric superstrate and RIS structure

truncated corner, RIS structure as a ground plane and dielectric superstrate are shown in a three-dimensional view in fig. 2.30. The size of square patches (P) and periodicity (Q) are adjusted to get wide impedance bandwidth. The optimized parameter values are shown in Table 2.3.

Table 2.3. Optimized Parameter Values

Parameter	Values(mm)
L	70
M	11.9
dl	3.3
P	4
Q	10
h	32
H1	1.6
H2	3.2
H3	0.8

The composite structure containing a patch with RIS structure and dielectric superstrate is simulated using HFSS software. It is observed from fig. 2.31 that the antenna has an impedance bandwidth of 18% (4.97-5.95GHz), the gain of the antenna is 9.75dB, and the axial ratio of the antenna is 2.9%. There are huge improvements in the gain and impedance bandwidth simultaneously. The proposed antenna simulation results are presented in Table 2.4. The proposed antenna results are compared with published literature results are presented in Table 2.5.

Table 2.4. Comparison Table

S. No.	**Configuration**	**Impedance Bandwidth (%)**	**Gain (dBi)**	**Axial Ratio (%)**
1.	Truncated Corner Square Patch Antenna	6.4% (5.13-5.47)	3.75-4.2	1.7% (5.23-5.32)
2.	FPR Antenna with Dielectric superstrate	7.36% (5.10-5.49)	9.61	1.15% (5.17-5.23)
3.	FPR Antenna with Dielectric superstrate and RIS surface	18% (4.97-5.95)	9.75	2.9% (5.15-5.30)

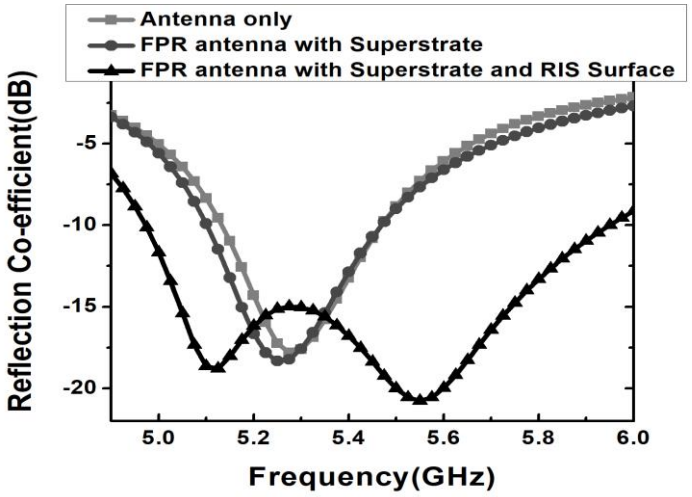

(a)

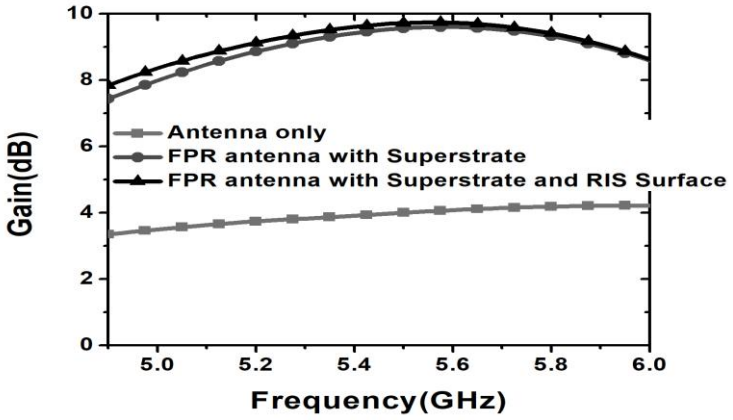

(b)

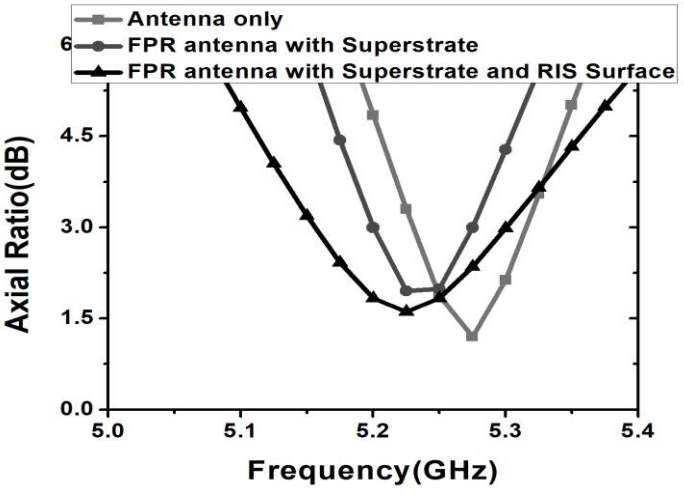

(c)

Fig. 2.31. Comparison of Simulated results (a) Reflection Coefficient (b) Gain (c) Axial Ratio

The simulation results for the LHCP gain and RHCP gain are shown in fig. 2.32. It is observed that the left-hand circular polarization (LHCP) gain is very high over the resonant frequency range. Hence the antenna is left-hand circular polarization (LHCP) antenna. The right-hand circular polarization (RHCP) gain is less over the resonant frequency range. The proposed antenna has shown very less RHCP gain at 5.25GHz where the antenna is maintaining an axial ratio of less than 3dB.

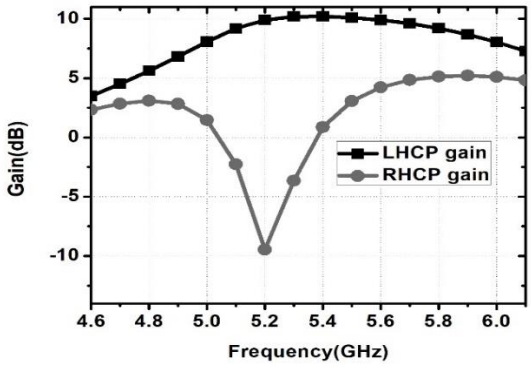

Fig. 2.32. The LHCP gain and RHCP gain

2.5.3 Fabrication and Measured Results

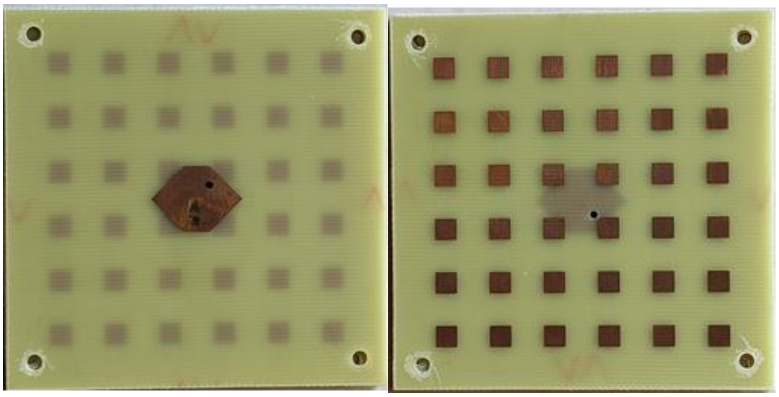

(a) (b)

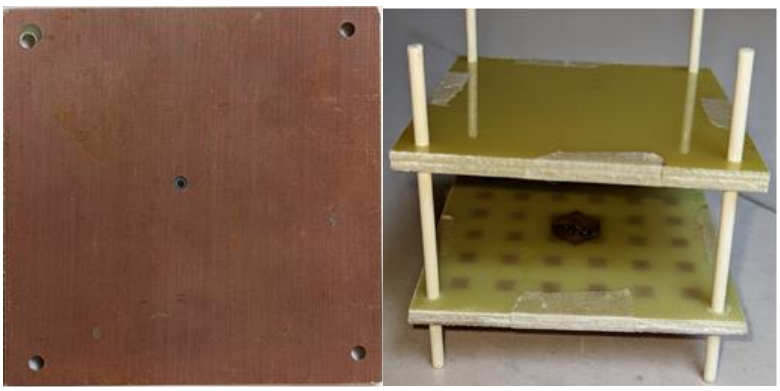

(c) (d)

Fig. 2.33. The model of fabricated prototype (a) Truncated corner square patch (b) RIS structure (c) Ground plane (d) Proposed antenna

The proposed antenna is fabricated using an LPKF milling machine. The fabricated prototype is shown in fig. 2.33. The reflection coefficient is measured using a network analyzer and it is plotted in fig. 2.34a. The antenna measurements are done in an anechoic chamber. The gain of the antenna measured using gain transfer method and it is plotted in fig. 2.34b. The axial ratio is calculated from the pattern and it is plotted in fig. 2.34c. The radiation patterns are measured at 5GHz, 5.25GHz and 5.5 GHz as shown in fig. 2.35.

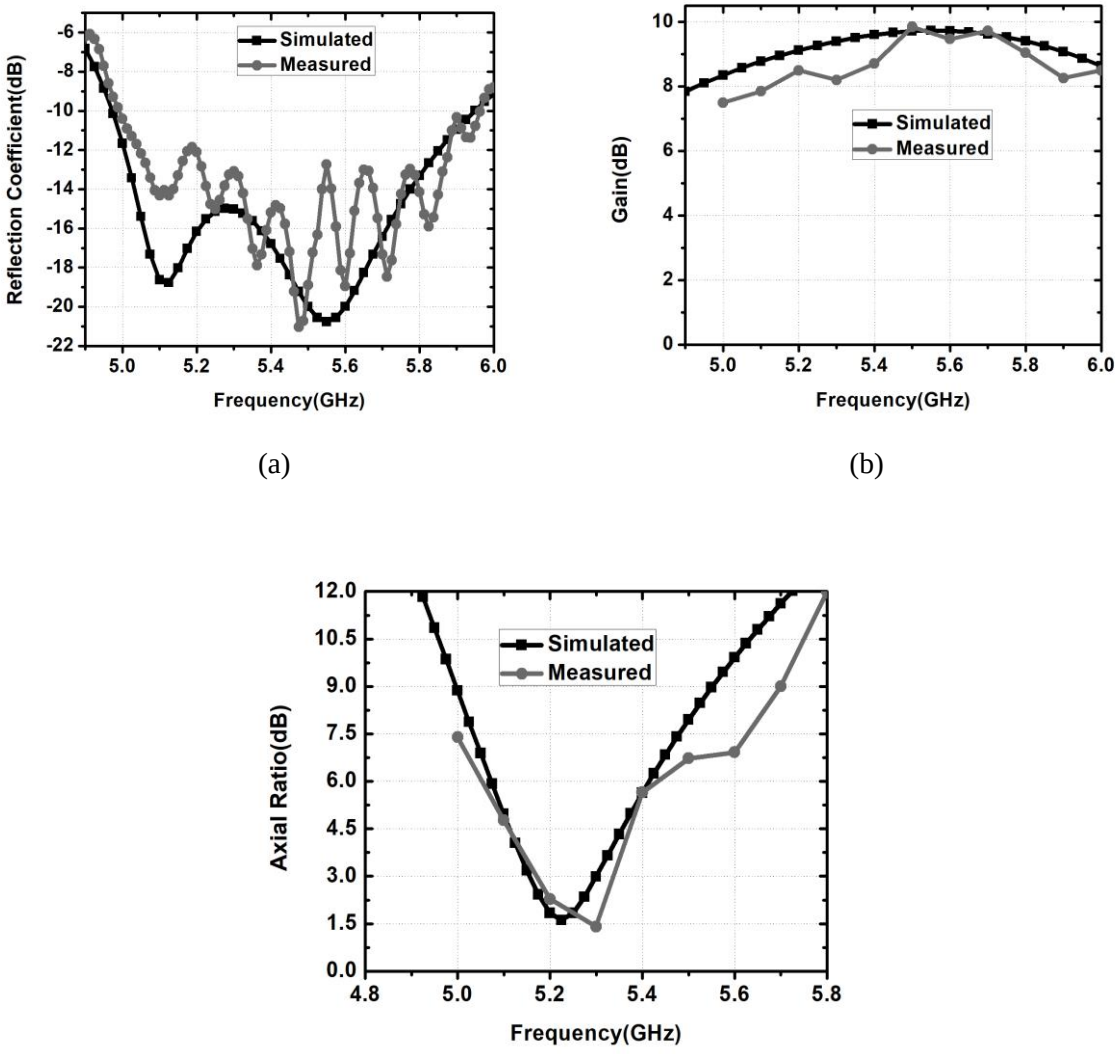

(a) (b)

(c)

Fig. 2.34. Comparison of simulated and measured results (a) Reflection Coefficient (b) Gain (c) Axial Ratio

X-Z Plane Y-Z Plane

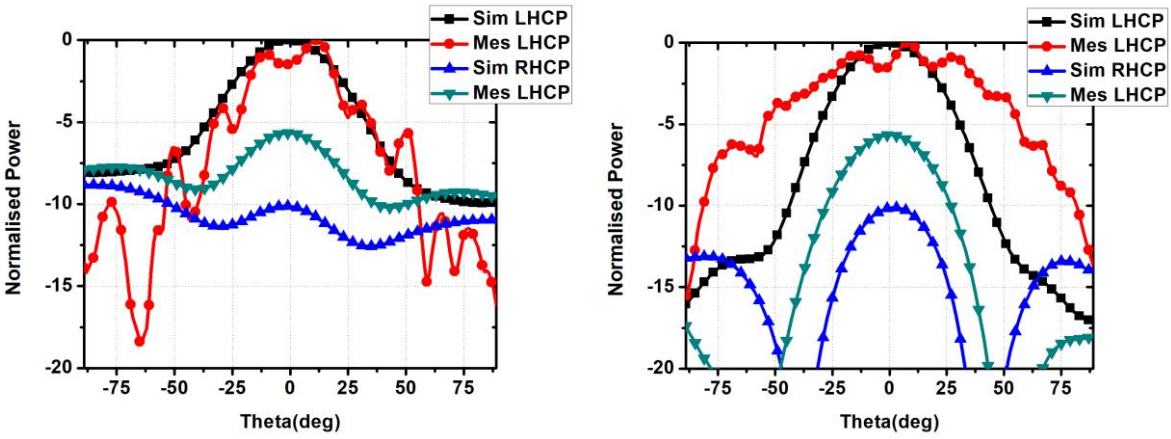

(a)

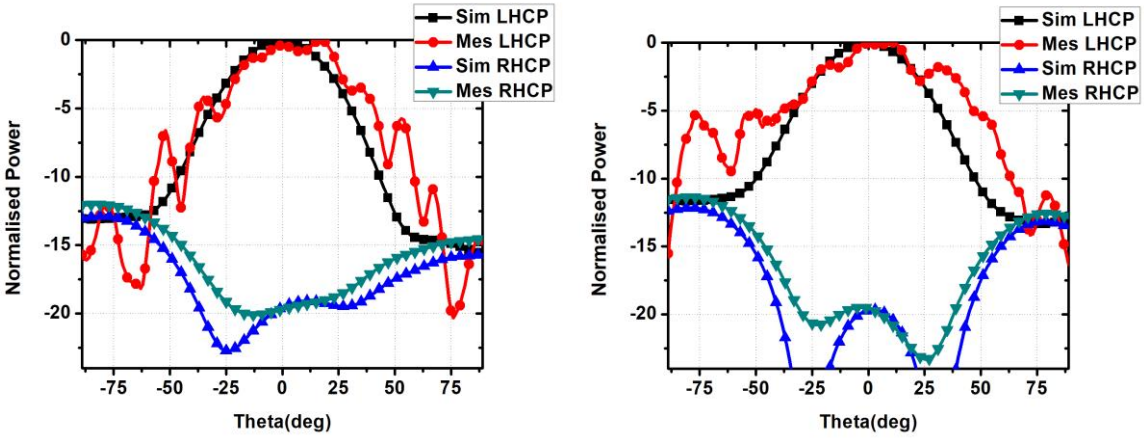

(b)

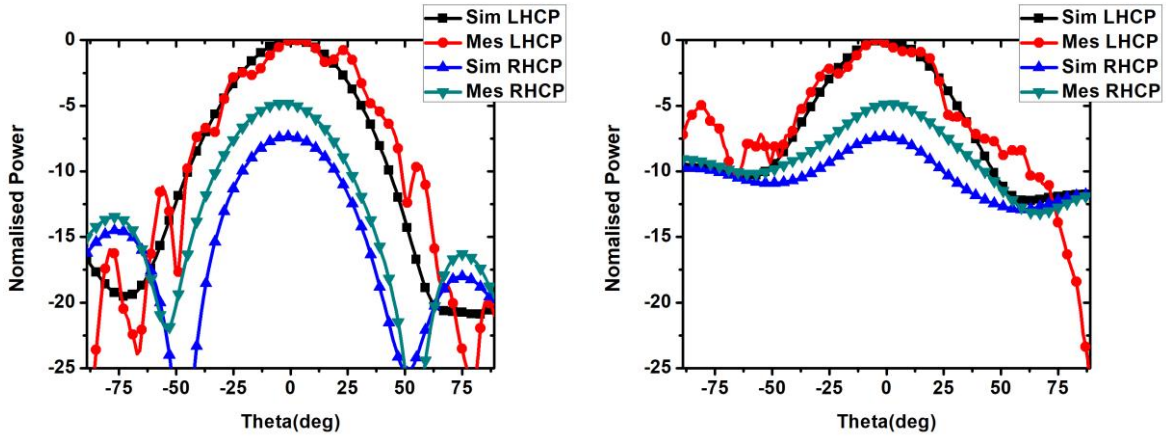

(c)

Fig. 2.35. Radiation patterns of proposed antenna at (a) 5GHz (b) 5.25GHz (c) 5.5GHz

Table 2.5. Comparison of antenna with published literature

Ref	Frequency range (GHz)	Planar Size (mm×mm)	Height of Superstrate (mm)	Gain(dBi)	Impedance Bandwidth (%)	Axial Ratio (%)
[10]	9.42–11.35	2.20 λo×2.20 λo	≈λo/2	12 dBi	18.56%	-
[16]	13.1-15.2	3 λo × 3 λo	≈λo/2	13 dBi	15.50%	-
[19]	29.1-31.6	2.5 λo× 2.5λo	≈ λo/2	15.2 dBi	9.60%	2.67%
[45]	55.4 - 66.6	4.44 λo× 3.6 λo	Greater than λo/2	15.6 dBi	18.40%	
[46]	27.5-30	2.98 λo ×2.98 λo	≈λo/2	15.5 dBi	8.60%	
[47]	9.85-10.1	2.758 λo×2.758λo	≈ λo/2	15 dBi	2.30%	0.60%
[48]	14.9-15.3	7λo × 7 λo	≈ λo/2	21 dBi	2.50%	7%
[51]	11.7–19.8	1.75 λo ×1.75 λo	≈ λo/2	11.5 dBi	54%	29%
2.4	**4.93-5.89**	**1.3 λo ×1.3 λo**	**≈ λo/2**	**12.48dBi**	**17.72%**	**2.40%**
2.5	**4.97-5.95**	**1.3 λo ×1.3 λo**	**≈ λo/2**	**9.75dBi**	**18%**	**2.90%**

2.6 Summary

A square microstrip patch antenna is designed for 5GHz Wi-Fi applications. By implementing the RIS structure, the bandwidth is enhanced to 6.9% and the dielectric lens is also attempted successfully to improve the gain up to 9.5dBi for a square patch with RIS. Instead of using the dielectric lens, the Fabry Perot resonator is applied extensively in all the antennas designed and discussed in the chapters. By using a highly reflective FSS superstrate, the gain is increased up to 8.5dBi in the case of the square patch with RIS surface. Similarly partially reflective surfaces are studied and designed. A highly reflective FSS superstrate is also applied for the pentagonal patch with RIS and the gain is increased substantially up to 12.48dBi and impedance bandwidth of 17.72%. Similarly, a truncated corner square patch is also designed with high gain up to 9.75dBi and impedance bandwidth of 18%. All the antennas in this chapter are presented in Table.2.6. All the antennas are suitable for 5GHz Wi-Fi systems.

Table 2.6. Comparison of all antennas

Antenna	Technique	S_{11} bandwidth	Gain	Axial Ratio(dB)
2.2	Square Patch with RIS and Vertical Dielectric Sheets	6.9% (5.13- 5.50GHz)	9.5-10.23dBi	-
2.3	Square Patch with RIS and FSS superstrate	5.85% (5.11-5.42GHz).	8.5dBi	-
2.4	Pentagonal Patch with RIS and FSS Superstrate	17.72% (4.93-5.89GHz)	12.48dBi	2.40% (5.01-5.14GHz)
2.5	Truncated Corner Patch with RIS and Dielectric Superstrate	18% (4.97-5.95GHz)	9.75dBi	2.9% (5.15-5.30GHz)

Chapter 3

Unconventional Patch Antennas with Reactive Impedance Surface and Superstrates

3.1 Introduction

The conventional patches with FR4 substrate are not able to generate broadband circular polarization. But the broadband circular polarization is needed for the present applications due to their inherent features. The signal reception is possible independent of the orientation of the receiver and polarization loss due to multipath propagation can also be eliminated. So the generation of broadband circular polarization is required for present applications. The circular polarization can be generated by exciting two orthogonal fields with the same magnitude and in phase quadrature. This mechanism was achieved by dual feeding. However, researchers in the last few decades are interested in designing single-feed circularly polarized antennas. The single-feed antennas with the techniques of slots, truncated corners, and slits to the square patch are producing circular polarization. There are perturbations on the patch due to slots, truncated corners, and slits. The generation of circular polarization without using slots, slits and truncated corners to the patch is a challenging problem. The broadband antenna is necessary for the present wireless communication devices such as 5GHz Wi-Fi to transmit the data with a high data rate. These devices also need high gain to transmit the data to longer distances. However, the broadband circularly polarized antenna design is a challenging problem with high gain requirements.

In the published literature, the impedance bandwidth and axial ratio bandwidth are improved by using reactive impedance surfaces to the H-shaped patch or dipole as listed below. Fan Yang (2005) et al proposed a circularly polarized dipole antenna using RIS structure as a ground plane. The antenna achieves impedance and axial ratio bandwidth of 5.6% at 3.56GHz [53]. Joysmitha Chatterjee (2018) et al proposed a circularly polarized H-shaped patch antenna using a 4×4 array of square patches as a RIS structure. The designed structure achieved an impedance bandwidth of 44.5% with axial ratio bandwidth of 27.5% in the 5GHz Wi-Fi region [54].

In chapter 2, published literature is cited for gain enhancement of antenna using Fabry Perot resonator principle. Similar works are listed below. Naizhi Wang (2014) et al proposed a positive reflection phase gradient superstrate with complementary FSS's. The superstrate is

placed above the air-loaded patch antenna to improve the gain of the antenna at the X band i.e from 8.6 GHz to 11.2 GHz and the peak gain of 13dBi[55]. Hang Ying Yuan (2016) et al designed a superstrate with a complementary cross element for a stable reflection phase. The gain of the patch antenna is increased when the superstrate is placed above the antenna at 13GHz [56]. Chen Zhang (2018) et al has proposed the superstrate with 3 different sizes to form a shared aperture superstrate with positive reflection phase gradient property. After loading the antenna with the superstrate, the impedance bandwidth is 44.7% from 7.8GHz to 12.3GHz and the peak gain is 7dB[57]. Peddakrishna samineni (2018) et al proposed a slotted elliptical patch antenna. The gain of antenna is further improved by 5.1dBi by placing FSS superstrate of highly reflective behavior and the impedance bandwidth is improved by 0.13 GHz [58]. Sarath Sankar Vinnakota et al proposed two orthogonal H shaped patches for generating dual polarization at two different frequencies. When the superstrate is placed above the antenna, the gain of the antenna enhanced by 9.8dBi and 10.1dBi at respective frequencies [59]. In the above-discussed papers [55-59] the circular polarization is not reported.

In chapter 2, published literature is cited for gain enhancement of circularly polarized antenna using Fabry Perot resonator principle. Similar works are listed below. Basit Al zeb (2015) et al published two corner truncated patches to get dual-band operation with different polarizations. The gain improvement in dual-band is attained by two dielectric superstrates with higher refractivity. The antenna achieves peak gains of 16.1dB, 16.2dB and axial ratios of 1.9dB, 1.5dB are attained at 9.65GHz and 11.75GHz respectively [60]. Zhen Guo Liu (2016) et al presented a circular polarization from the linearly polarized source by tilting the patch by 45^{o}. Nonstandard AMC surface is acting as a ground plane and cross slot FSS acts as a top plane to the Fabry Perot resonator to improve the gain of an antenna. The maximum gain is observed as 12.7dB at 13.9GHz. The antenna attains a common (impedance and axial ratio) bandwidth of 6.4%[61]. Son Xuat Ta (2019 et al investigated a PRS with a square aperture array for the improvement of axial ratio bandwidth and gain of truncated corner square patch. The antenna achieves axial ratio bandwidth of 13.7 %(5.45-6.25), a peak gain of 13.3dBic [62]. The above-mentioned techniques [55-62] have focused mainly on the improvement of antenna gain only.

In the published literature, the impedance bandwidth and axial ratio bandwidth of the antenna improved by using a reactive impedance surface. The gain of the antenna improved by using the Fabry Perot principle. Both the gain and impedance bandwidth can be improved simultaneously by combining RIS structure and superstrate. Unconventional structures like H,

C, E and S with RIS structure on FR4 substrate are designed for the broadband circular polarization.

The authors investigated that the unconventional structures like H, C, E and S are excited in such a way that their lengths are divided into two parts as shown in fig. 3.1. The feed position is optimized such that the length difference between two parts is selected at approximately λ/4 for generating orthogonal fields over broadband frequency ranges in the presence of the RIS structure. Therefore these structures are designed to generate broadband circularly polarized antennas in the presence of RIS structure.

Fig.3.1. Unconventional structures for broadband circular polarization

In this chapter, the design of broadband circularly polarized antennas using unconventional structures H, C, E and S with RIS structure on FR4 substrate is studied. The simulation results are only discussed for H, C and E structures with RIS structure on FR4 substrate because these structures' impedance matching is not good enough. The S-shaped patch with RIS structure and positive phase gradient FSS superstrate is designed to get high gain and broadband circularly polarized antenna for 5GHz Wi-Fi applications.

3.2 H Shaped Patch with RIS

The patch is designed in the form of an H shape on a grounded FR4 substrate (ε_r=4.4, loss tangent tanδ=0.02, h=5.2mm). The patch is excited by using the SMA connector. The inner conductor of SMA is connected to H shaped patch after inserting through the substrate. The outer conductor of SMA is connected to the ground plane. The feed position is optimized to get resonance at 5.4GHz. The RIS structure is designed with a 6×6 array of square patches and it is added in the middle of H shaped patch and ground plane [54] as shown in fig. 3.2.

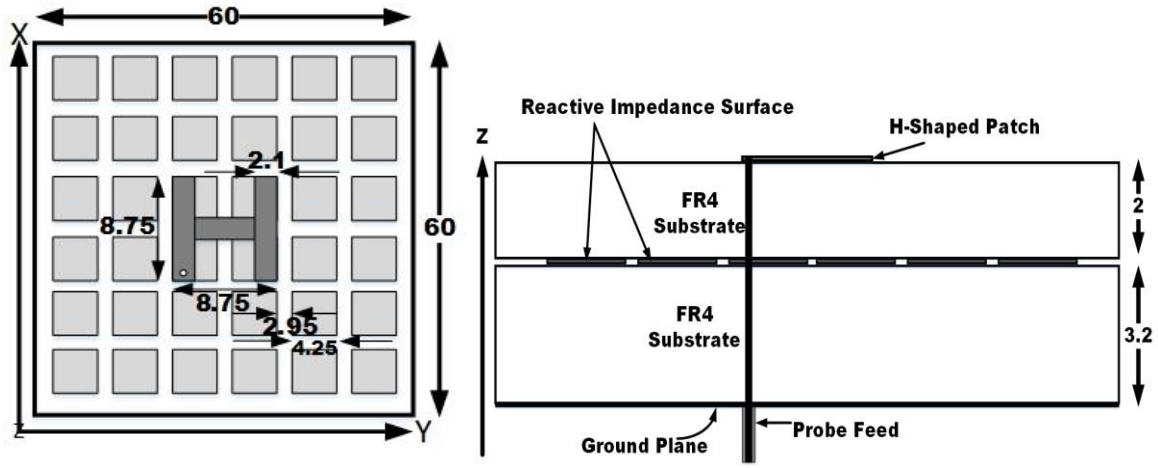

(a) (b)

Fig.3.2. Geometry of H-shaped patch antenna with RIS surface (a) Top View (b) Side View

The electric field in the broadside direction (z-axis) can be estimated by the addition of directly transmitting wave E_d and reflected wave from the RIS surface E_r [53]:

$$E = Ed + E_r \quad (1)$$

$$E_d = \frac{E_o}{2}(\hat{X} + \hat{Y})e^{-jkz} \quad (2)$$

$$E_r = \frac{E_o}{2}\left(\hat{X}e^{-2jkd+\theta_x} + \hat{Y}e^{-2jkd+\theta_y}\right)e^{-jkz} \quad (3)$$

Where E_o is the magnitude of the electric field component, d indicates the antenna height above the ground plane, k indicates the wavenumber, θ_x is the phase of the incident wave polarized along X direction, and θ_y is the phase of the incident wave polarized along Y direction. Here, the antenna is placed very near to the ground plane, 2kd is approximately zero in (3).

The RIS surface is chosen with suitable polarization-dependent reflection phases i.e. $\theta_x = -90^o$ and $\theta_y = 90^o$.

$$E = \frac{E_o}{2}((\hat{X}+\hat{Y})-j(\hat{X}-\hat{Y}))e^{-jkz} \quad (4)$$

From equation (4), it can be observed that the RIS surface converts the linear polarized wave into a circularly polarized (LHCP) wave. Therefore RIS surface converts linearly polarized antenna into circularly polarized antenna in [53]. The H-shaped patch antenna and H-shaped patch with RIS structure are simulated using HFSS 13 software and the simulation results are compared in fig. 3.3. The H-shaped patch with RIS structure has shown an impedance bandwidth of 23.9% (5.04GHz-6.41GHz), gain of the antenna is 0-4.5dBi. In addition to that, the axial ratio bandwidth is 16.2 %(4.92GHz-5.79GHz). It can be observed that there is a huge improvement in impedance bandwidth and 3dB axial ratio bandwidth when RIS structure is

added. The authors have also investigated that C, E, and S structures also generate broadband circular polarization in the presence of the RIS structure.

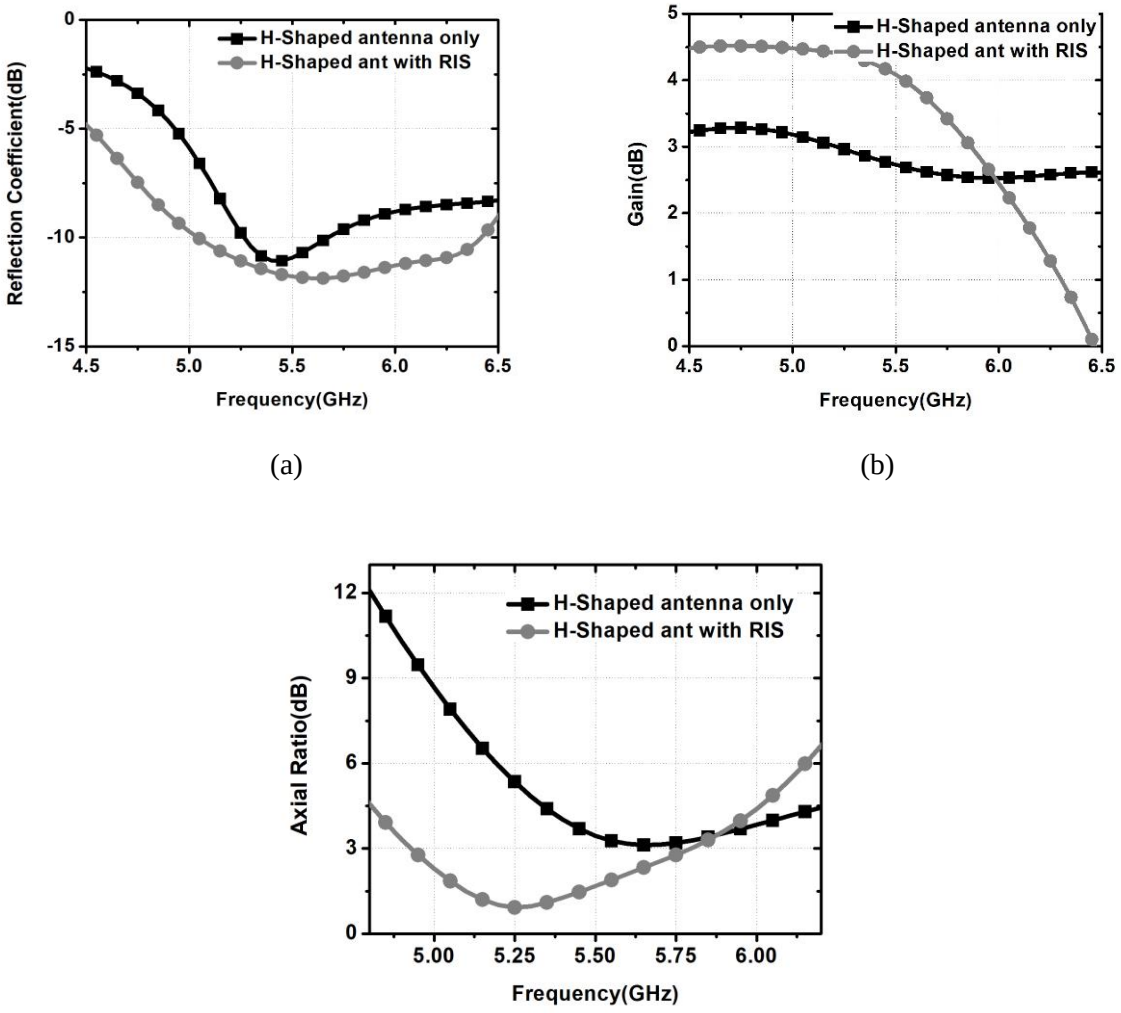

(a) (b)

(c)

Fig.3.3. Comparison of simulation results for the H-shaped patch antenna, and H-shaped patch antenna with RIS (a) Reflection Coefficient (b) Gain (c) Axial Ratio

3.3 C Shaped Patch with RIS

The patch is designed in the form of a C shape on a grounded FR4 substrate (ε_r=4.4, loss tangent tanδ=0.02, h=5.2mm). The patch is excited by using the SMA connector. The inner conductor of SMA is connected to the patch after inserting through the substrate. The outer conductor of SMA is connected to a ground plane. The feed position is optimized to get resonance at 5.4GHz. The RIS structure is designed with a 6×6 array of square patches and it is added in the middle of C shaped patch and ground plane as shown in fig. 3.4.

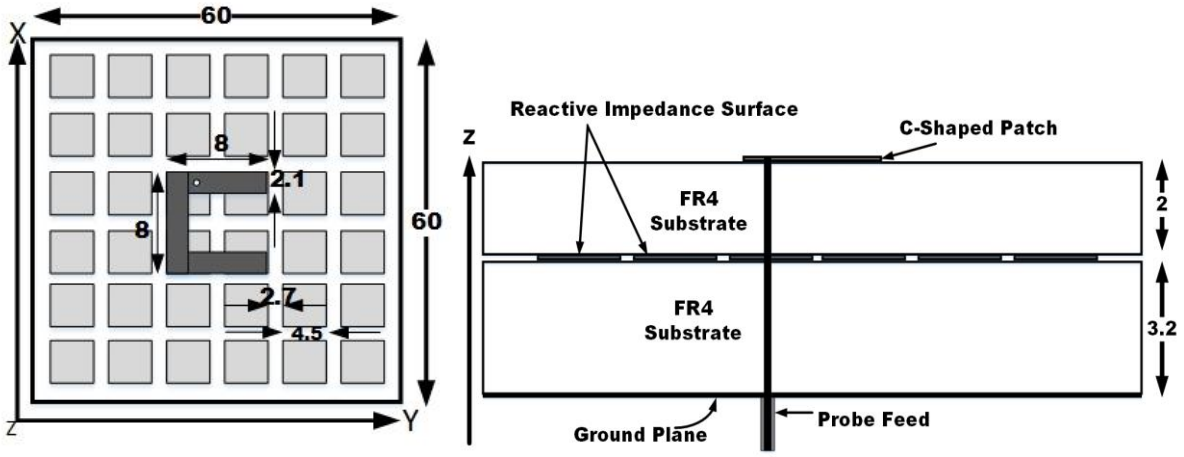

(a) (b)

Fig.3.4. Geometry of C-shaped patch antenna with RIS surface (a) Top View (b) Side View.

The C-shaped patch antenna and C-shaped patch with RIS structure are simulated using HFSS 13 software and the simulation results are compared in fig. 3.5. The C-shaped patch with RIS structure has shown an impedance bandwidth of 24.9% (4.81GHz-6.18GHz), the gain of an

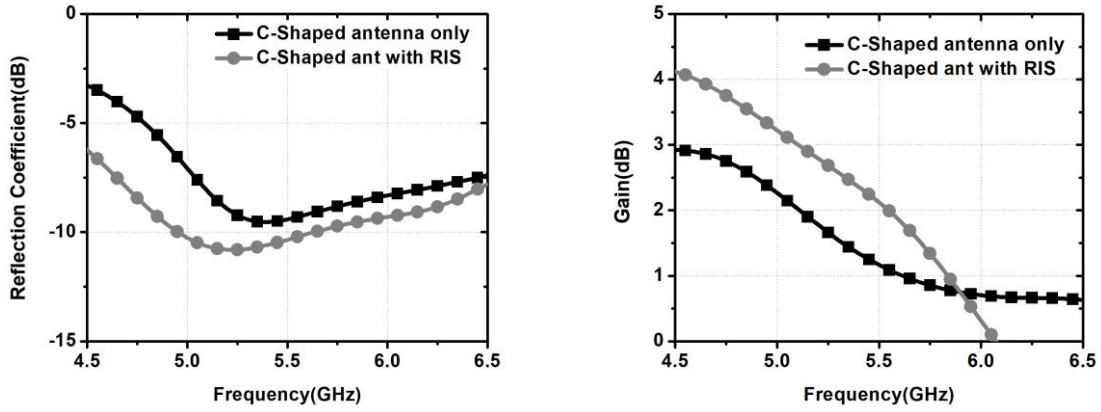

(a) (b)

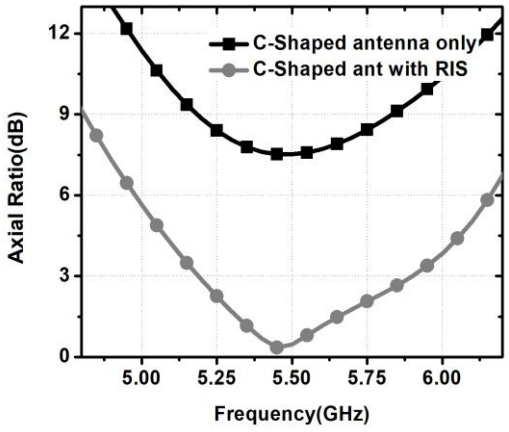

(c)

Fig.3.5. Comparison of simulation results for the C-shaped patch antenna, and C-shaped patch antenna with RIS (a) Reflection Coefficient (b) Gain (c) Axial Ratio

antenna is 0-4dBi. In addition to that, the axial ratio bandwidth is 12.9 %(5.18GHz-5.90GHz). It can be observed that there is a huge improvement in 3dB axial ratio bandwidth when RIS structure is added. The impedance matching is not good for these structures.

3.4 E-Shaped Patch with RIS

The patch is designed in the form of an E shape on a grounded FR4 substrate (ε_r=4.4, loss tangent tanδ=0.02, h=5.2mm). The patch is excited by using the SMA connector. The inner conductor of SMA is connected to the patch after inserting through the substrate. The outer connector of SMA is connected to a ground plane. The feed position is optimized to get resonance at 5.4GHz. The RIS structure is designed with a 6×6 array of square patches and it is added in the middle of E shaped patch and ground plane as shown in fig. 3.6.

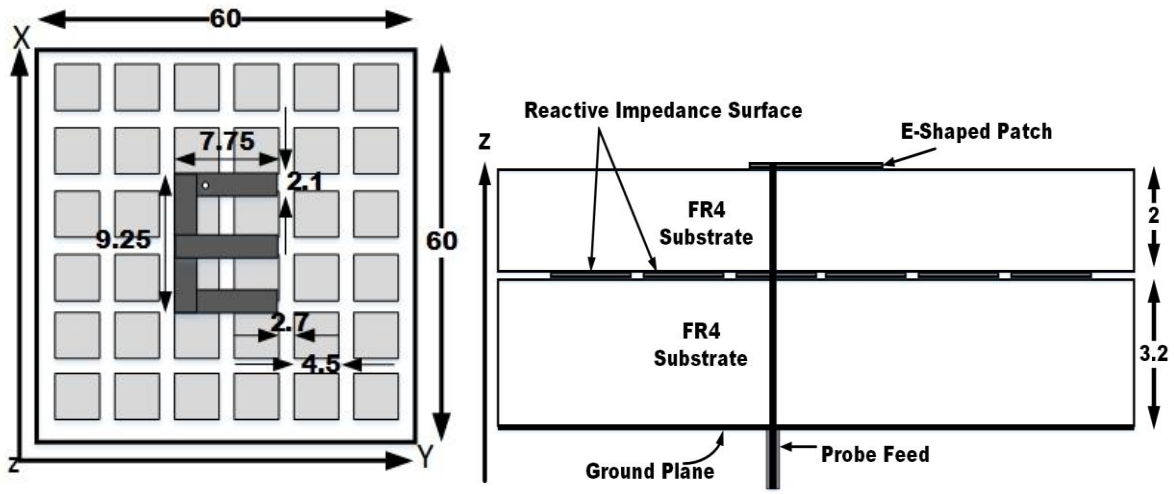

(a) (b)

Fig.3.6. Geometry of E-shaped patch antenna with RIS surface (a) Top View (b) Side View

The E-shaped patch antenna and E-shaped patch with RIS structure are simulated using HFSS and the simulation results are compared in fig. 3.7. The E shaped patch with RIS structure has shown an impedance bandwidth of 27.7% (4.82GHz-6.37GHz), the gain of antenna is 0-4dBi. In addition to that, the axial ratio bandwidth is 12.4 %(5.11GHz-5.79GHz). It can be observed that there is a huge improvement in impedance bandwidth and 3dB axial ratio bandwidth when RIS structure is added.

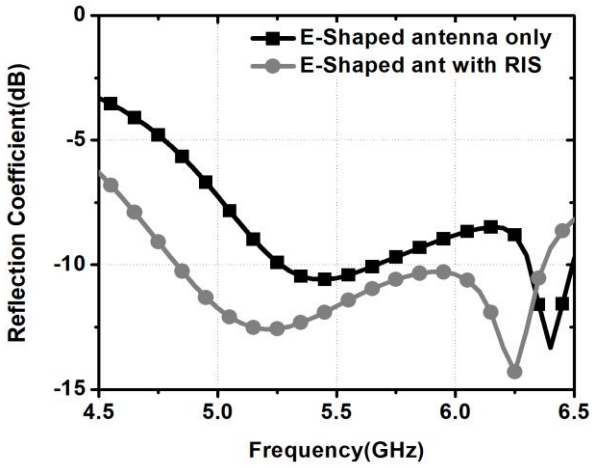

(a)

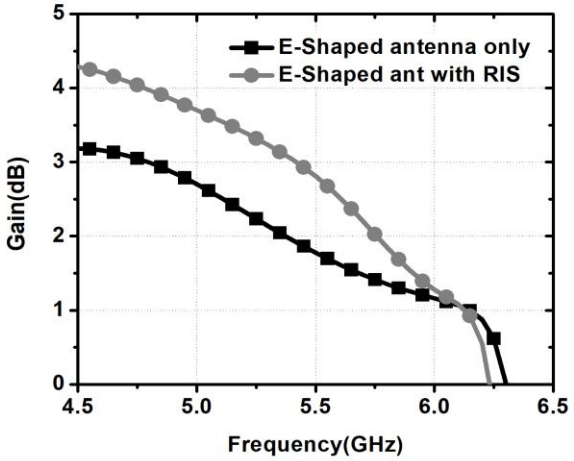

(b)

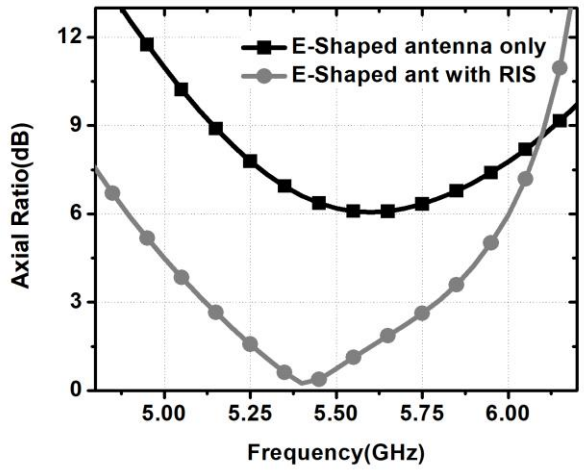

(c)

Fig.3.7. Comparison of simulation results for the E-shaped patch antenna, and E-shaped patch antenna with RIS (a) Reflection Coefficient (b) Gain (c) Axial Ratio

3.5. S-Shaped Patch with RIS Structure as a Ground Plane and Positive Phase Gradient FSS Superstrate for High Gain and Broadband Circular Polarization

The impedance matching of H, C, E shaped patches with RIS structure on FR4 substrate is not good. These structures are designed and simulated for the analysis of unconventional structures. Whereas the S-shaped patch is showing good impedance matching. Therefore, the S-shaped patch with RIS structure is selected for the design of broadband and high gain circularly polarized antenna. The S-shaped patch with RIS structure is showing good impedance matching with broadband axial ratio bandwidth. In order to improve the gain of the antenna, the positive phase gradient FSS superstrate is placed above the antenna.

3.5.1 S-Shaped Patch Antenna with RIS Structure

The square patch is trimmed in the form of an S-shaped patch on a grounded FR4 substrate (ε_r=4.4, tanδ=0.02, h=5.2mm). The patch is excited by using the SMA connector. The inner connector of SMA is connected to the patch after inserting through the substrate. The outer connector of SMA is connected to a ground plane. The feed position is optimized to get resonance at 5.3GHz. The RIS structure is designed with a 6×6 array of square patches and it is added at a height of 3.2mm from the ground plane as shown in fig. 3.8.

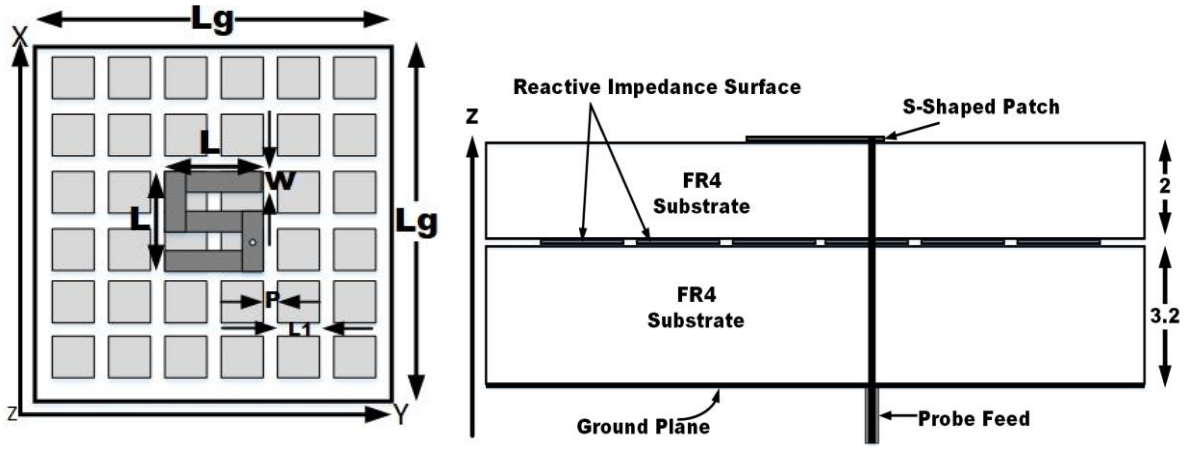

(a) (b)

Fig.3.8. Geometry of S-shaped patch antenna with RIS surface (a) Top View (b) Side View

The length of square patches (L_1) and their periodicity (L_1+P) are chosen to obtain broadband impedance bandwidth and 3dB axial ratio bandwidth. The length of the square patches L_1 is optimized to 4.5mm and the gap between the patches P is optimized to 2.8mm.

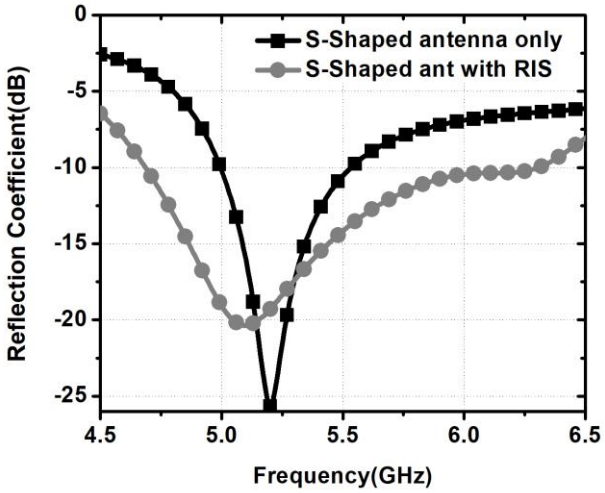

(a)

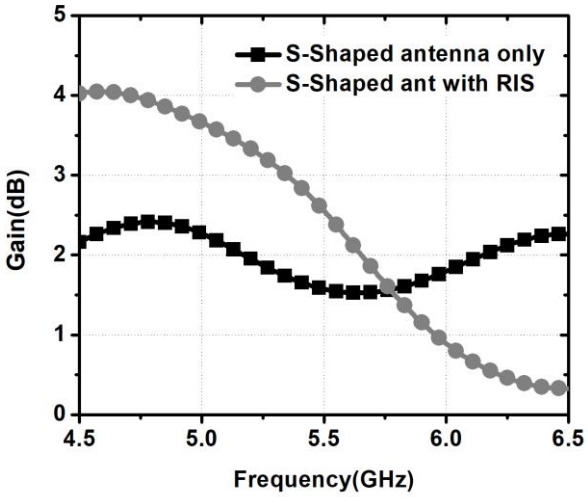

(b)

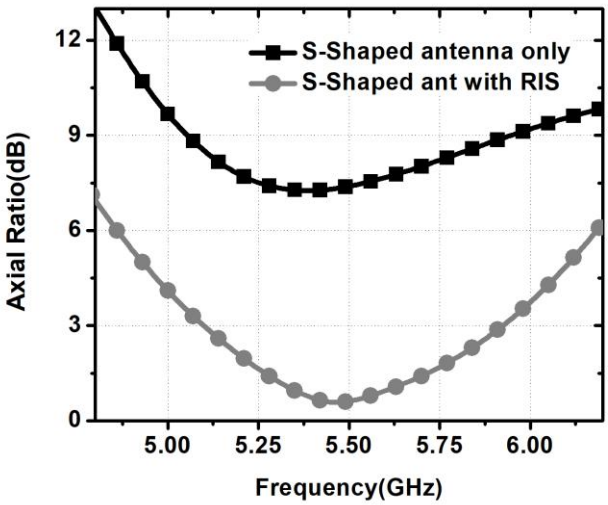

(c)

Fig.3.9. Comparison of simulation results for the S-shaped patch antenna, and S-shaped patch antenna with RIS (a) Reflection Coefficient (b) Gain (c) Axial Ratio

The S-shaped patch antenna with RIS structure simulations are carried out in HFSS 13 Simulator software and simulated results are presented in fig. 3.9. The antenna has shown an impedance bandwidth of 29.5% (4.68GHz-6.30GHz) and a 3dB axial ratio bandwidth of 15.1 %(5.09GHz-5.92GHz), but the antenna gain is 1-3dBi only. There is a huge improvement of around 19.3% in impedance bandwidth compared with the simple S-shaped patch antenna and the antenna attains the 3dB axial ratio bandwidth of 15.1%. Still, the gain of an antenna is not adequate for many applications. The partially reflective surface superstrate is deployed above the antenna to enrich the antenna gain. Here the frequency selective surface is used as a partially reflecting surface.

3.5.2 Frequency Selective Surface (FSS) Superstrate

It is designed with a periodic array of meta-structure unit cells whose characteristics are varied with the dimension of the unit cell. It has the property to allow the selected frequency ranges and improve the gain in that selected frequency range. A positive phase gradient unit cell is selected for the proposed antenna.

3.5.2.1 Positive Phase Gradient Unitcell: It is constructed as a circle-shaped patch printed on the top face of Rogers RO 4003C substrate and circle-shaped etching on the bottom face of the substrate as displayed in fig. 3.10 a. The PEC and PMC boundary conditions are assigned to four sides of the unit cell as displayed in fig. 3.10 b. The above-mentioned unit cell is simulated in the High-Frequency Structure Simulator software.

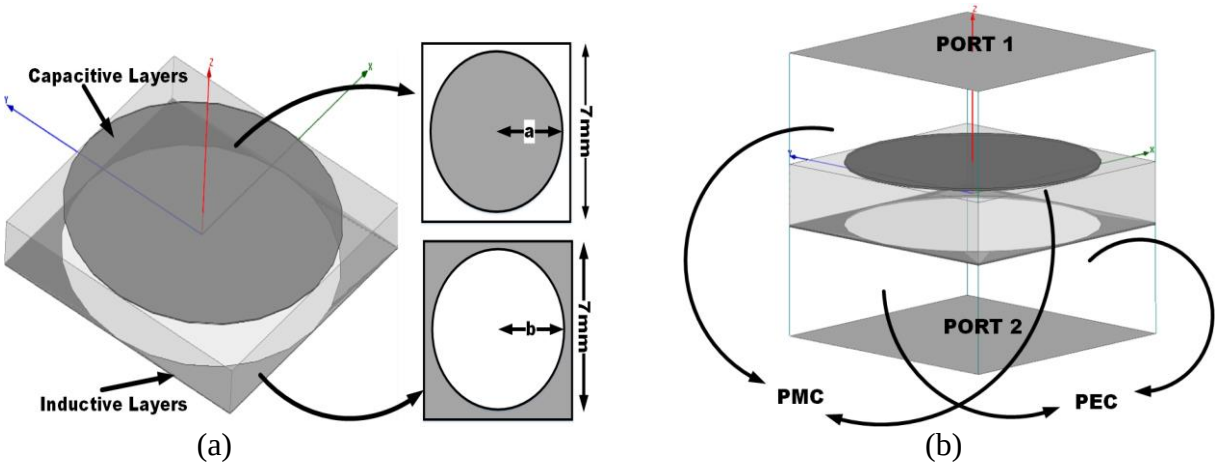

Fig.3.10. Positive Phase Gradient Unit Cell (a) Geometry (3D view) (b) Boundary conditions

The superstrate is formed by a 6 × 6 array of positive phase gradient unit cells. The FSS superstrate is deployed at approximately λ/2 height above the ground plane. Fabry Perot cavity

resonator is formed between the RIS structure and FSS superstrate, this leads to multiple reflections in the cavity. The rays in the cavity move forward and backwards. Finally, the constructive interference in the cavity increases the antenna gain towards the broadside direction when the FSS is deployed at a distance (h) above the ground plane.

$$h = \frac{\lambda}{2}\left(\frac{\phi}{2\pi} + 0.5\right) + N\frac{\lambda}{2} \qquad (5)$$

Where ϕ is the phase of reflection of the FSS superstrate, and λ is the free-space wavelength. N is the order of resonant mode and equal to 0,1,2,3… N. The equation of phase can be written from equation (5)[46]. To get the optimum phase and the air gap height (h) is selected as 25mm.

$$\phi = \frac{4\pi h}{c} f - (2N - 1)\pi \qquad (6)$$

Equation (6) shows the condition to get maximum gain in the broadside direction in terms of positive phase gradient property over the selected frequency range [46]. To achieve the suitable positive phase gradient property, circle-shaped patches are used on the top face of the superstrate and circle-shaped etching on the bottom face of the superstrate. Top layers act like capacitive layers and bottom layers act as an inductive layer to form an FSS.

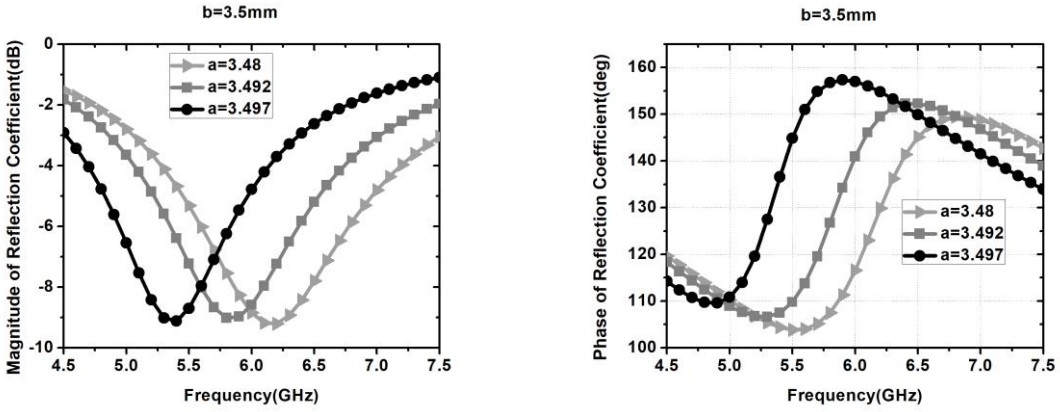

(a) (b)

Fig.3.11. Simulated results of unit cell a) Magnitude of Reflection Coefficient b) Phase of Reflection Coefficient

The optimized values are obtained by doing a parametric study on the a and b values and simulation results are displayed in fig. 3.11. It is noticed that the positive phase gradient property is shifted to the lower frequencies as "a" value increases. The parameters a=3.497mm and b=3.5mm are selected for the design to get maximum gain enhancement in the 5GHz to 6 GHz frequency region.

3.5.3. S-Shaped Antenna with RIS and FSS Configuration

The RIS structure is utilized as a ground plane to the S-shaped patch antenna. The FSS is deployed at approximately λ/2 height above the ground plane as displayed in fig. 3.12 and a three-dimensional view of the composite structure of the S-shaped patch with RIS and FSS is shown in fig. 3.13. The combination of RIS and FSS enhances impedance bandwidth and the gain simultaneously. Besides that, the composite structure enhances 3 dB axial ratio bandwidth. The optimized parameter values are mentioned in Table.3.1.

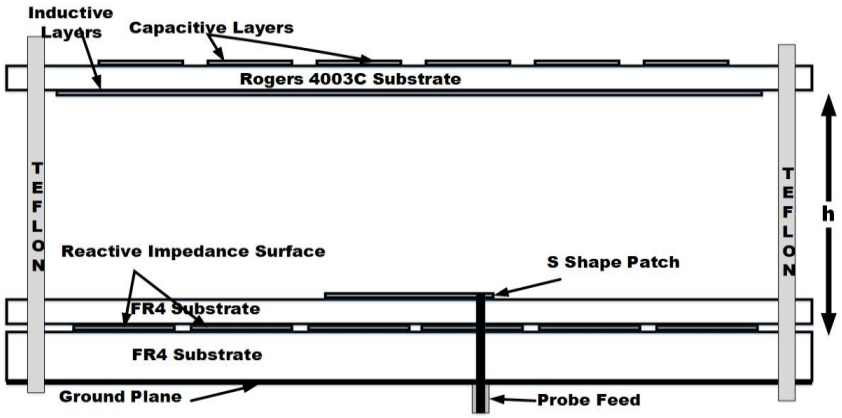

Fig.3.12. Geometry of composite structure of S shape antenna with RIS and FSS at h=25mm (front view)

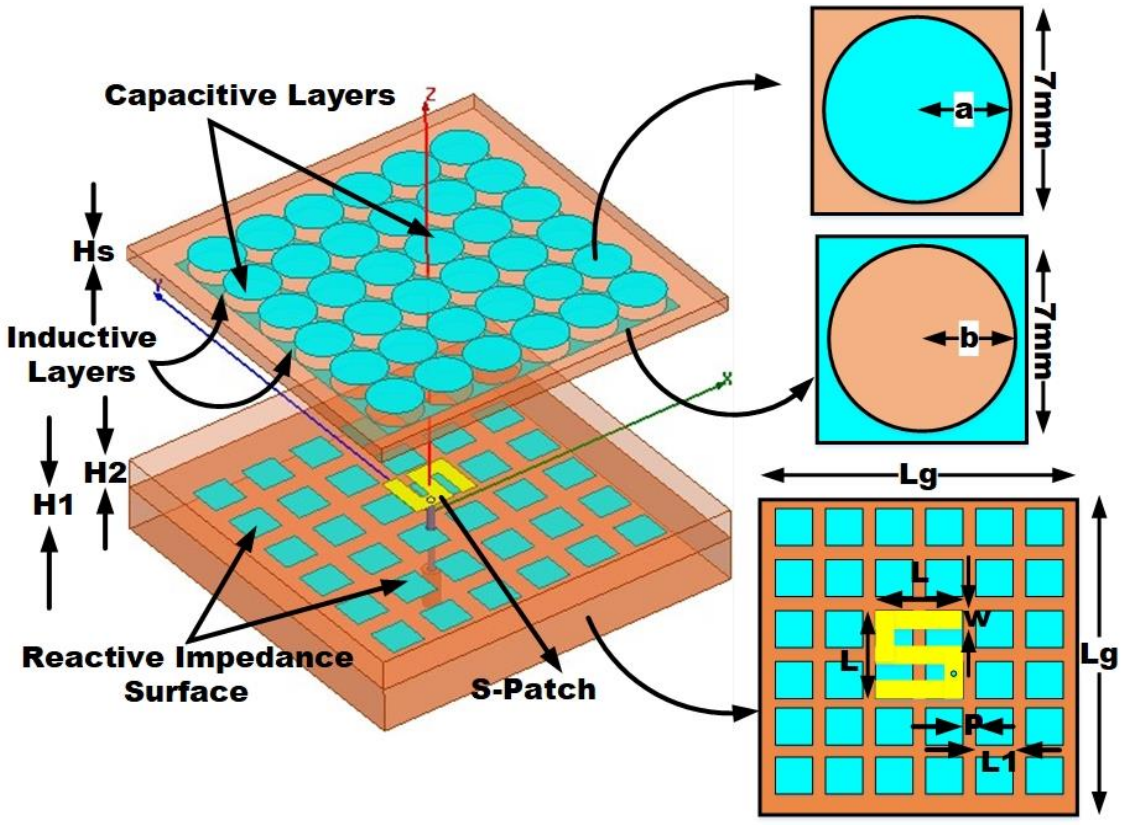

Fig.3.13. Three-dimensional view of S-shaped antenna with RIS and FSS at h=25mm

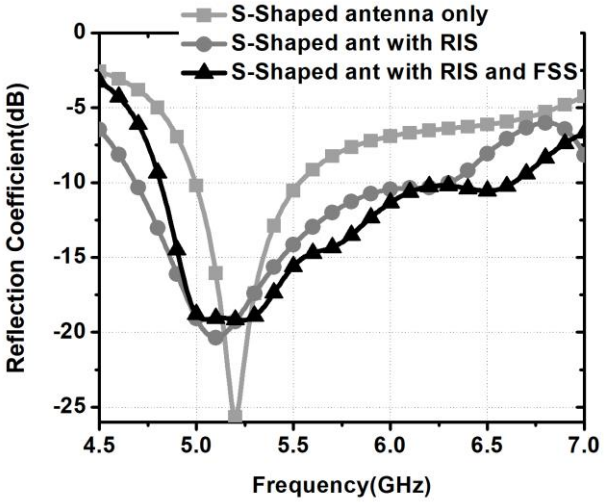

(a)

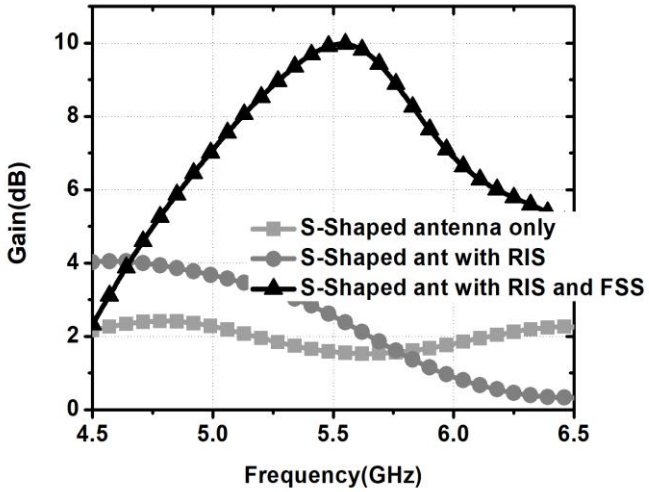

(b)

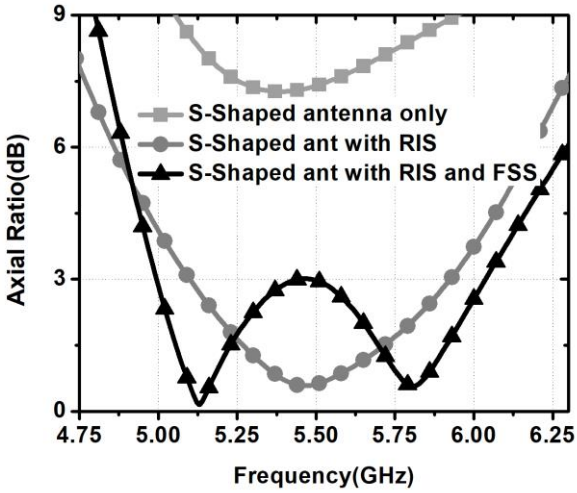

(c)

Fig.3.14. Comparison of simulation results for the antenna, antenna with RIS, and antenna with RIS and FSS at h=25mm (a) Reflection Coefficient (b) Gain (c) Axial Ratio

Table 3.1: Optimized parameter values for the S-shaped antenna with RIS and FSS

Parameter	Values(mm)
Lg	60
H1	3.2
H2	2
Hs	0.787
L	7.3
W	2.1
L1	4.5
p	2.8
a	3.497
b	3.5
h	25

The composite structure consists of an S-shaped patch, RIS structure, and FSS superstrate. The composite structure is simulated in HFSS 13 Simulator software and simulated results are displayed in fig. 3.14. The composite structure has shown impedance bandwidth of 31.8% (4.81GHz-6.63GHz**)** as displayed in fig. 3.14 a and 3dB axial ratio bandwidth of 18.9 %(4.99GHz-6.03GHz) as displayed in fig. 3.14 c. The proposed antenna gain is around 10dBi as displayed in fig. 3.14b. It is observed that there are improvements in impedance bandwidth, 3dB axial ratio bandwidth and gain of an antenna compared with a simple S-shaped patch antenna. The comparison is done for the simple S-shaped patch, patch with RIS, and patch with RIS and FSS as displayed in Table 3.2. The composite structure is compared with published literature as mentioned in Table 3.3.

Table 3.2: Comparison of simulation results for the patch, patch with RIS, and patch with RIS and FSS

S.No.	Antenna	Impedance Bandwidth	Gain	Axial Ratio
1	S-shaped patch	10.2% (4.99GHz-5.53GHz)	1.5-3 dBi	NA
2	S shaped patch with RIS	29.5% (4.68GHz-6.30GHz)	1-3dBi	15.1% (5.09GHz-5.92GHz)
3	S shaped patch with RIS and FSS	31.8% (4.81GHz-6.63GHz)	10dBi	18.9% (4.99GHz-6.03GHz)

Table 3.3: Comparison of the composite structure of patch with RIS and FSS with published literature

Ref	Frequency range (GHz)	Planar Size (mm×mm)	Height of Superstrate (mm)	Gain(dBi)	Impedance Bandwidth (%)	Axial Ratio (%)
[11]	8.75-9.04, 9.34-9.52	1.78λ×1.78λ	≈0.1λ	10.2,8.5	3.3%, 1.9%	-
[15]	8.35-8.56, 9.5-10.1	3.2 λ× 3.2λ	≈λ/2	17.6,19	2.5%, 6.1%	-
[17]	2.49-2.59	1.6 λ×1.6λ	≈0.8 λ	13.5	1.12%	1.90%
[18]	3.84–3.96	4 λ × 4 λ	≈ λ	18	3%	3%
[58]	5.07-5.56	λ × λ	≈λ/2	9.8	0.49%	-
[59]	5.8, 6.2	2.9 λ×2.9 λ	≈λ	10.1,9.8	-	
[60]	9.65,11.25	3.6 λ×3.6 λ	≈0.82 λ	16.1,16.2	-	1.9%,1.5%
[61]	13.3-13.8	2.1 λ×2.13 λ	≈0.25 λ	12.4	6.40%	6.40%
[62]	5.23-7.2	2.4λ×2.4λ	≈λ/2	10.3	31%	10.80%
3.5	**4.81-6.63**	**λ × λ**	**≈λ/2**	**10dBi**	**31.8**	**18.90%**

In the S-shaped patch antenna with RIS, the feed position is set at a position to create two different arm lengths. The shorter arm generates the E_x component and the longer arm generates the E_y component. The length difference between the shorter arm and the longer arm is approximately λ/4. E_x component leads the E_y component by 90^0 in the presence of RIS structure. It will lead to the left hand circularly polarized (LHCP). The simulation results are mentioned in fig. 3.15.

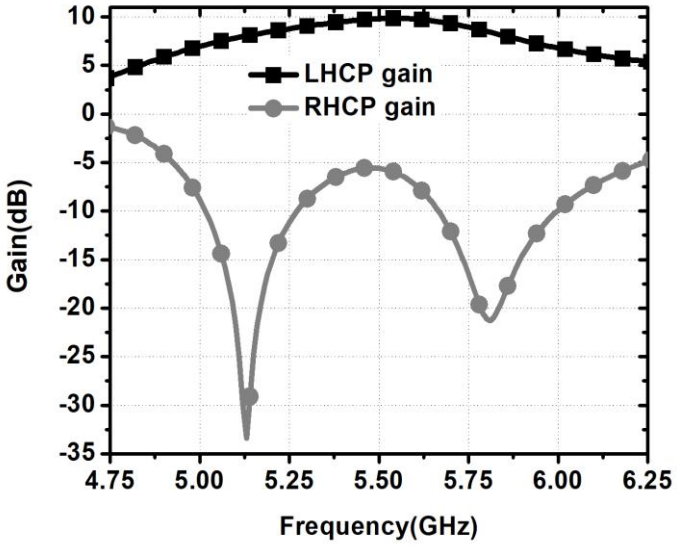

Fig.3.15. Simulated LHCP gain and RHCP gain for the composite structure of S-Shaped antenna with RIS and FSS

3.5.4 Fabrication and measured results

The layers of a composite structure are fabricated by an LPKF protomat S100 milling machine. The S-shaped patch is milled on an ungrounded FR4substrate with a height of 2mm. The RIS structure is milled on a grounded FR4(ε_r=4.4) substrate with a height of 3.2mm. The RIS structure is attached as a ground plane to the S-shaped antenna. A four-hole flange female SMA connector is used to feed an S-shaped patch. A hole diameter of 1.3mm is cut to the FR4 substrates. The inner conductor of SMA is passed through the hole of FR4 substrates and the projected part is soldered to an S-shaped patch. The outer conductor of the SMA is soldered to the ground of the RIS structure. The periodic array of circle-shaped patches is milled on the top face of the Rogers RO 4003C (ε_r=3.38) substrate and the circle-shaped etching is milled on the bottom face of the substrate. This substrate is deployed as an FSS superstrate. The Teflon rods are used to place the FSS superstrate at approximately $\lambda/2$ height above the ground plane as displayed in fig. 3.16. The radiation pattern of the antenna is not affected by Teflon rods because they do not have any conductive property.

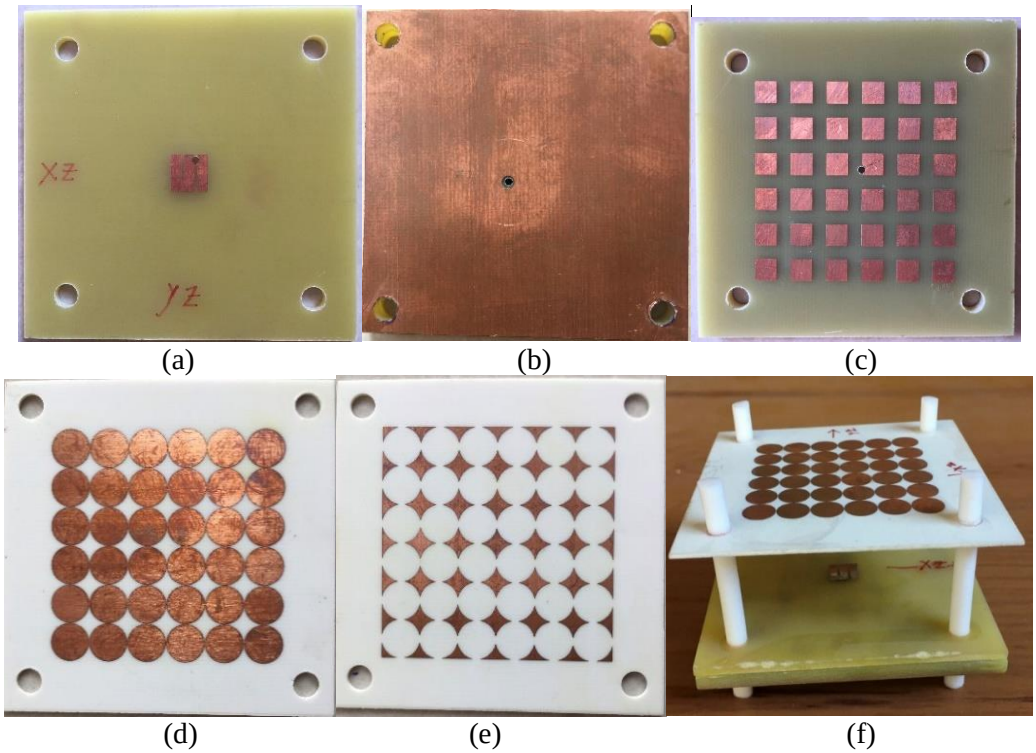

Fig.3.16. Photograph of fabricated prototypes (a) S-shaped with RIS (top view) (b) S-shaped with RIS (bottom view) (c) RIS structure (d) FSS (top view) (e) FSS (bottom view) (f) S-shaped with RIS and FSS (3D view)

The network analyzer is used to measure the reflection coefficient from 4.5GHz to 6.5GHz frequency range as displayed in fig. 3.17a. The gain transfer method is applied to measure the gain where the standard gain values are already noted for the transmitting antenna.

Here, the standard horn antenna is chosen for the measurement and it is connected as a transmitting antenna. The fabricated prototype is connected as a receiving antenna in the anechoic chamber and it is arranged to rotate around its axis by using the software. The gain values are calculated from the measured power values. The measured results are almost similar to the simulated results as displayed in fig. 3.17b. The axial ratio values are calculated from the pattern and it is displayed in fig. 3.17c. The results were disturbed slightly due to fabrication errors. The fabricated antenna and simulated antenna radiation patterns are displayed at 5.5GHz, and 5.8 GHz as shown in fig. 3.18. It is observed that the radiation pattern is directional towards the z-direction at the center frequency i.e 5.5GHz where side lobes are very much low. But the radiation pattern is spread in other directions for other frequencies i.e 5.8GHz where the side lobes are moderately increased. There is a variation between simulation radiation patterns and measured radiation patterns due to fabrication errors.

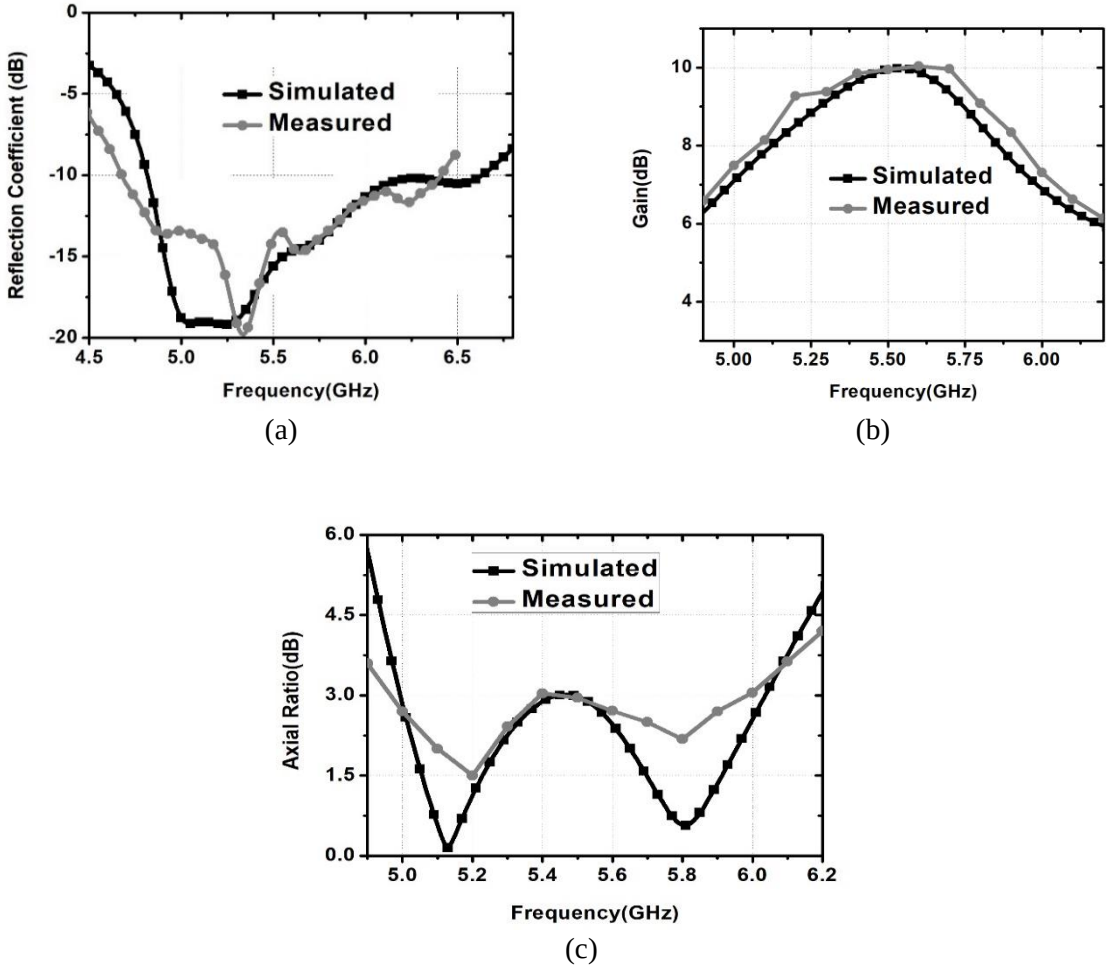

Fig.3.17. Comparison of simulated results and measured results for the S-shape patch antenna with RIS and FSS at h=25mm (a) Reflection Coefficient (b) Gain (c) Axial Ratio.

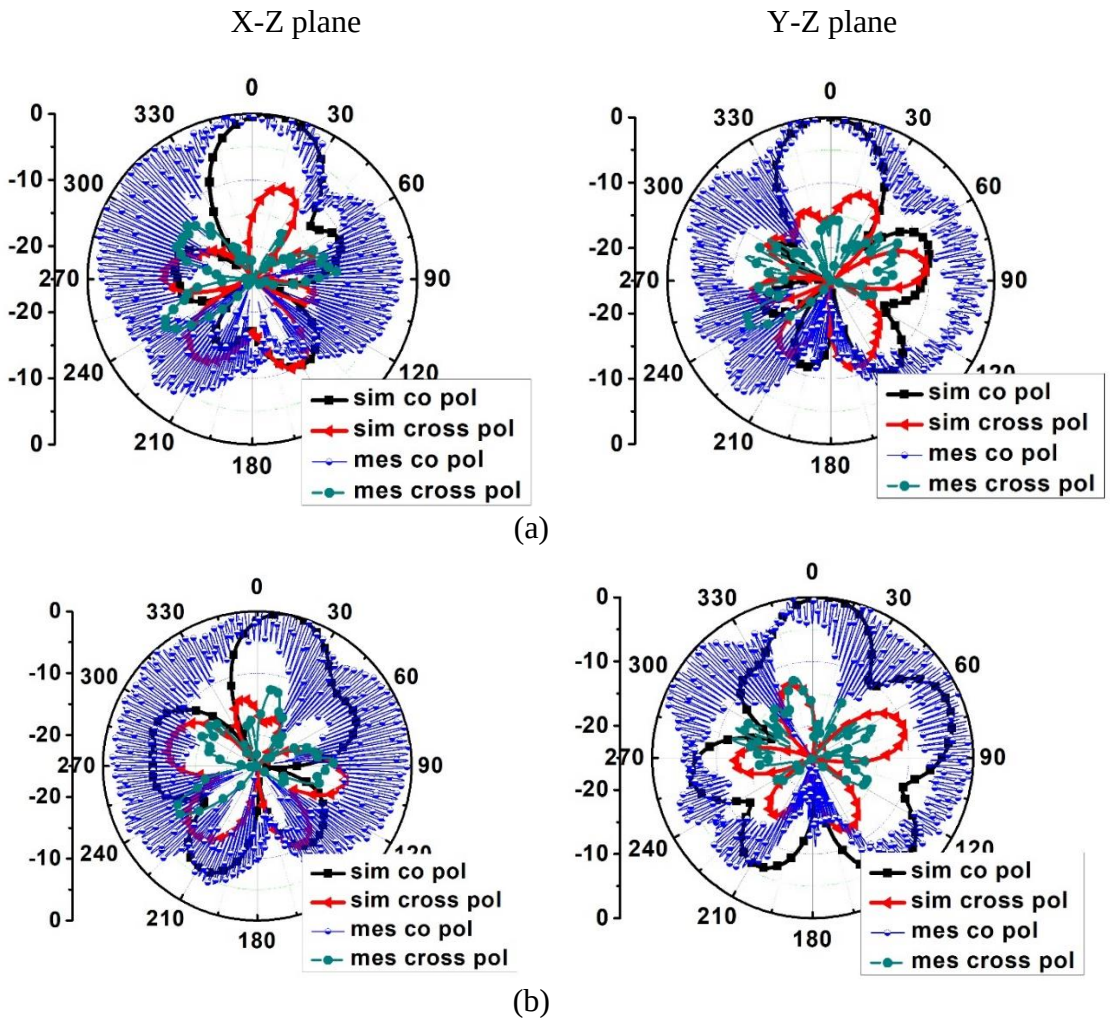

Fig.3.18. Simulated and measured radiation patterns for the antenna with RIS and FSS at h=25mm (a) 5.5GHz (b) 5.8GHz

3.6 Summary

Several types of patch structures like H, E, C and S are proposed to generate broadband circularly polarized antennas using RIS structure as a ground plane on FR4 substrate. The S shape patch with the RIS structure is producing good impedance matching over other structures. Furthermore, the S-shaped patch with a RIS structure is combined with a positive phase gradient FSS superstrate to improve the gain of the antenna over broadband frequency ranges. The S-shaped patch with RIS and FSS is achieved an impedance bandwidth of 31.8 %(4.81GHz-6.63GHz), 3dB axial ratio bandwidth of 18.9 %(4.99GHz-6.03GHz), and a peak gain is around 10 dBi at the center frequency. All the antennas in this chapter are compared in Table 3.4. The proposed can be used in various wireless applications like WLAN, and Wi-Max at 5GHz frequency region.

Table 3.4: Comparison of all antennas

Antenna	Technique	S11 bandwidth	Gain	Axial Ratio(dB)
3.2	H Shape with RIS	23.9% (5.04GHz-6.41GHz)	0-3dBi	16.2 % (4.92GHz-5.79GHz)
3.3	C Shape with RIS	24.9% (4.81GHz-6.18GHz)	0-3dBi	12.9 % (5.18GHz-5.90GHz)
3.4	E Shape with RIS	27.7% (4.82GHz-6.37GHz)	0-4dBi	12.4% (5.11GHz-5.79GHz).
3.5	S Shaped Patch with RIS and FSS Superstrate	31.80 (4.81GHz-6.63GHz)	10dBi	18.90% (4.99GHz-6.03GHz)

Chapter 4

Metasurface with L-Shaped Aperture CPW Feed

4.1 Introduction

The antennas designed in the previous chapters are volumetric structures. The superstrate has to be placed at an approximately half-wavelength distance above the antenna. But the compactness is a major requirement of wireless devices. In order to design a compact antenna, the metasurface with aperture CPW feed technique has opted. In the published literature, the metasurface and radiating elements are designed on the different substrate layers. The metasurface is designed on another substrate and it is placed on the top side of radiating element to improve the gain and bandwidth of the antenna. The design of metasurface and radiating element in single layer substrate can be realized by using metasurface on the top face of the substrate and aperture CPW feed on the bottom face of the substrate. The slot antenna and its coplanar feed line exist in the ground plane only. The design of a high gain and broadband circularly polarized antenna in the single-layer substrate is a challenging problem.

Normally superstrates are working at half-wavelength or quarter wavelength distance above the ground element. Papers are published with high gain and broadband circularly polarized antennas using RIS structure and superstrates [63-65]. Some of the papers have designed superstrates or metasurfaces working at a height less than the quarter wavelength as listed below. Tarakeshwar Shaw(2016) et al presented a single-layer metamaterial superstrate with a 3×3 ring unit cell on both sides of the dielectric sheet at a height less than λ/4 above the ground plane. The metamaterial superstrate has zero refractive index property to improve the gain of the CPW fed slot antenna[66]. JA sheersha (2019) et al proposed a metasurface at a height less than λ/4 to improve the gain of the microstrip antenna. The metasurface is designed with rectangular unit cells of non-uniform size to achieve circular polarization [67]. In the above-discussed papers [66-67], the superstrate or metasurface is placed at a height less than λ/4. In the following section, the metasurface is placed above the radiating element without any air gap.

In the published literature, the metasurface is placed above the radiating element without an air gap to improve the gain and bandwidth of linearly polarized or circularly polarized antennas. Wei Liu (2014) et al proposed an antenna consisting of an array of mushroom cells on the substrate to improve the impedance bandwidth and gain at 5GHz to 6GHz. The

mushroom cells are fed by a microstrip line through a rectangular slot in the ground plane. The slot is cut orthogonal to the microstrip line on the conductor which is present between the mushroom cells and the microstrip line [68]. Wei Liu(2015) et al proposed a metasurface with a grid-slotted patch antenna to improve the impedance bandwidth and gain from 5GHz to 6GHz. The grid slotted patches are fed by a microstrip line through a rectangular slot in the ground plane. The slot is cut orthogonal to the microstrip line on the conductor which is present between the grid slotted patches and the microstrip line [69]. Wen quan Cao (2016) et al proposed a metasurface with 4 × 4 arrays of square patches. The metasurface is excited by a microstrip line through L shaped slot in the ground plane. The designed antenna achieves an impedance bandwidth of 55.4% ranging from 4.66 to 8.23GHz and 3 dB axial ratio bandwidth of 23.6% and a gain of 7-8dBic [70]. These papers [68-70] have published a metasurface using dual substrate layers. One layer is used for the metasurface and another layer is used for radiating slot and microstrip feed line.

In the published literature, a single layer substrate is used for the metasurface and CPW fed aperture to improve the gain and bandwidth of linearly polarized antenna as listed below. The idea of designing metasurface in single layer substrate is implemented by using a patch with aperture CPW feed [71-73]. They have designed a patch on the top face of the substrate and a slot is designed on the bottom face of the substrate. The slot is connected to or coupled to the coplanar feed line in the bottom plane of the substrate. The patch is replaced with metasurface in [36-37] to design a high gain and broadband linearly polarized antenna. Broadband and high gain linearly polarized antenna in single layer substrate is designed with aperture CPW feed with a stepped slot on the bottom of the substrate and the top of the substrate is designed with a 3×3 array of two-step dipoles in a tapered manner[36]. Broadband and high gain linearly polarized antenna in a single layer substrate is designed with aperture CPW feed with stair-shaped slots on the bottom of the substrate and the top of the substrate is designed with a 3×3 array of square patches[37]. In the above-discussed papers [36-37], the linearly polarized antenna with high gain and broadband is discussed.

In this chapter, the high gain and broadband circularly polarized antenna in single layer substrate is designed using a metasurface with aperture CPW feed technique. Initially, the metasurface and its features are studied. Different types of feeding techniques for aperture CPW feed antennas are discussed. The patch antenna with aperture CPW feed technique in single layer substrate is discussed. Then the high gain and broadband antenna is designed with metasurface with aperture CPW feed technique in single layer substrate. The realization of high

gain and broadband circularly polarized antenna in single layer substrate is achieved with metasurface and CPW fed L-shaped aperture.

4.1.1 Metasurface

Metasurfaces are special types of metamaterials. They are composed of planar arrays of resonant or non-resonant subwavelength elements. Electromagnetic properties and functionalities of metasurface are defined by structure and their coupling type. Metasurface offers full control of transmitted fields and reflected fields as shown in fig. 4.1. Therefore the metasurface with proper dimension and excitation can be used to improve the gain and impedance bandwidth simultaneously.

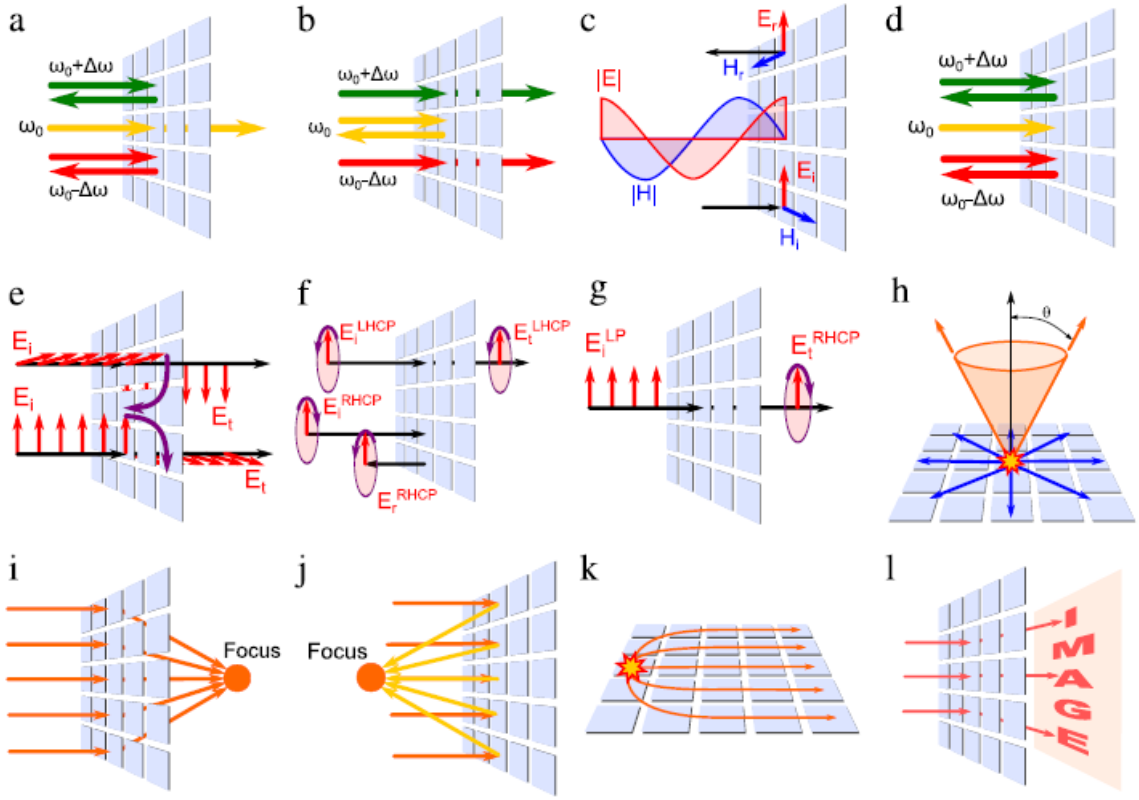

Fig.4.1. Functions of metasurface[100]

The metasurface is designed with 4×4 arrays of mushroom cells in [68] and an array of 4×4 square patches in [69]. This array of patches is excited simultaneously by aperture coupling. The gaps between the patches act like slots. The slots and radiating patches produce the dual adjacent resonant modes TM_{10} and TM_{20} close to each other. Hence, the broadband impedance bandwidth with broadside radiation is obtained. The gain of the antenna also improved with the combined radiation of all the patches in the metasurface. The changes are made in metasurface and aperture coupling to generate high gain and broadband circularly polarized antenna.

4.2 Slot Antenna and its feeding methods

The slot antenna is designed to study its radiation properties. The ground plane is designed on the bottom plane of the substrate. The slot is made in the center of the ground plane. In order to feed the slot, there are two types of coplanar feed line methods. One is an inductive type of feeding and another one is a capacitive type of feeding. In the case of inductive type of feeding, the coplanar feedline is connected across the slot. In the case of capacitive type of feeding, the coplanar feedline is coupled to the slot. The slot antenna is designed as shown in fig. 4.2. The structure is simulated using HFSS software and its 3D polar plots are drawn in fig. 4.3. It can be observed that the slot antenna radiates bi-directionally above and below the slot antenna.

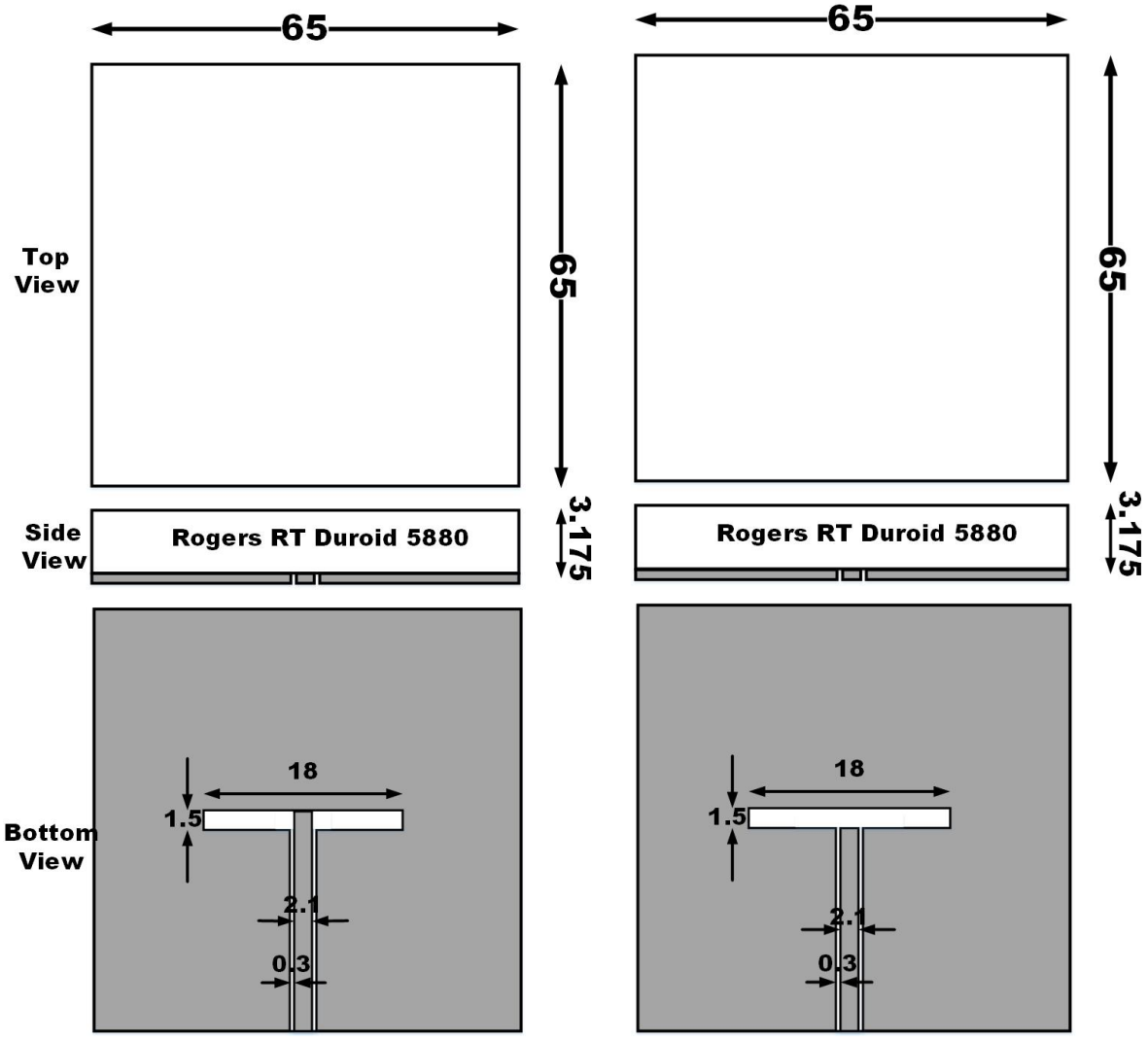

(a) (b)

Fig.4.2. Slot antenna with (a) inductive type of feeding (b) capacitive type of feeding

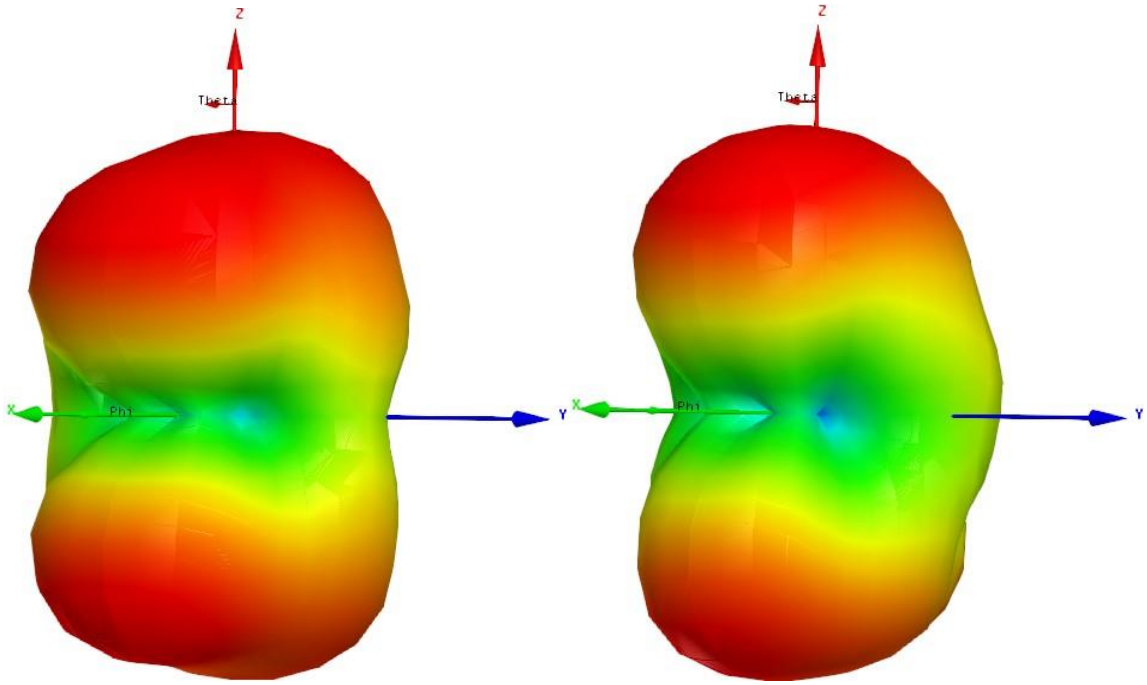

(a) (b)

Fig.4.3. 3D polar plots of slot antenna with (a) inductive type of feeding (b) capacitive type of feeding

4.3 High Gain and Broadband Antenna with H-Shaped Patch with Meta Patches

Initially, the slot antenna is designed with an inductive type of feeding as shown in fig. 4.2. To this antenna, H shaped patch is designed on the opposite side of the slot antenna to get a uni-directional antenna. The meta patches are added around the H-shaped patch to improve both gain and bandwidth simultaneously.

4.3.1 H Shaped Patch with Aperture CPW feed

The top plane of the substrate is designed with H-shaped patch and the bottom plane of the substrate is designed with a slot with an inductive type of feeding as shown in fig. 4.4. When the patch is placed on the top plane of the substrate, the patch is acting like a superstrate [71-72] and attracts radiation towards the top side of the patch. Even though the slot antenna has a bi-directional broadside radiation pattern, the H shape patch with a slot in the bottom plane is acting as a unidirectional broadside radiation pattern. The antenna radiation pattern is compared with the slot antenna alone at frequencies 4.6GHz, 5GHz, and 5.4GHz as shown in fig. 4.5. It can be observed that the H-shaped patch antenna with aperture CPW feed is converting the bidirectional pattern of the slot antenna into a unidirectional pattern with more gain in the normal direction of the antenna. The radiation pattern of slot antenna and slot antenna with H-

shaped patch are compared in fig. 4.5. The impedance bandwidth and the gain of H shaped patch antenna with aperture CPW feed are plotted in fig. 4.6. It can be observed that the antenna has an impedance bandwidth of 7% (5.21-5.59GHz) and a gain of 7.5-7.7 dBi.

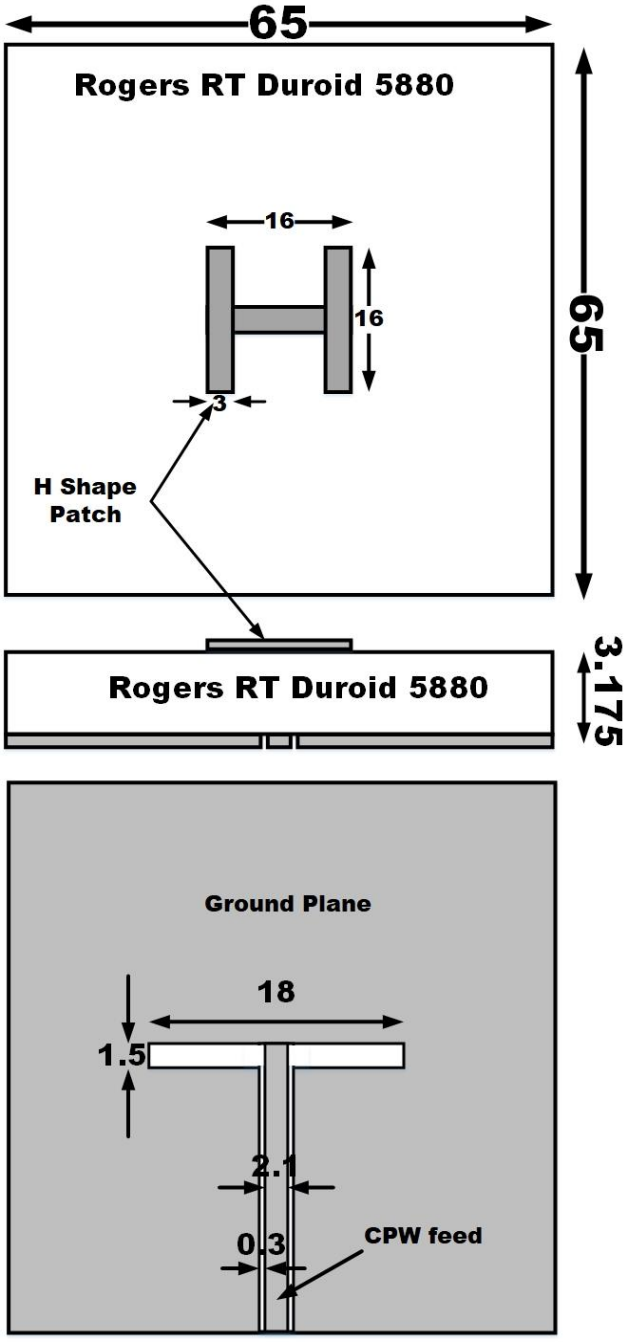

Fig.4.4. H shape patch with aperture CPW feed

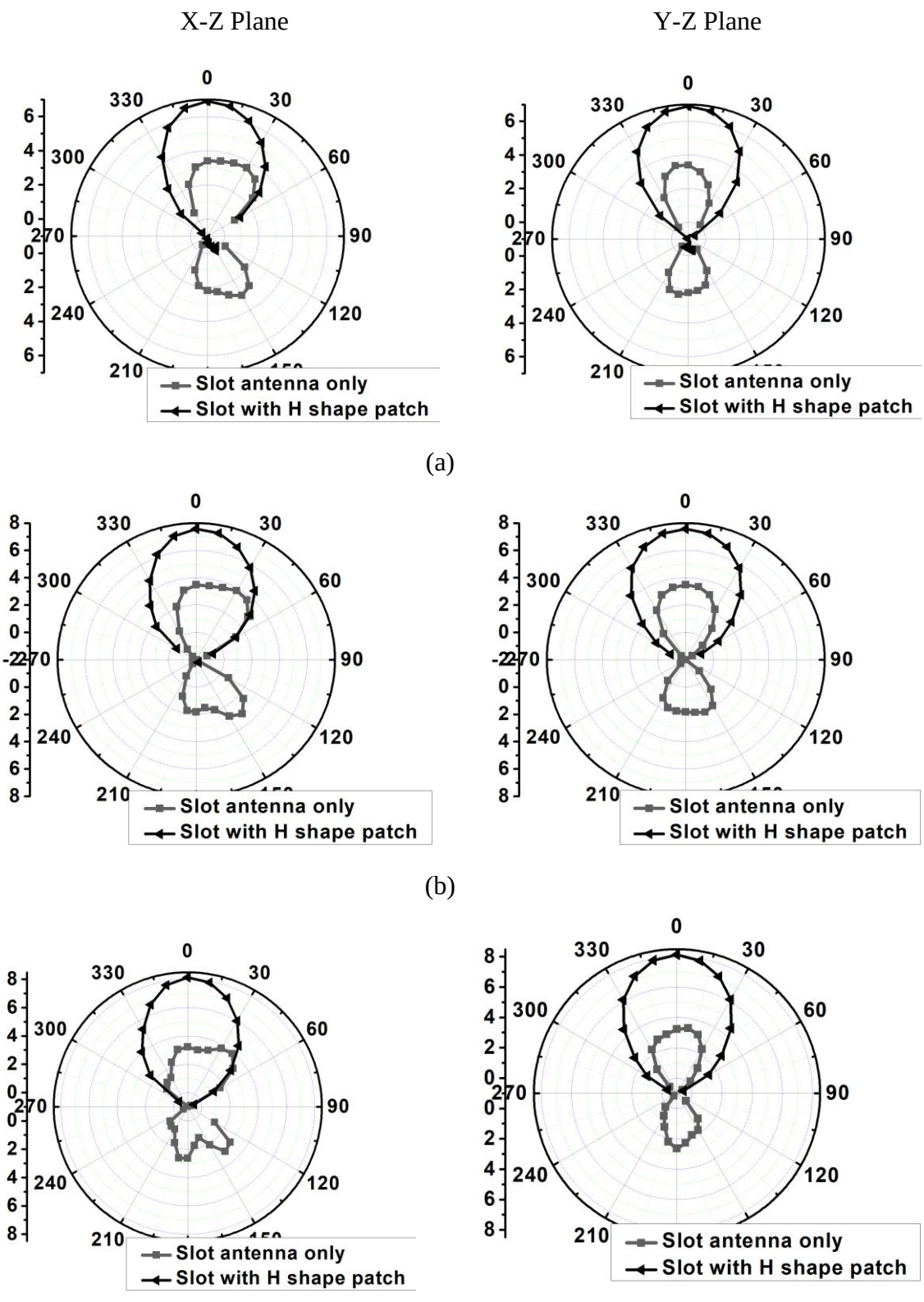

Fig.4.5. Radiation patterns of slot antenna, slot antenna with H shape patch at (a) 4.6GHz (b) 5GHz (c) 5.4GHz

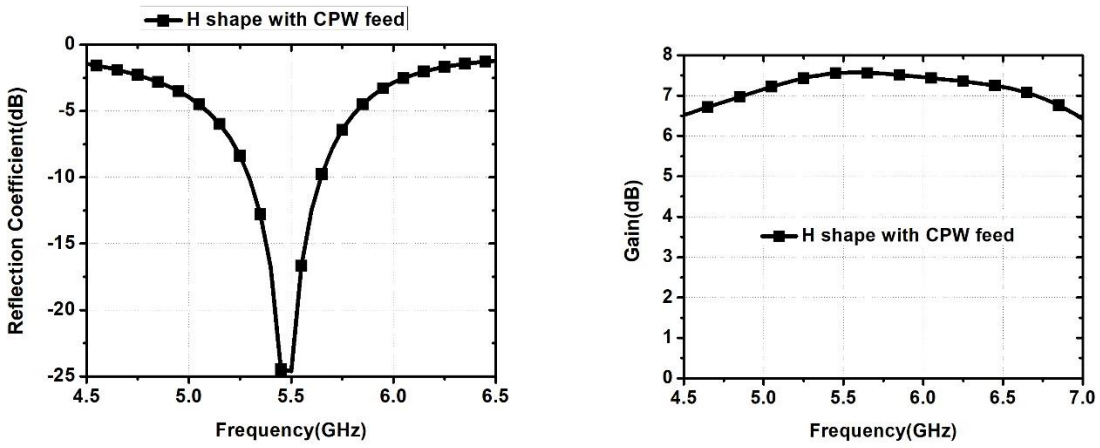

(a) (b)

Fig.4.6. Simulation results of H-shaped patch with aperture CPW feed (a) Reflection Coefficient (b) Gain

4.3.2 H Shaped Patch with Meta Patches

The H shape patch antenna with aperture CPW feed has an impedance bandwidth of 7% (5.21-5.59GHz) and the gain of the antenna is 7.5-7.7 dBi. The meta patches are added around the H-shaped patch as shown in fig. 4.7. This structure produces dual resonant modes close to each other[68-69] and hence the bandwidth of the antenna can be improved. All the patches are excited simultaneously. So the gain of the antenna is improved. The H shape patch with meta patches is simulated using HFSS 13 simulator software. When meta patches are added to H-shaped patch, the impedance bandwidth is improved to 34.8% (4.57-6.50GHz), and the gain of the antenna is improved to 10-11dB as shown in fig. 4.8.

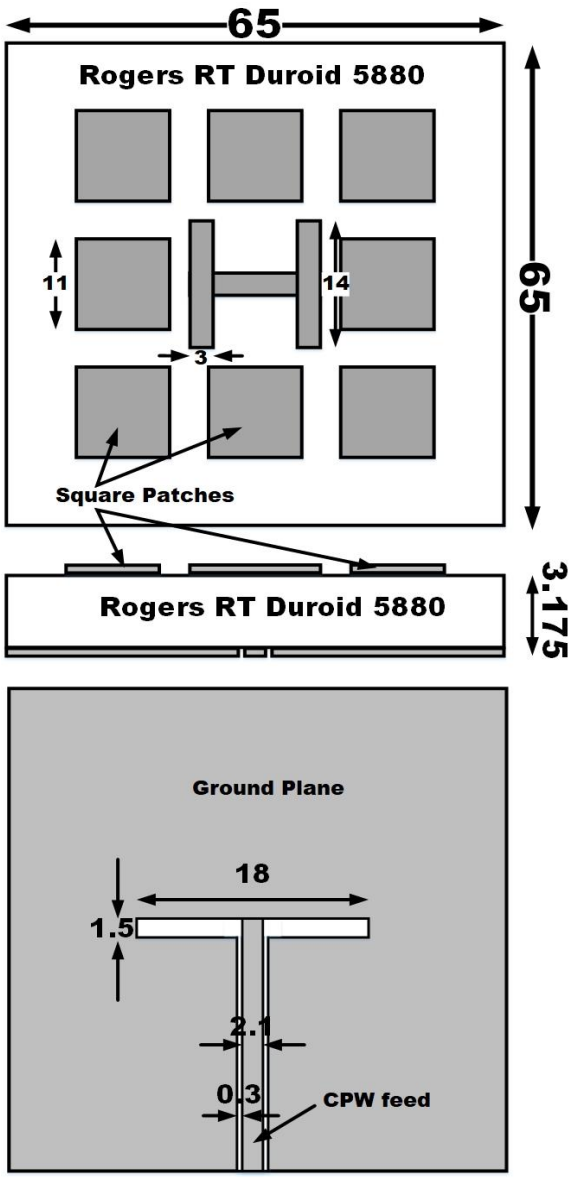

Fig.4.7. H Shaped patch with meta patches

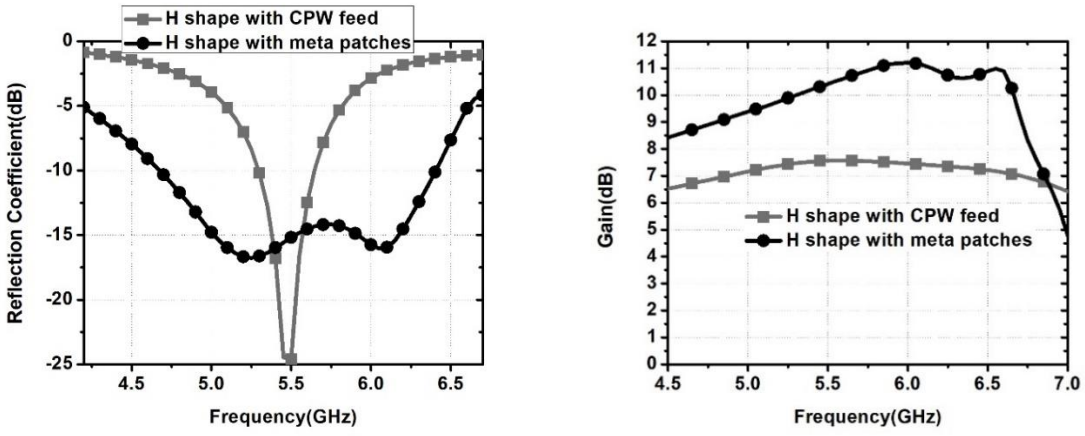

Fig.4.8. Comparison of simulation results of H shaped patch, H shape patch with meta patches (a) Reflection Coefficient (b) Gain.

4.4 Metasurface with L-Shaped Aperture CPW Feed for High Gain and Broadband Circularly Polarized Antenna

The H-shaped patch with meta patches has improved impedance bandwidth and gain of an antenna. But no circular polarization is achieved. In order to attain circular polarization, the metasurface with L shaped aperture CPW feed is proposed.

4.4.1 Antenna Configuration

The structure of the proposed antenna is displayed in fig. 4.9. The antenna is designed on Rogers RT/Duroid 5880 substrate (ε_r=2.2, tanδ=0.0009) with dimensions of W*W*H. The antenna is designed by printing a 3×3 array of circle patches as a metasurface on the top face of the substrate. The metasurface is fed by CPW fed stub-loaded L-shaped aperture CPW on the bottom face of the substrate. The radius of central patch R_2 is smaller than the radius of outer patch R_1. The optimized parameter values are shown in Table 4.1.A detailed analysis is given in the following section.

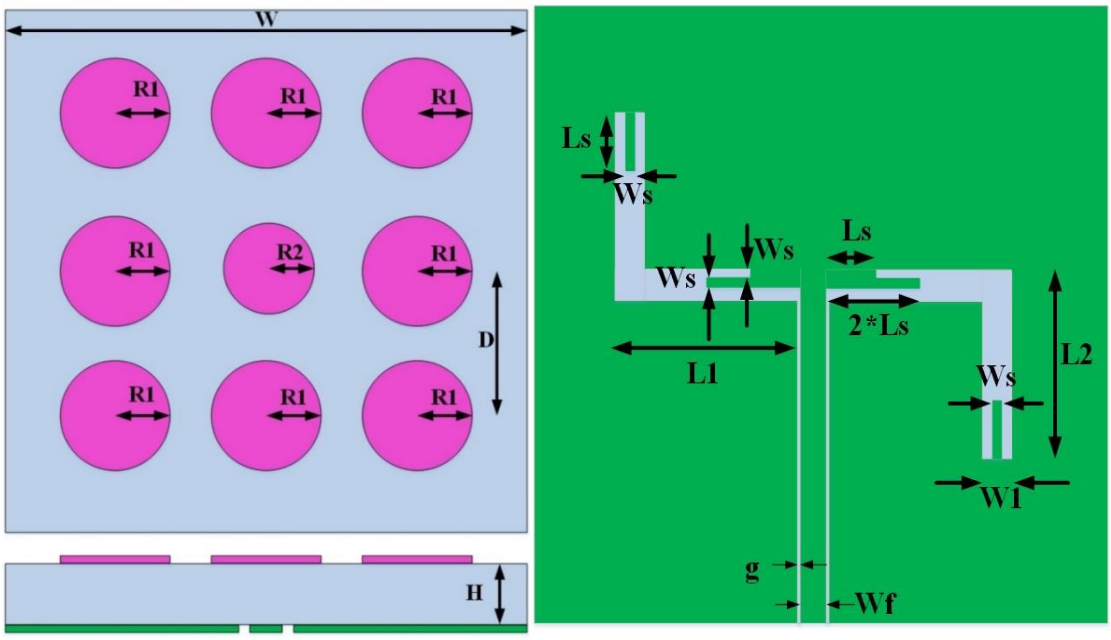

(a) (b)

Fig.4.9. Metasurface with L-shaped aperture (a) top-plane view and side view (b) bottom plane view

4.4.2 Design process of the antenna

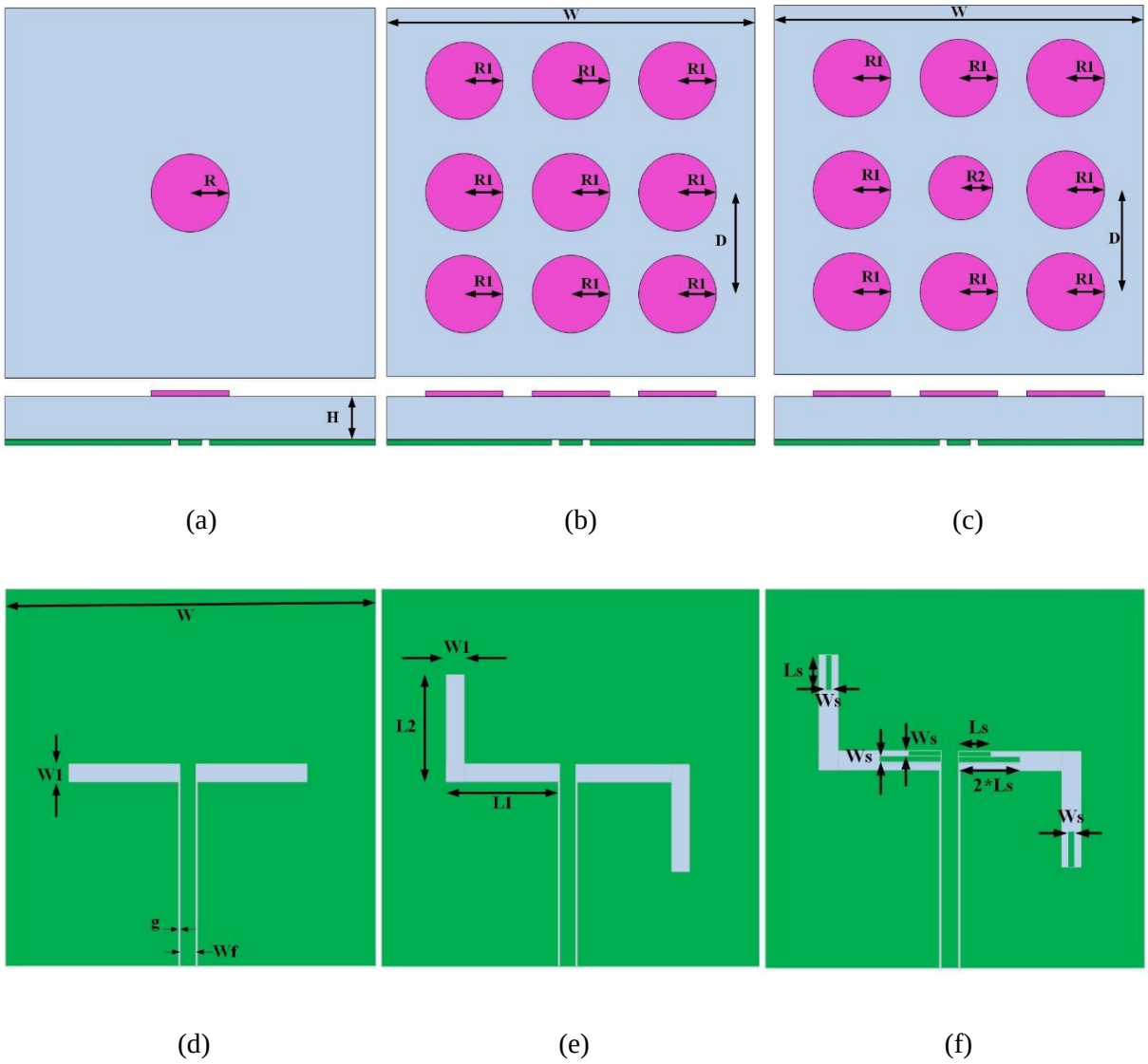

Fig.4.10. Design steps of proposed antenna (a) Ant-1 top plane view (b) Ant-2, Ant-3, Ant-4 top plane view (c) Proposed Antenna top plane view (d) Ant-1, Ant-2 bottom plane view (e) Ant-3 bottom plane view (f) Ant-4, Proposed Antenna bottom plane view

Table 4.1: Optimized Parameter Values

Parameter	Value(mm)	Parameter	Value(mm)
W	58	W_1	1.5
R_1	7.75	L_s	4
R_2	6.75	W_s	0.5
D	16.45	g	0.3
L_1	14.15	W_f	2.1
L_2	14.5	H	3.175

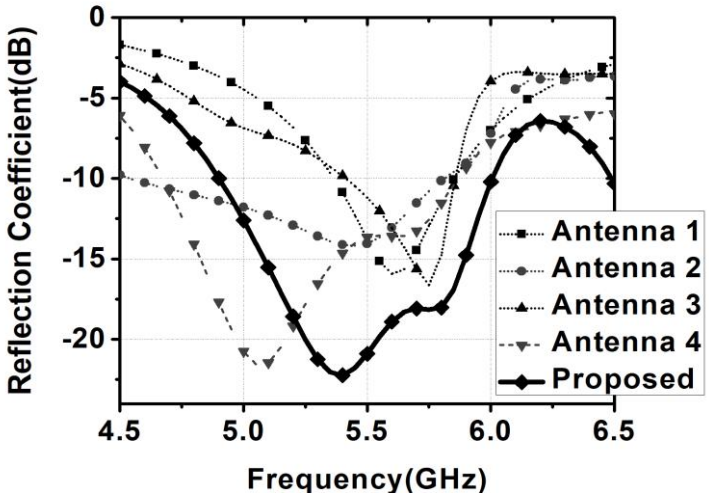

Fig.4.11. Reflection coefficient of Ant-1, Ant-2, Ant-3, Ant-4 and proposed Antenna vs frequency

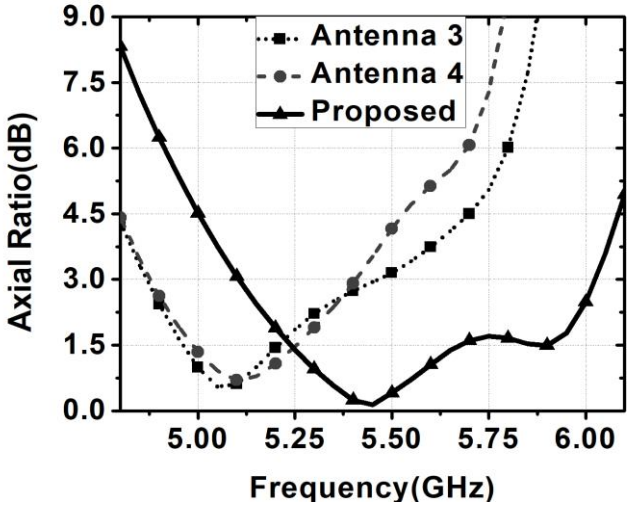

Fig.4.12. Axial ratio of Ant-3, Ant-4 and proposed Antenna vs frequency

The design steps of the proposed antenna are displayed in fig. 4.10. The reflection coefficients at each stage are displayed in fig. 4.11 and the respective axial ratio bandwidths are displayed in fig. 4.12.

Antenna 1 is designed with a circular-shaped patch on the top face of the substrate and this patch is fed by CPW fed uniform slot on the bottom face of the substrate. The circular-shaped patch is coupled to the slot. The slot is placed in the middle of the ground plane and fed by a coplanar feed line [71] as displayed in fig. 4.10. The CPW fed slot antenna in the ground plane is normally a dual dipole antenna that has a bi-directional broadside radiation pattern. When the patch is placed on the other side of the slot, the radiation pattern is converted into a unidirectional broadside radiation pattern. The impedance bandwidth and gain are very less for such types of antennas as shown in fig. 4.11.

High gain and broadband using metasurface radiator: Antenna 2 is designed by adding meta patches around the central patch. The circle-shaped metasurface is excited with CPW fed uniform slot as displayed in fig. 4.10. It is proved in [36],[37] that the Metasurface with CPW fed uniform aperture improves the impedance bandwidth and gain of the antenna. Uniform spacing between the patches contributes to exciting the dual adjacent resonant modes simultaneously [68],[69] and hence the impedance bandwidth is improved. It is observed from the fig. 4.11 that impedance bandwidth is enhanced to 25.2%. The gain of the antenna is around 10dB. No circular polarization is observed in this type of configuration.

Circular polarization using L-shaped slot: In antenna 3, the slot is proposed in the form of an L-shape as displayed in fig. 4.10. It is investigated that the L-shaped slot generates orthogonal fields with phase quadrature. The 3dB axial ratio bandwidth of 11.7% is noticed in this type of configuration as displayed in fig. 4.12. An impedance bandwidth of 8% is obtained as displayed in fig. 4.11. It is observed that the impedance bandwidth of the antenna is less when compared with the bandwidth of antenna 2. Antenna 3 has the same gain i.e. approximately 10dBic because of the metasurface on the top plane.

Impedance matching with stubs: It is investigated in [71], [37] that the impedance bandwidth can be improved either by adding soldering or stubs in the slot. In antenna 4, the stubs are added in the slot as shown in fig. 4.10. The impedance bandwidth is improved to 22.6% as shown in fig. 4.11. And the axial ratio bandwidth is maintained at 10.5% as shown in fig. 4.12. The antenna gain is around 10dBic.

Broadband circular polarization: In the proposed antenna, the central patch size is reduced. When the size of the central patch is reduced, the resonant frequency of the central patch shifts to higher frequencies. The surrounding patches maintain the impedance matching at lower frequencies only. A combination of all patches improves the impedance matching below -18dB over a broad frequency range. The impedance bandwidth is slightly shifted to higher frequencies with 20.18% bandwidth as shown in fig. 4.11. When the size of the central patch is reduced, the resonant frequency of the central patch shifts to higher frequencies, and the respective orthogonal fields are also generated at higher frequencies. The surrounding patches maintain orthogonal fields at lower frequencies only. The combination of all patches generates the orthogonal fields over a broad frequency range. Hence the 3dB axial ratio bandwidth shows a massive improvement of 16.21% as shown in fig. 4.12. The gain of the antenna is 10.43dBic. The simulation results for all the antennas are compared in Table 4.2.

Table 4.2: Comparison of simulation results

S.No	Antenna	Impedance bandwidth (%)	Axial Ratio (%)	Gain
1	Antenna 1	8.1	nil	7.5 dBi
2	Antenna 2	25.2	nil	10.68 dBi
3	Antenna 3	8	11.7	10.52 dBic
4	Antenna 4	22.6	10.6	10.14 dBic
5	Proposed Antenna	20.18	16.21	10.43 dBic

4.4.3 Parametric study by changing L_s

The parametric study is done by changing the stub lengths. It is observed that the antenna without stubs is not properly matched which causes a reduction in axial ratio bandwidth. When the stubs are inserted, the impedance matching is improved and the 3dB axial ratio bandwidth is also improved as shown in fig. 4.13 and fig. 4.14. The parametric study is done by changing the stub lengths and the best suitable value is chosen as L_s=4mm.

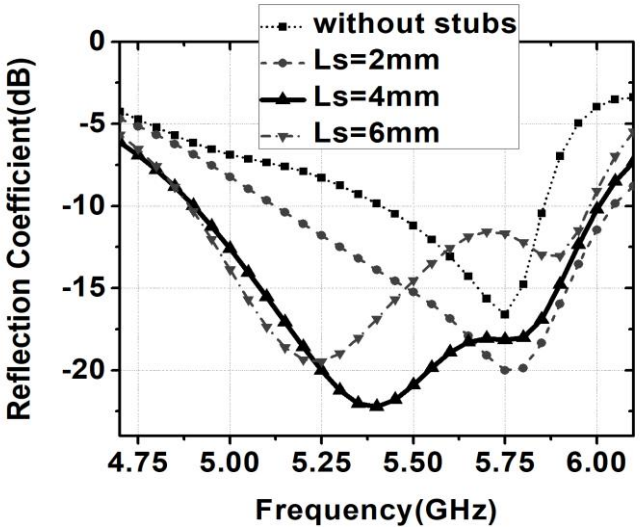

Fig.4.13. Reflection coefficient against L_s

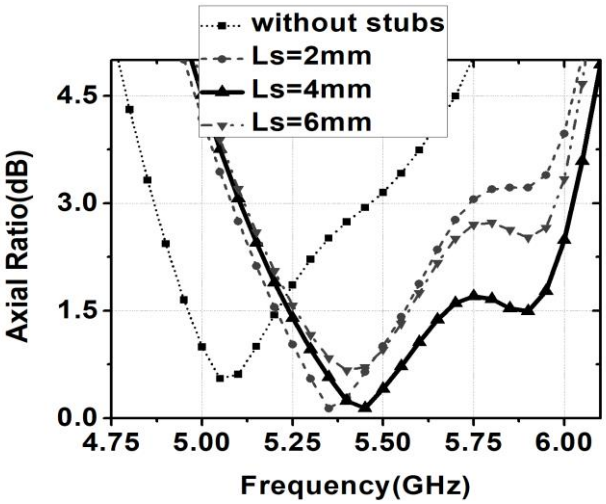

Fig.4.14. Axial ratio against L_s

4.4.4 Parametric study by changing R_2

The parametric study is done by changing the radius R_2 of the central patch. The simulation results of the reflection coefficient and axial ratio for different values of R_2 are displayed in fig. 4.15 and fig. 4.16. It can be observed that the impedance bandwidth shifted to higher frequencies as the radius of the central patch is reduced as displayed in fig. 4.15.

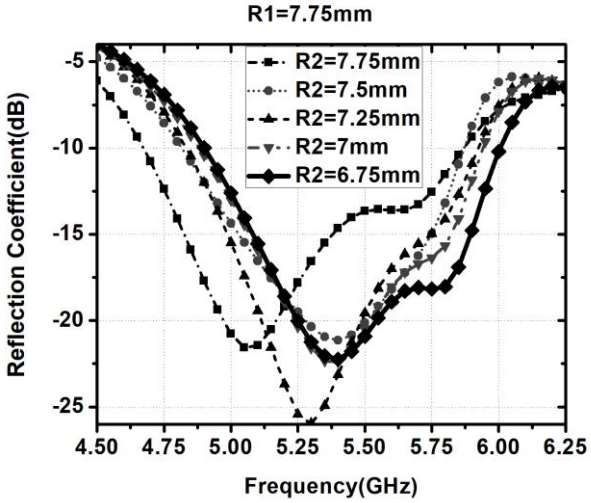

Fig.4.15. Reflection Coefficient against R_2

When all the patches on the metasurface are of the same size (R_1=R_2=7.75mm), the orthogonal fields are generated by L-shaped slots at lower frequencies. When the size of the central patch is decreased, the resonant frequency of the central patch is shifted to higher frequencies and the respective orthogonal fields are also generated at higher frequencies. The surrounding patches maintain orthogonal fields at lower frequencies only. A combination of the central patch and surrounding patches achieves orthogonal fields over a broad frequency range

as shown in fig. 4.16. The best suitable value is chosen as R_2=6.75mm to obtain broadband 3dB axial ratio bandwidth.

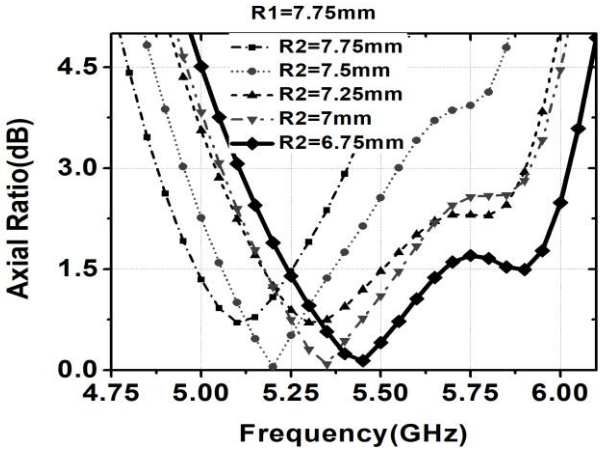

Fig.4.16. Axial ratio against R_2

The simulation results for orthogonal fields are shown in fig. 4.17 to justify the 3dB axial ratio bandwidth. It can be observed from fig. 4.17 that the magnitude of orthogonal fields is almost the same (less than 3dB magnitude difference). A 90^0 phase difference is maintained at a broadband of frequencies (5.1GHz to 6GHz) for R_2=6.75mm. Hence, the required conditions to meet the wideband 3dB axial ratio bandwidth is observed for R_2=6.75mm.

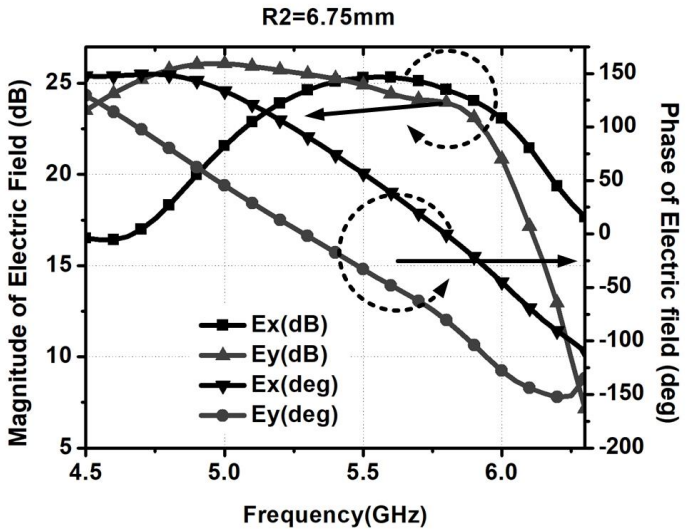

Fig.4.17. Electric field magnitude and phase for R_2=6.75mm

In the proposed antenna, the L-shaped slot generates orthogonal fields in phase quadrature. In the orthogonal fields, the E_x component lags behind the E_y component by 90^0. Hence, the right-hand circular polarization (RHCP) is generated. The gain of co-polarization (RHCP) and cross-polarization (LHCP) is plotted in fig. 4.18. It is observed that the RHCP gain

is high over the resonant frequency range whereas the LHCP gain is low over the resonant frequency range.

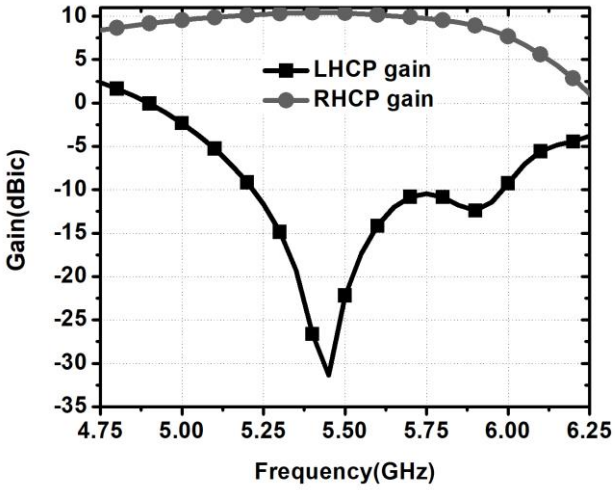

Fig.4.18. LHCP gain and RHCP gain of the proposed antenna

The comparison is done for the simulation results of the proposed antenna with published literature as displayed in Table.4.3. It can be noticed that in the published literature, two substrate layers are used for high gain and wideband circular polarization. A few works are published using the single-layered planar antenna to design high gain and wide bandwidth for

Table 4.3: Comparison of proposed antenna with the published literature.

Ref	**Substrates**	**Size(λ^3)**	**Frequency range(GHz)**	**IBW (%)**	**Gain**	**AR (%)**
[31]	Dual Layer	0.34 λ×0.34 λ×0.05λ	3.1-10.6	109	5.7 dBi	-
[32]	Dual Layer	1.78λ× 1.78λ×0.07λ	4.8-6.2	31	14 dBi	-
[34]	Dual Layer	0.58λ×0.58λ×0.056λ	4.70–7.48	45.6	7-7.6	23.4
[35]	Dual Layer	3 λ× 3 λ× 0.1 λ	10.8-12.4	13.7	6.52 dBic	6
[38]	Dual Layer	7.69 λ×7.69 λ×0.06λ	2.2-2.4	14	2.5-5.7	15.3
[39]	Dual Layer	0.72λ×0.74λ×0.088λ	4.52 - 7.42	48.6	6.6	20.4
[40]	Dual layer	0.822λ×1.18λ×0.06λ	3.22-4.63	35.6	7-7.5 dBic	28.6
[54]	Dual Layer	0.58λ×0.58λ×0.1λ	4.64–7.3	44.5	7.2 dBic	27.5
[68]	Dual Layer	1.10λ×1.10λ×0.06λ	4.85-6.28	25	9.9 dBi	-
[69]	Dual Layer	1.10λ×1.10λ×0.06λ	4.60–6.17	29	9.8 dBi	-
[70]	Dual Layer	0.93λ×0.93λ×0.054λ	4.66-8.23	55.4	7.3-8.1	23.6
[64]	Multilayer + Air gap	λ×λ×0.5λ	4.93-5.89	17.72	12.48	2.4
[65]	Multilayer + Air gap	λ×λ×0.5λ	4.81-6.63	31.8	10	18.9
[36]	Single Layer	λ×λ×0.053λ	9.07-11.36	22.1	7.5 dBi	-
[37]	Single Layer	1.28λ×1.28 λ×0.09λ	4.81 -9.69	67.3	9.18 dBi	-
4.4	**Single Layer**	**λ×λ×0.052λ**	**4.9-6**	**20.18**	**10.43 dBic**	**16.21**

linear polarization. In this thesis, a high gain and broadband circularly polarized antenna using a single-layered planar substrate is designed.

4.4.5 Fabrication and measured results

The fabrication of the prototype is made using an LPKF ProtoMat S100 PCB milling machine. The metasurface is milled on the top plane of Rogers RT/Duroid 5880 substrate. CPW -fed L-shaped aperture is milled on the bottom plane of the substrate. A straight 4-hole flange SMA connector is used for feeding the antenna. The co-planar feedline is soldered to the inner conductor of the SMA connector as shown in fig. 4.19. The ground plane is soldered to the outer conductor of the SMA connector as shown in fig. 4.19. The measurement of the reflection coefficient is obtained by a vector network analyzer and it is plotted in the frequencies of 4.5GHz to 6.5GHz as displayed in fig. 4.20a. The measurement of the gain of the antenna is calculated in the anechoic chamber. The standard horn antenna is connected as a transmitting antenna in the chamber. The standard antenna gain values are already noted. The proposed antenna prototype is connected as a receiving antenna. Software is used for rotating the prototype antenna itself to measure gain at each angle. The simulated and measured gain values are then compared as shown in fig. 4.20b. The axial ratio values are calculated from these measured data and it is plotted in fig. 4.20c. The radiation pattern is plotted in the X-Z plane and Y-Z plane as shown in fig. 4.21. The measurement results follow the simulation results closely. There is a slight difference due to fabrication errors.

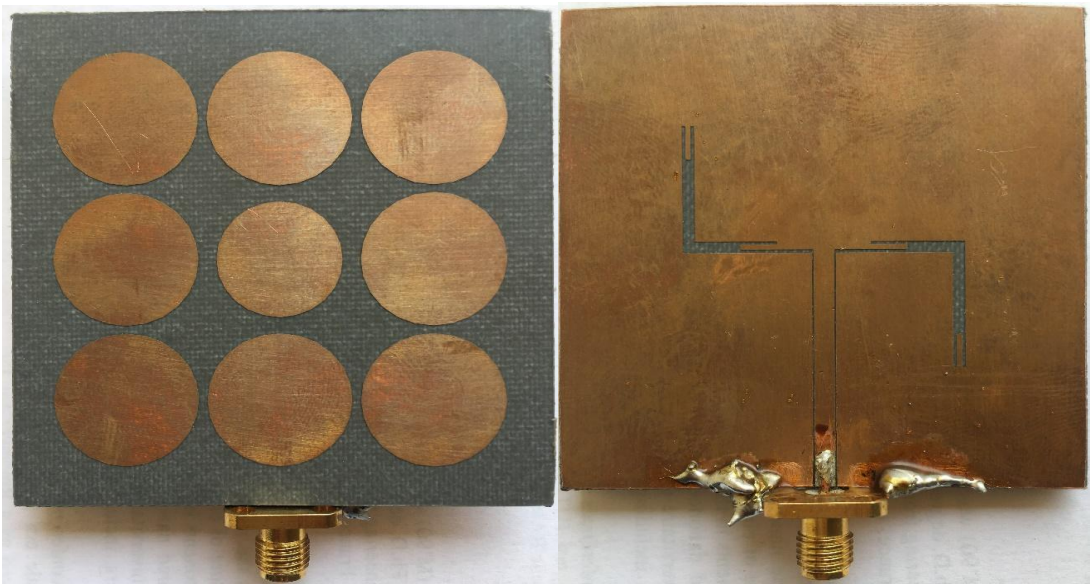

Fig.4.19. Fabricated prototype of proposed antenna (a) top plane view (b) bottom plane view

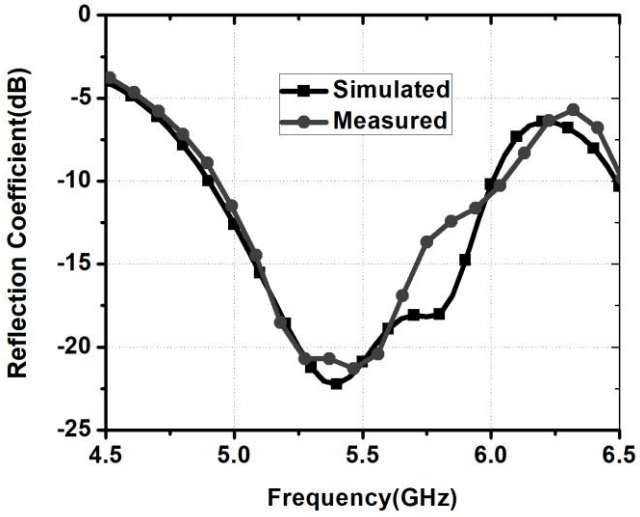

(a)

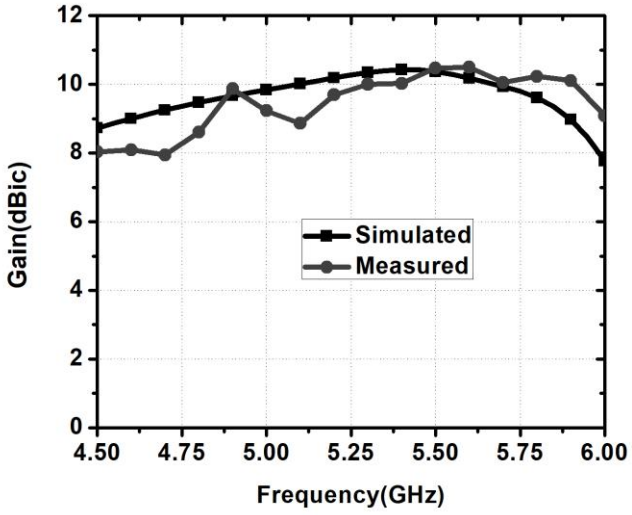

(b)

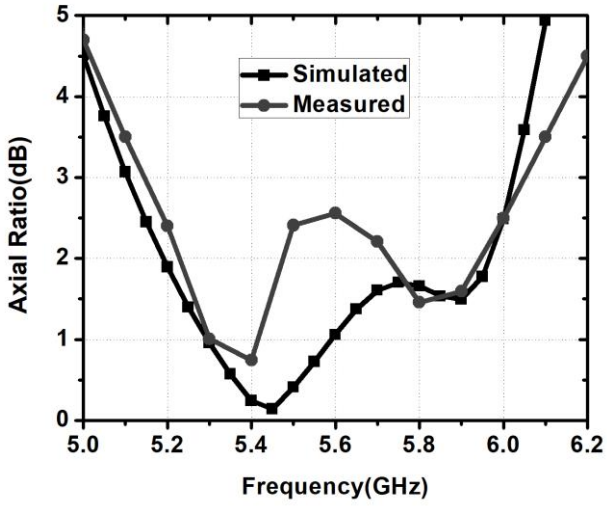

(c)

Fig.4.20. Comparison of simulated and measured results for the proposed antenna (a) Reflection Coefficient (b) Gain (c) Axial Ratio

X-Z plane Y-Z plane

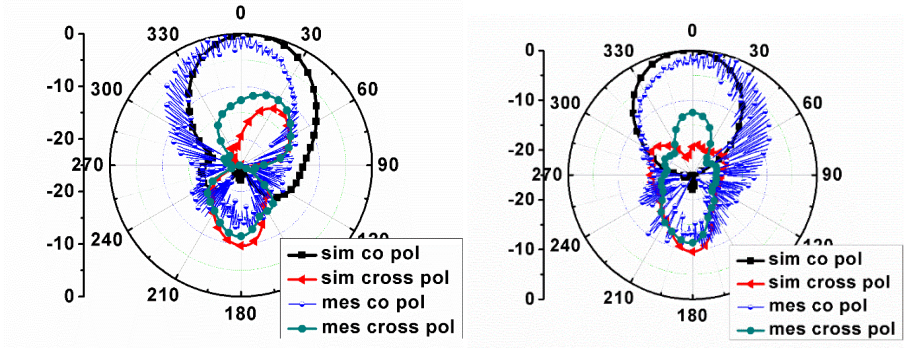

(a)

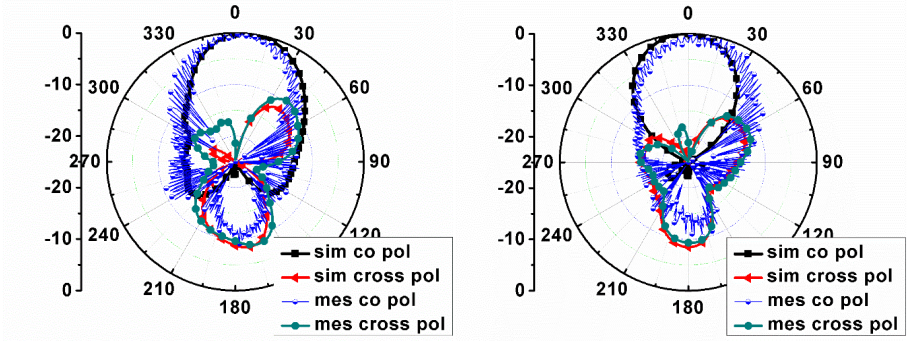

(b)

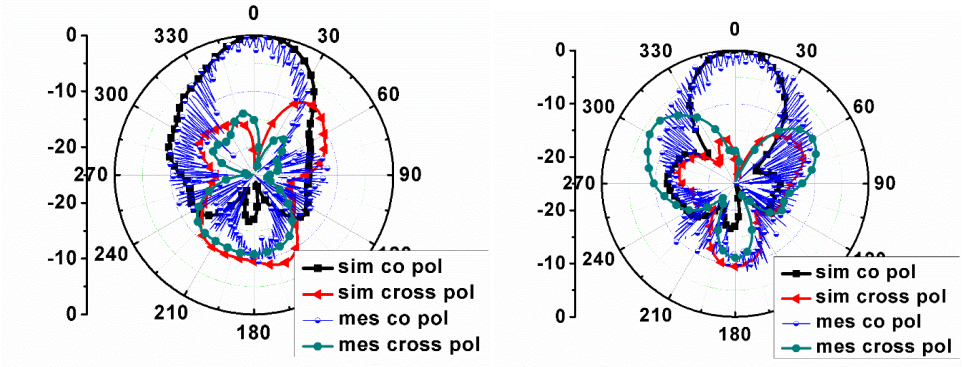

(c)

Fig.4.21. Radiation patterns of proposed antenna at (a) 5.2GHz (b) 5.5GHz (c) 5.8GHz

4.5 Summary

A slot antenna with different types of feeding techniques are discussed. Furthermore, the H-shaped patch is printed on another side of the slot antenna to convert a bidirectional pattern into a unidirectional pattern. The gain and impedance bandwidth are improved simultaneously by adding meta patches around the H-shaped patch.

Alternately, an array of 3x3 circle patches are used as a metasurface to increase the impedance bandwidth and gain of the antenna. Moreover, an L-shaped aperture CPW with stubs is designed to achieve circular polarization. Furthermore, the radius of the central patch is reduced to enhance the 3dB axial ratio bandwidth. A combination of all such aspects results in impedance bandwidth of 20.18%, and axial ratio bandwidth of 16.21%. Furthermore, the antenna is achieved a high gain of 10.43dBic which is remarkably very high in single-layered planar antennas at 5GHz used for WLAN and Wi-Max applications. All the antennas in this chapter are presented in Table 4.4.

Table 4.4: Comparison of all results

Antenna	**Technique**	**S11 bandwidth**	**Gain**	**Axial Ratio(dB)**
4.3	H shape with CPW fed aperture antenna with meta patches	34.8% (4.57-6.50GHz)	10-11dB	-
4.4	CPW fed L shaped aperture coupled metasurface antenna	20.18 (4.9-6GHz)	10.43 dBic	16.21

Chapter 5

Metasurface with Uniform Aperture CPW Feed

5.1 Introduction

In the previous chapter, the high gain and broadband circularly polarized antennas in single layer substrate are designed using metasurface with CPW fed L shaped aperture. Instead of using L shaped slot in the ground plane, the changes can be made in the metasurface to design a high gain and broadband circularly polarized antenna. In the published literature, the metasurface is designed with truncated corner square patches or 45^o rotated rectangular loops where the uniform slot is used in the ground plane [34], [74] and [75]. These antennas have used an array of conventional patches like truncated corner square patches and 45^o rotated rectangular loops in the metasurface to get circular polarization. But they used another substrate layer for the metasurface. The design of a high gain and broadband circularly polarized antenna in a single layer substrate using conventional patches in the metasurface is a challenging problem.

A high gain and broadband circularly polarized antennas are implemented by using RIS structure as a ground plane and superstrate at a height half wavelength above the antenna [63-65]. The metasurface or superstrates are proposed at a height less than λ/4 to design high gain and broadband linearly polarized antennas[30, 31, 66] or circularly polarized antenna [67].

Some of the papers have designed metasurface without a gap to radiating source in [68-69] to design high gain and broadband linearly polarized antenna. They have designed metasurface with 4x4 arrays of square patches or mushroom cells. The slot is used to excite the metasurface. The slot is fed by a microstrip line in the ground plane. The metasurface is designed with an array of truncated corner square patches in [74], and the metasurface is designed with 45^o rotated rectangular loops in [75] to design high gain and broadband circularly polarized antennas. But they have used dual substrate layers.

The idea of designing in single layer substrate is realized by using a patch with aperture CPW feed [71]-[73]. Where a patch is placed on the top face of the substrate and a slot is made in the bottom face. The slot is fed by a coplanar feed line. The patch is replaced with a metasurface containing a 3x3 array of patches to design a high gain and broadband linearly polarized antenna [36]-[37].

In this chapter, the high gain and broadband circularly polarized antennas in single layer substrate are designed with conventional patches like truncated corner square patches and 45^o rotated slot-loaded square patches. Initially, a metasurface is designed with an array of truncated corner square patches on one side of the substrate and this metasurface is excited by uniform aperture CPW feed on the other side of the substrate. Then the central patch size is increased and truncation in surrounding patches reduced to achieve a high gain and broadband circular polarization. Later the metasurface is designed with an array of 45^o rotated slot-loaded square patches and this metasurface is excited by uniform aperture CPW feed on the other side of the substrate. Then the middle patch sizes are increased and slot sizes in the middle patches are increased to achieve a high gain and broadband circular polarization.

5.2. Truncated Corner Square Patch Metasurface Antenna with Uniform Aperture CPW feed

5.2.1 Antenna Design

The structure of the proposed antenna is depicted in fig. 5.1. The antenna's modelling is done on a Rogers RT/Duroid 5880 substrate with a dimension of W×W×H. The antenna is made up of a 3×3 array of truncated corner square patches on the substrate's top face. The central patch's size is selected as L with the amount of truncation p on two diagonal corners. The surrounding patch's size is selected as M with the amount of truncation q on two diagonal corners. On the opposite side of the substrate, a stub-loaded CPW-fed uniform aperture is designed. The slot width of W_1 is extended on both sides with a length of L_1. The stubs of dimension L_s×W_s are arranged in the slot. The coplanar feed of width W_f is connected across the slot. The gap between the coplanar feed and ground plane is 'g'. The following section has a detailed analysis.

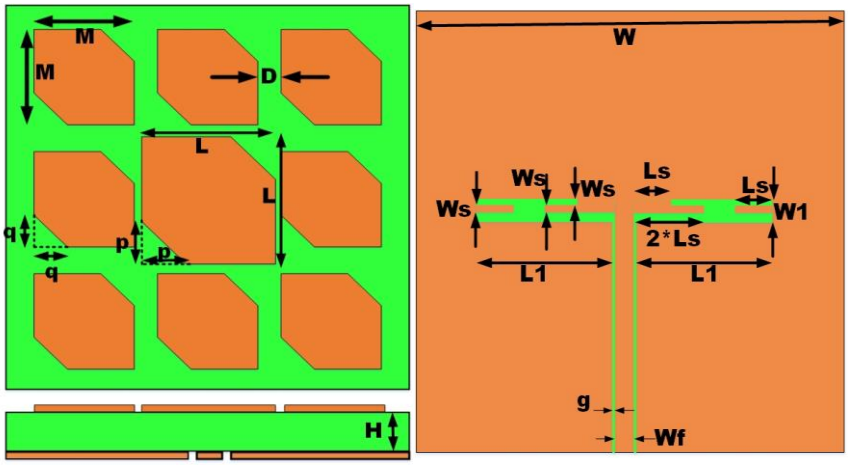

a) b)

Fig. 5.1. Geometry of proposed antenna (a) top view and side view (b) bottom view

5.2.2 Design steps

The design steps of each antenna are depicted in fig. 5.2. The respective impedance bandwidth (S_{11}), gain and axial ratio (AR) are shown in fig. 5.3. The dimensions of all the patches are the same in antenna 1 and antenna 2, whereas the central patch and surrounding patch dimensions are different in antenna 3 and the proposed antenna. Optimized parameter values are displayed in Table.5.1.

The metasurface is designed with patches on one side and CPW fed aperture on another side of the substrate in [36], [37] to design wideband and high gain linearly polarized antennas. Antenna 1 is composed of square patches with a truncated corner metasurface antenna on the top plane of the substrate and the metasurface antenna is driven by aperture CPW feed on the opposite side. The impedance bandwidth has multiple resonant modes apart from each other and the 3dB axial ratio bandwidth is nil for antenna 1. In antenna 2, the stubs are inserted across the slot [37] as displayed in fig. 5.2. Here, the stubs are helpful to get resonant modes close to each other. When all the truncated corner square patches are the same size for antenna 2, the impedance bandwidth has two resonant modes close to each other as shown in fig. 5.3.

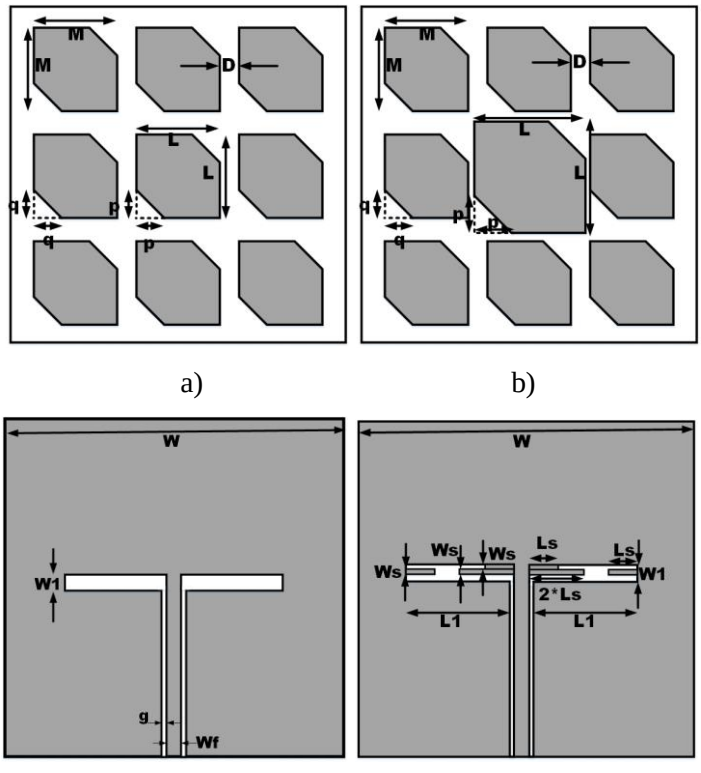

Fig. 5.2. Evolutions of proposed antenna (a) Top plane view of antenna 1, antenna 2 (b) Top plane view of antenna 3, proposed (c) Bottom plane view of antenna 1 (d) Bottom plane view of antenna 2, antenna 3, proposed.

Table 5.1. Optimized parameter values

Parameter	Value(mm)	Parameter	Value(mm)
W	58	L	16.25
W_1	1.5	M	13.75
L_1	14	D	2
L_s	3	p	5.3
W_s	0.5	q	4.85
W_f	2.1	H	3.175
g	0.3		

In antenna 3, the central patch dimension is chosen larger than the surrounding patches. When the central patch's size is increased for antenna 3, the first and second resonance frequencies overlap with each other. Hence, the impedance bandwidth and 3dB axial ratio bandwidth are improved as displayed in fig. 5.3. In the proposed antenna, the same truncation is maintained in a central patch and the truncation in surrounding patches is reduced. The upper resonant frequencies and lower resonant frequencies overlap with each other to further enhance the

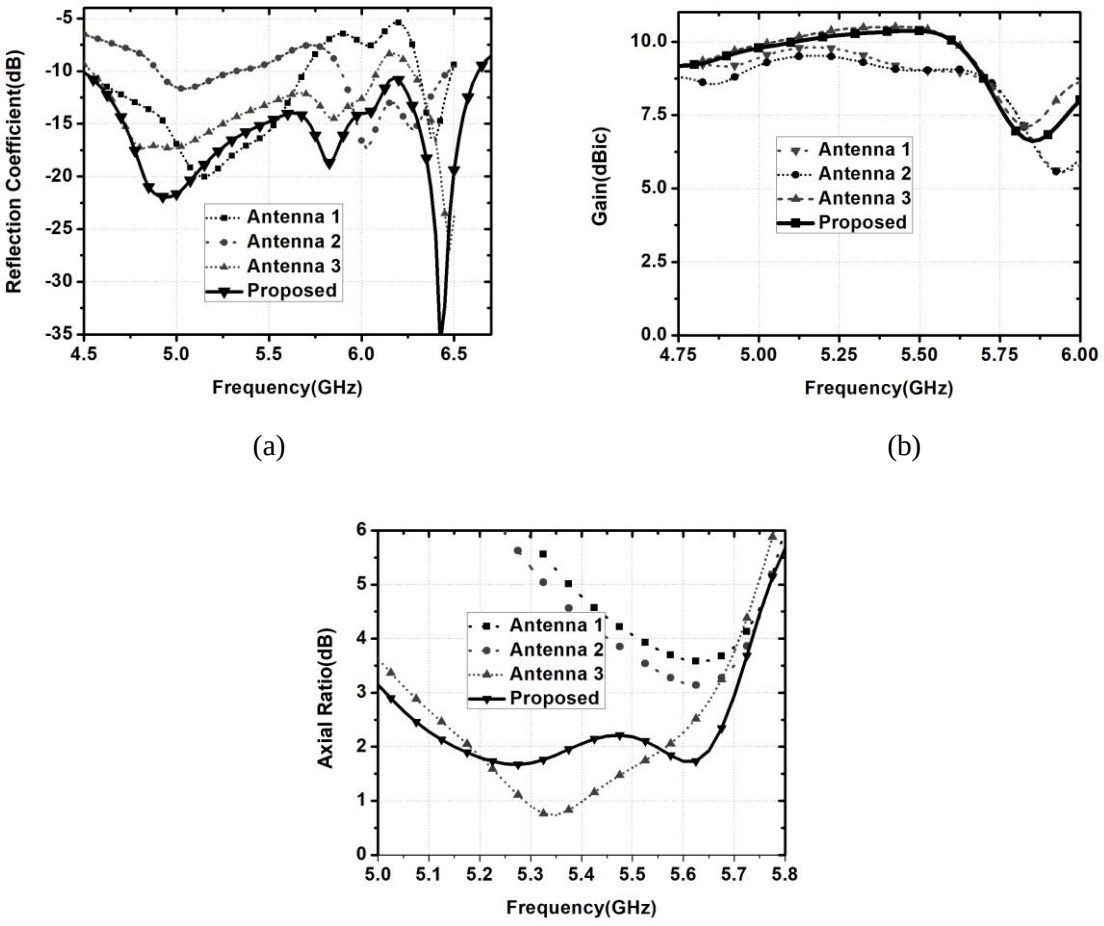

(a) (b)

(c)

Fig.5.3. Simulated results of four designs (a) S_{11} (b) Gain (c) AR.

impedance bandwidth and 3dB axial ratio as shown in fig. 5.3. All these antennas are maintaining a gain at around 10dBi because of the metasurface. The variations are explained in detail in the following section.

5.2.3 Consider the values of 'p' and 'q' as 5.3mm and varying the dimension 'L'

In antenna 2, the size of all truncated corner square patches are the same i.e., 'L' and 'M' are taken as 13.75mm. When the size of central patch 'L' is increased, the resonant frequency of the central patch is shifted to lower frequencies. The resonant frequency of surrounding patches is maintained in the same frequency range as there is no change in the dimensions. Further, the resonance frequency range of the central patch and surrounding patches are overlapping with each other for 'L'=16.25mm and impedance bandwidth is enhanced as shown in fig.5.4 a. The axial ratio (AR) of the antenna gradually increases as the 'L' value increases, finally, the broadband axial ratio bandwidth is obtained at 'L' considered as 16.25mm as shown in fig. 5.4b.

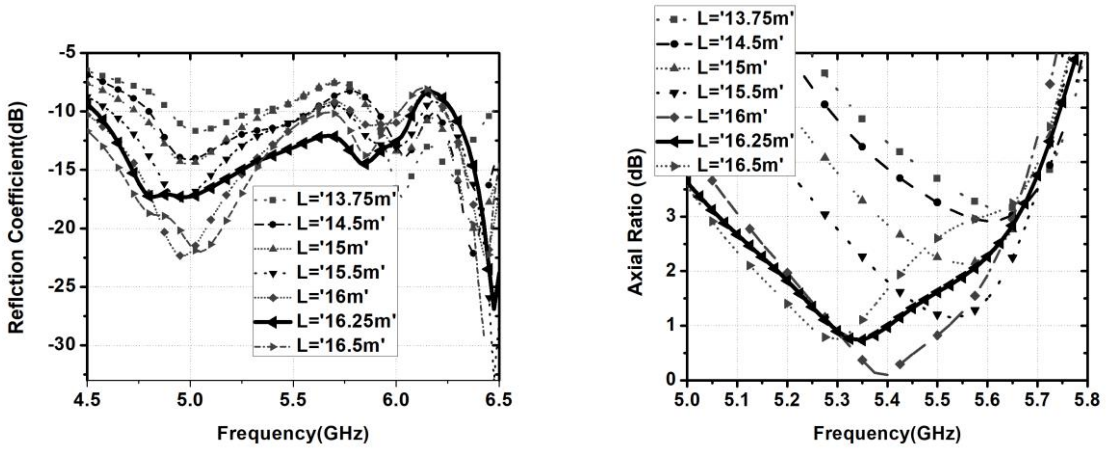

(a) (b)

Fig. 5.4. Simulated results with respect to 'L' (a) S_{11} (b) AR

5.2.4 Considering the dimension 'L' as 16.25mm, 'M' as 13.75mm, 'p' as 5.3mm, and varying the dimension 'q'

In antenna 3, the size of the central patch is chosen as 16.25mm and the truncation in the central patch is maintained at 5.3mm. When the truncation in surrounding patches is reduced, the size of surrounding patches is increased. As a result, the resonant frequency of surrounding patches shifts to lower frequencies and the resonant frequency of the central patch is maintained at the same frequency range. Hence, the upper and lower resonance frequencies

overlap with each other and the impedance bandwidth is further enhanced as the truncation in the surrounding patches is reduced as shown in fig.5.5a.

When the uniform truncation (p=q=5.3mm) is maintained in all patches in antenna 3, the orthogonal fields are generated for circular polarization. When the non-uniform truncation is provided (p ≠ q), the orthogonal fields are spread in other frequencies also. Hence, the axial ratio bandwidth is further increased. The truncation in surrounding patches 'q' is chosen to get maximum 3dB axial ratio bandwidth as shown in fig.5.5b. Therefore in the proposed antenna, the dimension 'L' of a central patch is taken as 16.25mm, dimension 'M' of surrounding patches is taken as 13.75mm and truncation 'p' of a central patch is selected as 5.3mm. The truncation 'q' of the surrounding patch is considered as 4.85mm to achieve the broad bandwidth in impedance bandwidth and axial ratio as depicted in fig.5.5.

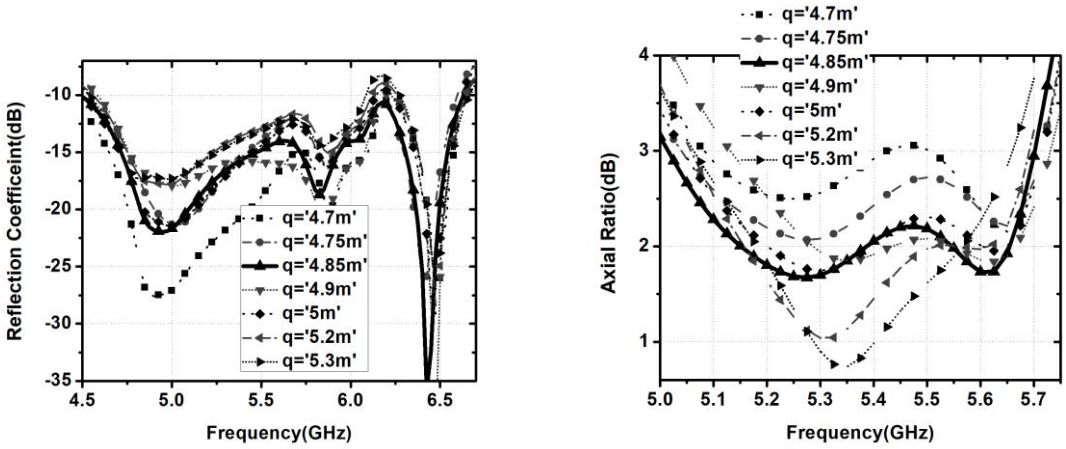

(a) (b)

Fig. 5.5. Simulated results with respect to 'q' (a) S_{11} (b) AR

5.2.5 Variation of L_s

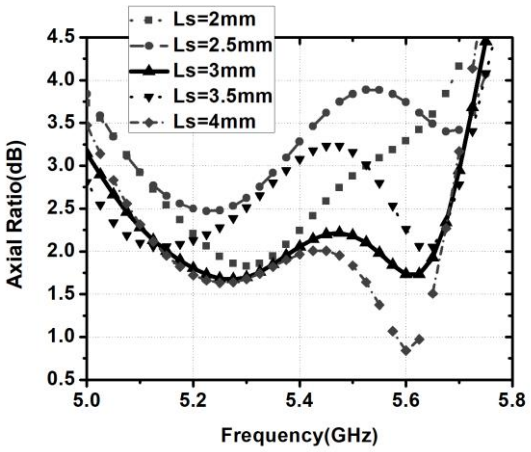

Fig.5.6. Simulated AR results with respect to L_s

The parametric study is performed by varying the length of the stubs in the slot. It is observed from fig. 5.6 that the proposed antenna has shown a maximum 3dB axial ratio bandwidth when the dimension 'L_s' as 3mm and results are represented for the other values less than 3mm also.

The simulation results for the orthogonal fields (E_x and E_y) of proposed antennas are displayed in fig. 5.7. It can be noticed that the amplitude of orthogonal fields (E_x and E_y) is the same (less than 3dB difference) and the phase difference is 90^0 attained throughout broadband frequency ranges (5.0GHz-5.7GHz). Hence, the axial ratio below 3dB is achieved over a broadband frequency range (5.0GHz-5.7GHz).

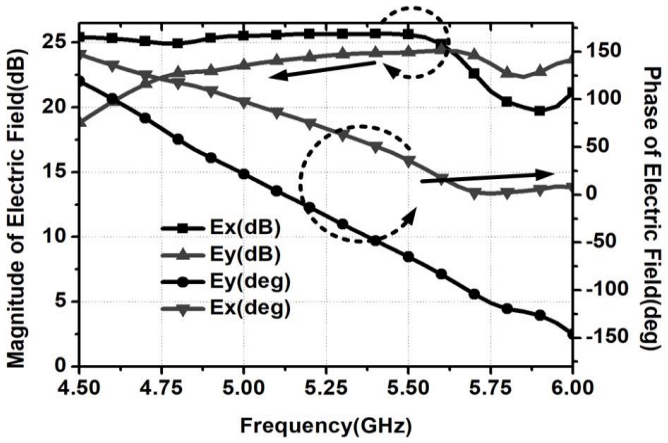

Fig. 5.7. Orthogonal fields for the proposed antenna

The simulation results for the left-hand circularly polarized (LHCP) gain and right-hand circularly polarized (RHCP) gain are displayed in fig. 5.8. Over a resonant frequency range, the RHCP gain is observed to be high and the LHCP gain is observed to be quite low. As a result, the proposed antenna is a right-hand circularly polarized antenna.

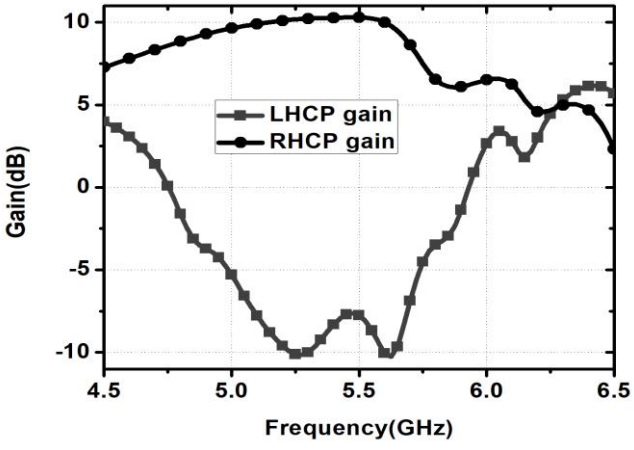

Fig.5.8. Simulated results for the LHCP gain and RHCP gain.

Table.5.3 shows a comparison of proposed antenna simulation results with published literature. It can be noticed that the published literature used a dual substrate layer, multilayer substrates, and air gap to attain broadband circular polarization. In recent works, broadband circular polarization is achieved in single-layer substrates using parasitic elements to the truncated radiating patch [76-79]. But the holes are required for the probe-fed radiating patch and soldering problems to the radiating patch. Such problems are avoided in some of the works to generate broadband linear polarization in single-layer substrates. In this thesis, the above-noticed problems are avoided to create a broadband and high gain circularly polarised antenna in single-layer substrates.

The proposed antenna has been fabricated and is shown in fig. 5.9. The measurements for the proposed antenna have been performed. The measured results seem to be very similar to the simulation results. Due to fabrication errors, there is a slight variation. A vector network analyzer is used to calculate the reflection coefficient, which is presented in fig. 5.10a. In an anechoic chamber, the antenna gain is measured and plotted in fig. 5.10b. The patterns are used to calculate the axial ratio, which is presented in fig. 5.10c. In an anechoic chamber, the radiation patterns are measured and plotted in the X-Z and Y-Z planes, as illustrated in fig. 5.11.

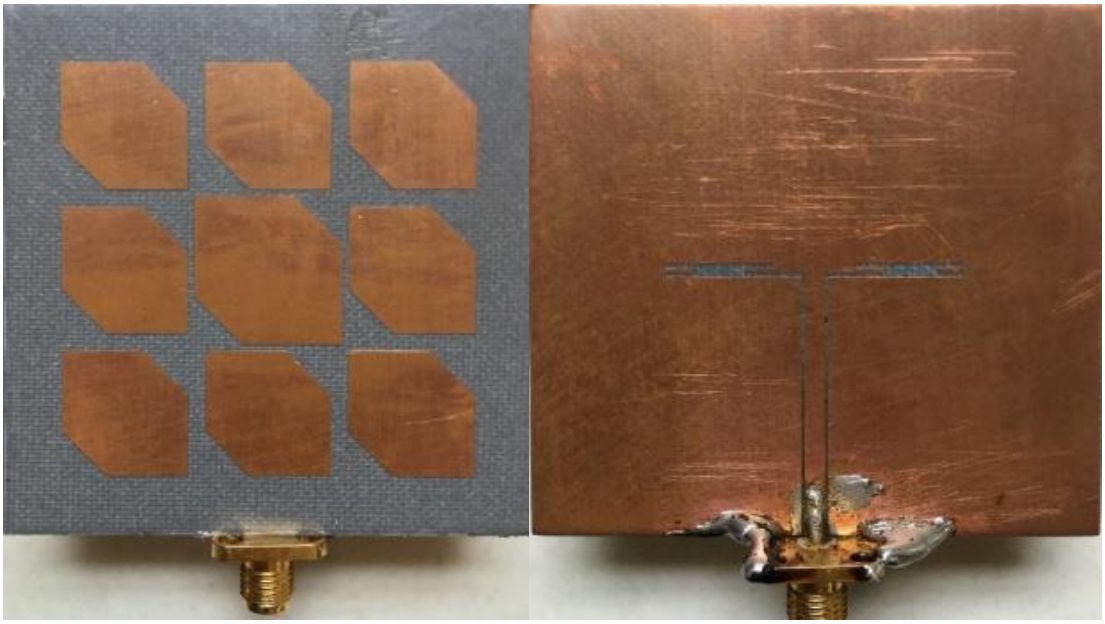

a) b)

Fig. 5.9. Fabricated Prototype model for the proposed antenna (a) top plane view (b) bottom plane view

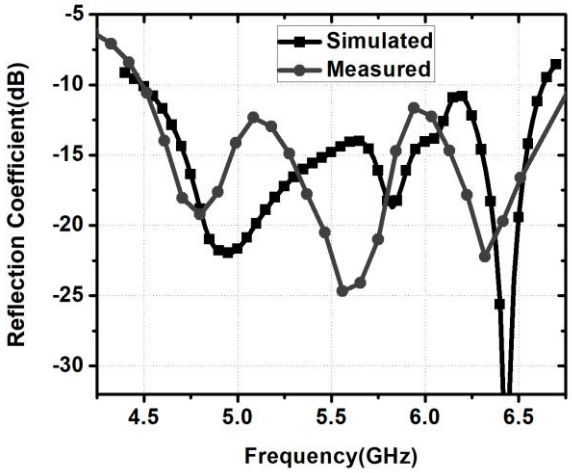

(a)

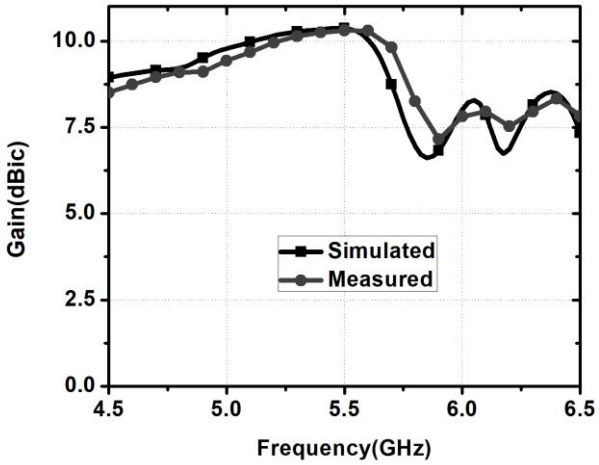

(b)

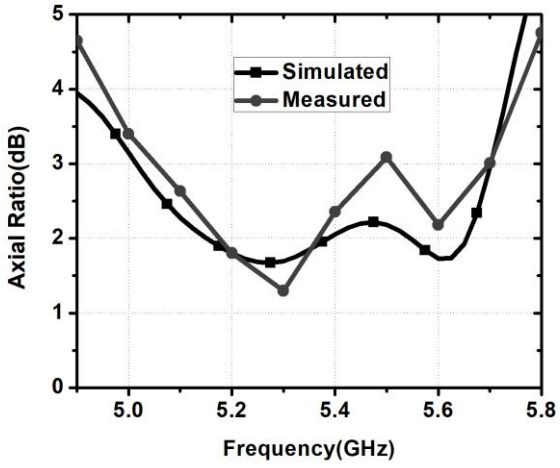

(c)

Fig. 5.10. Simulated and measured results are compared for the proposed antenna (a) S_{11} (b) Gain (c) AR.

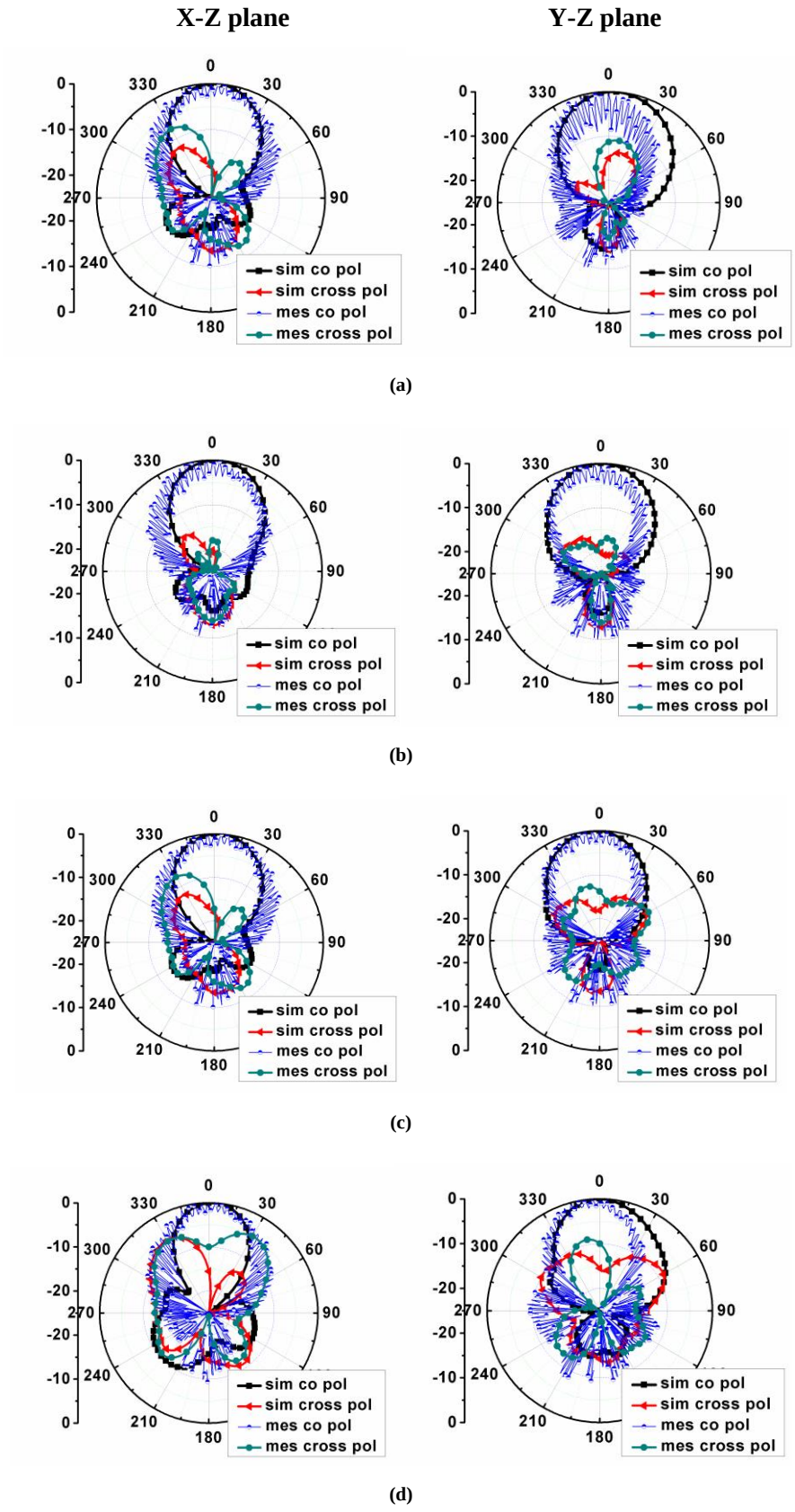

Fig. 5.11. Normalized gain patterns for the proposed antennas at X-Z plane(left) and Y-Z plane (right) (a) 5GHz (b) 5.3GHz (c) 5.5 GHz(d) 5.7GHz.

5.3. 45º Rotated Slot Loaded Square Patch Metasurface Antenna with Uniform Aperture CPW feed

5.3.1 Antenna Design

The proposed antenna geometry is designed on Rogers RT/Duroid 5880 substrate with dimensions of L×W×H as shown in fig. 5.12. The metasurface antenna consists of a 3×3 array of 45^0 rotated slot-loaded square patches separated by a distance d on one side of the substrate. The size of square patches in the middle row is selected as P with the 45^0 rotated slot of dimension r×t. The size of square patches in other rows is selected as Q with the 45^0 rotated slot of dimension s×t. The metasurface antenna is fed by a stub-loaded aperture CPW feed. The aperture is extended on both sides of length L_s with the width of W_s. The stubs of dimension L_t×W_t are inserted across the slot. Coplanar feed of width W_f is connected across the slot. The gap 'g' is maintained between the ground plane and microstrip feed. The following section has a detailed analysis.

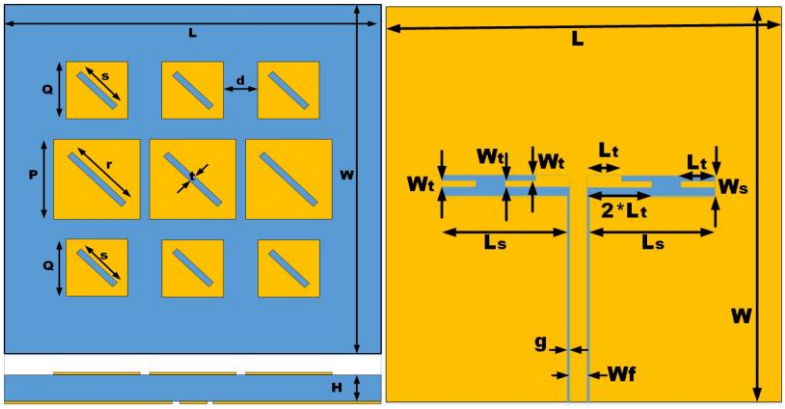

(a) (b)

Fig.5.12. Proposed antenna configuration (a) top plane view and side view (b) bottom plane view.

5.3.2 Design steps

The formulation of the proposed antenna is explained in step by step procedure in fig. 5.13. The corresponding reflection coefficient, gain and axial ratio are displayed in fig. 5.14. The size of middle patches (P) and other patches (Q) are the same for antenna 1 and antenna 2 whereas it is different in the case of antenna 3 and the proposed antenna. The truncation in middle patches (r) and the truncation in other patches (s) are the same for antenna 1 and antenna 2 whereas it is different in the case of antenna 3 and the proposed antenna. The optimized parameter values are shown in Table.5.2.

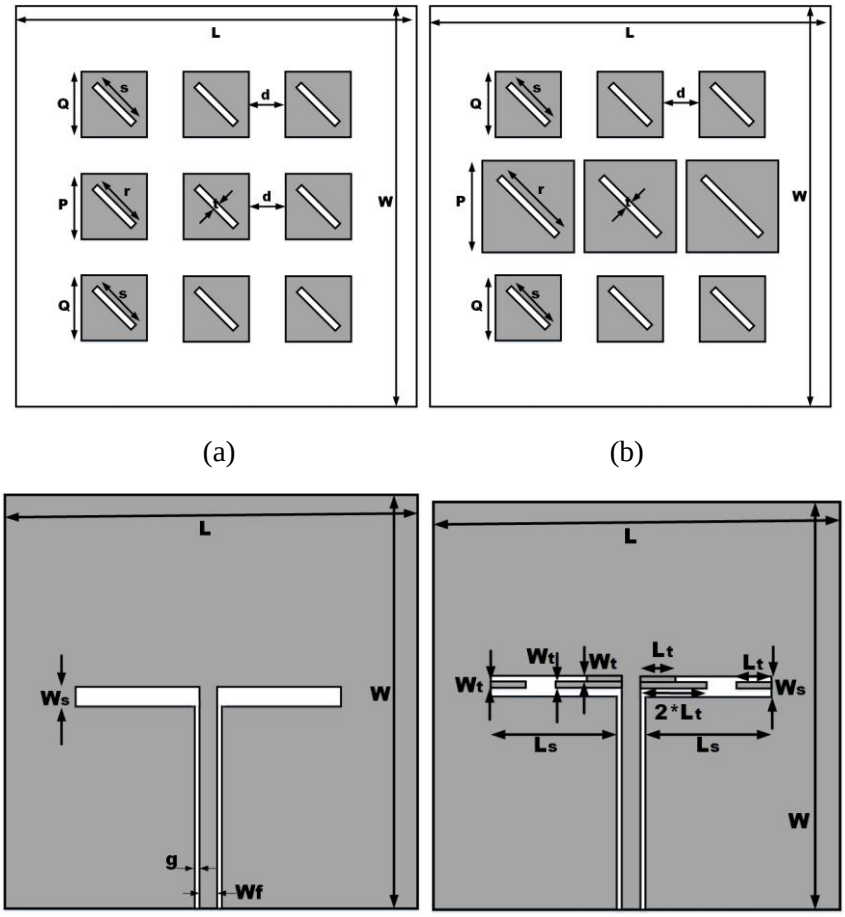

(a) (b)

(c) (d)

Fig.5.13. Design steps of a proposed antenna (a) top plane view of Antenna1, Antenna 2. (b) top plane view of Antenna 3, proposed (c) bottom plane view of Antenna 1(d) bottom plane view of Antenna 2, 3, proposed.

Table 5.2: Optimized parameter values

Parameter	Values(mm)	Parameter	Values(mm)
L	54	P	12.1
W	54	Q	11
L_t	2.5	r	12.8
W_t	0.5	s	12.5
L_s	14	t	0.9
W_s	1.5	d	2.5
g	0.3	H	3.175
W_f	2.1		

In Antenna 1, one side of the substrate is designed with a 3×3 array of equal square patches loaded with 45^0 rotated slots. These patches are excited by a uniform slot on the other side of the substrate. The slot is connected to the coplanar feed line. The simulated results of antenna 1 are shown in fig. 5.14. It can be observed that the antenna has multiple resonances with zero 3dB axial ratio bandwidth in the resonant frequency range. When the stubs are inserted across the slot in antenna 2, the resonant frequencies are coming closer to each other.

The lower resonance frequencies overlap with each other for antenna 2. When the size of middle patches is increased in antenna 3, the impedance bandwidth and 3dB axial ratio bandwidth is improved. In the proposed antenna, the length of slots in the middle patches is increased further to enhance the bandwidth of the impedance bandwidth and 3dB axial ratio. The gain of all antennas is maintained at around 10dBi because of the metasurface on one side of the substrate.

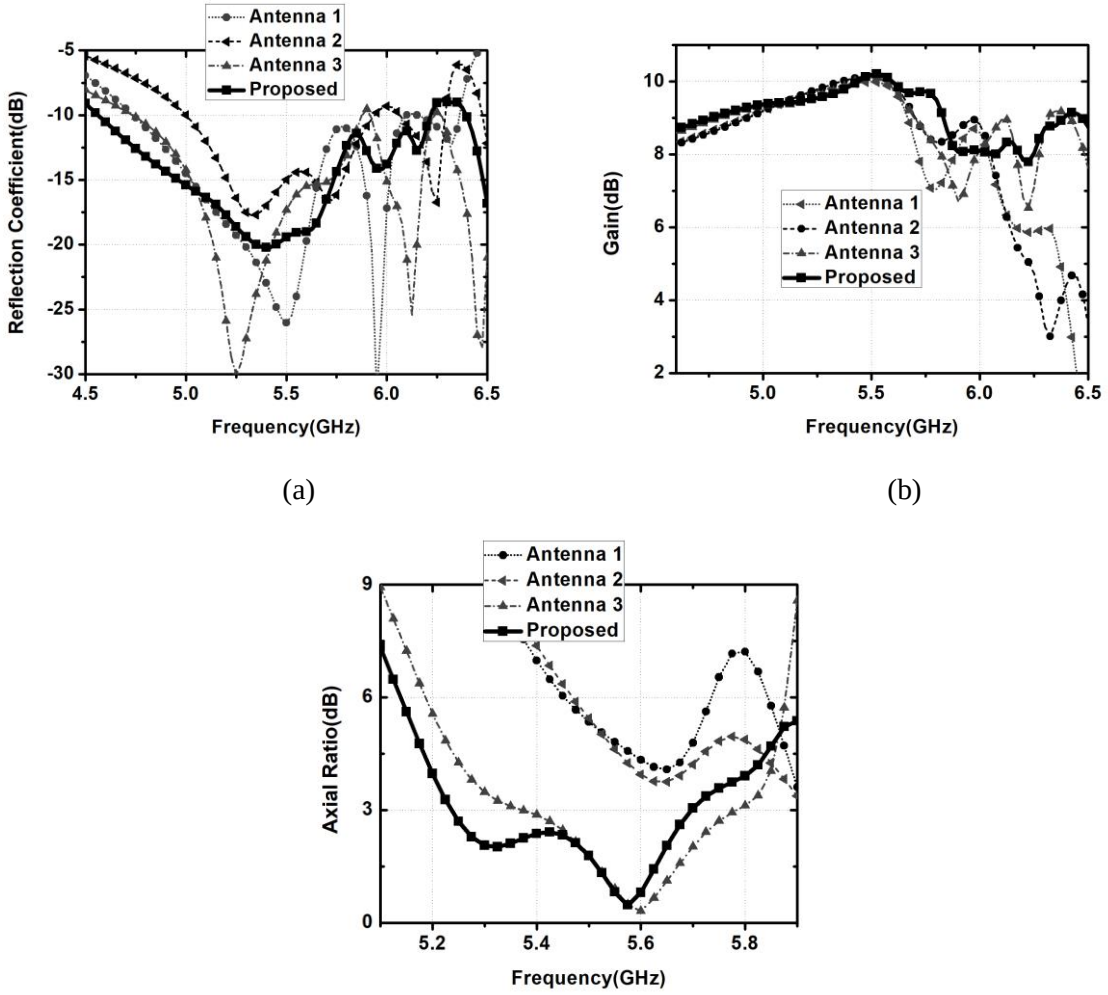

Fig.5.14. Simulated results of all antennas (a) Reflection coefficient (b) Gain (c) Axial Ratio

5.3.3 Considering the 'Q' as 11mm, 'r' and 's' as 12.5mm and changing the dimension 'P'

In antenna 2, the size of all patches is the same with the same slot loaded. When the size of middle patches (P) is increased, it can be observed that the bandwidth of reflection coefficient and 3dB axial ratio is increased. It can be noticed in fig. 5.15 that 'P' is 12.1mm is showing fine bandwidth in reflection coefficient and 3dB axial ratio. Hence, the value of 'P' is selected as 12.1mm for the proposed antenna.

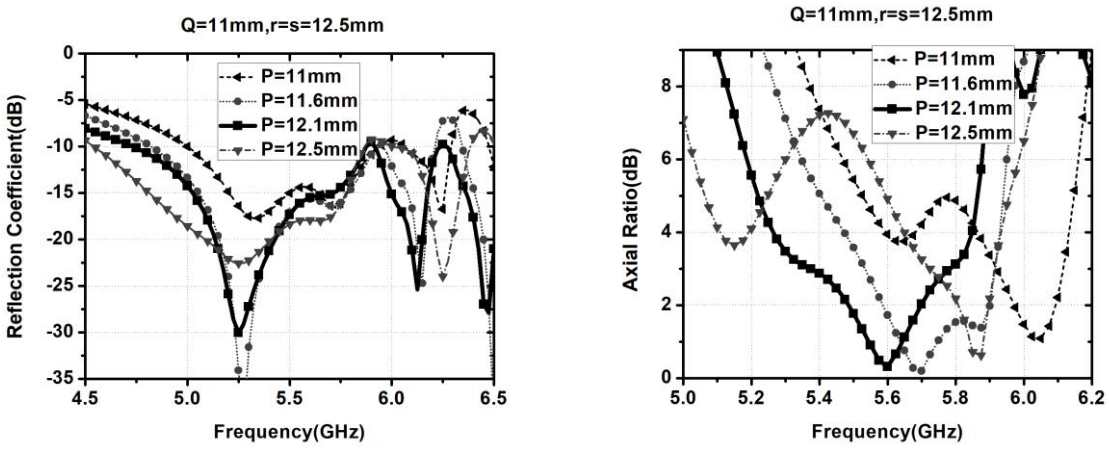

(a) (b)

Fig.5.15. Parametric study of "P" (a) Reflection Coefficient (b) Axial ratio

5.3.4 Considering the 'P' as 12.1mm, 'Q' as 11mm, 's' as 12.5mm and changing the dimension of 'r'

In antenna 3, the size of middle patches (P) is selected as 12.1mm and the size of other patches (Q) is selected as 11mm. When the size of the slots is increased in middle patches, the bandwidth of reflection coefficient and 3dB axial ratio is further enhanced as shown in fig. 5.16. Hence, the value of 'r' is selected as 12.8mm for the proposed antenna.

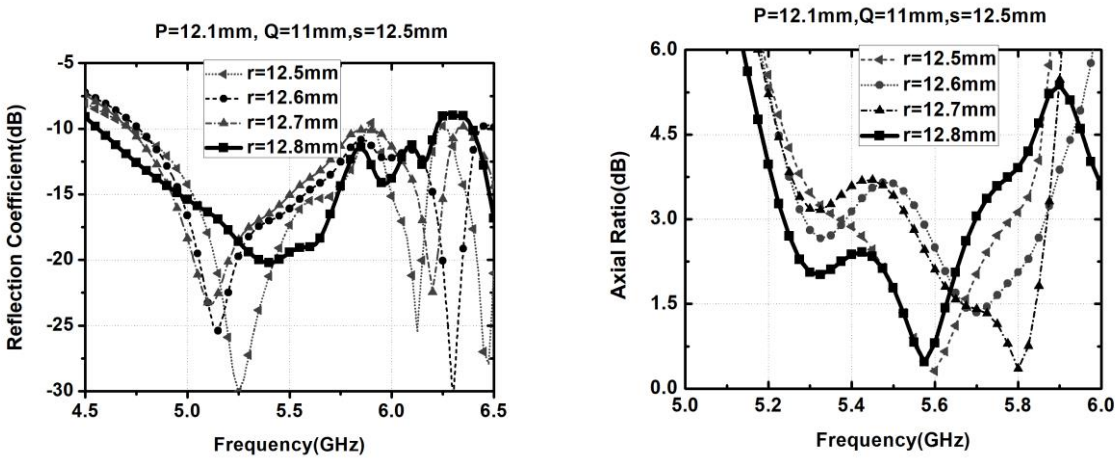

(a) (b)

Fig.5.16. Parametric study of "r" (a) Reflection Coefficient (b) Axial ratio

5.3.5 Varying stub lengths 'L_t'

The parametric study is performed on stub lengths (L_t) by changing the different values. It is clear from fig. 5.17 that the designed antenna has shown the maximum 3dB axial ratio bandwidth when the dimension of L_t is equal to 2.5mm.

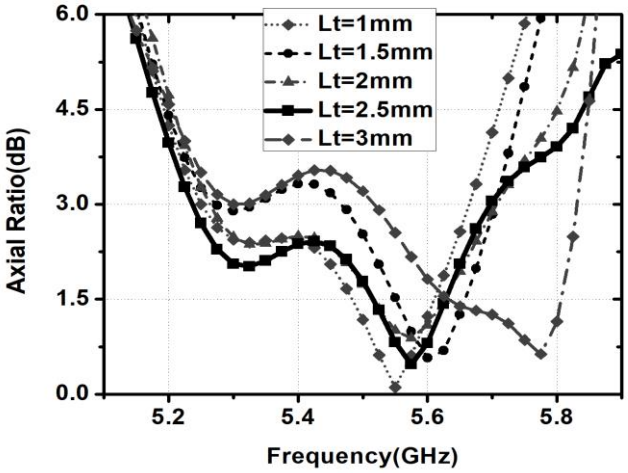

Fig.5.17. Parametric study of "Lt"

Orthogonal fields for the proposed antenna are simulated and it is shown in fig. 5.18a. The orthogonal fields are showing the same magnitude(less than 3dB) and 90^0 phase difference over a broad frequency range (5.23GHz-5.7GHz). Hence, the 3dB axial ratio bandwidth is observed in the frequency range (5.23GHz-5.7GHz). The gain of the left hand circularly polarized (LHCP) and the right hand circularly polarized (RHCP) are displayed in fig. 5.18b. The RHCP gain is high over the resonant frequency range. Whereas the LHCP gain is less over the resonant frequency range. Hence, the antenna is a right-hand circularly polarized antenna.

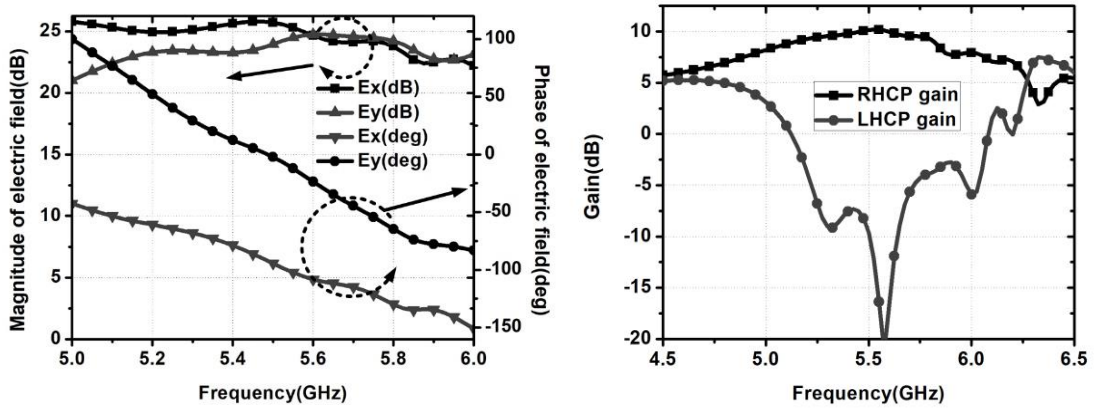

(a) (b)

Fig.5.18. Simulated results of proposed antenna (a) orthogonal fields (b) LHCP & RHCP gain

The proposed antenna is fabricated and the fabricated prototype is displayed in fig. 5.19. The S_{11} for the fabricated prototype is measured using a vector network analyzer. The measurements for the gain, axial ratio and radiation patterns are done in an anechoic chamber.

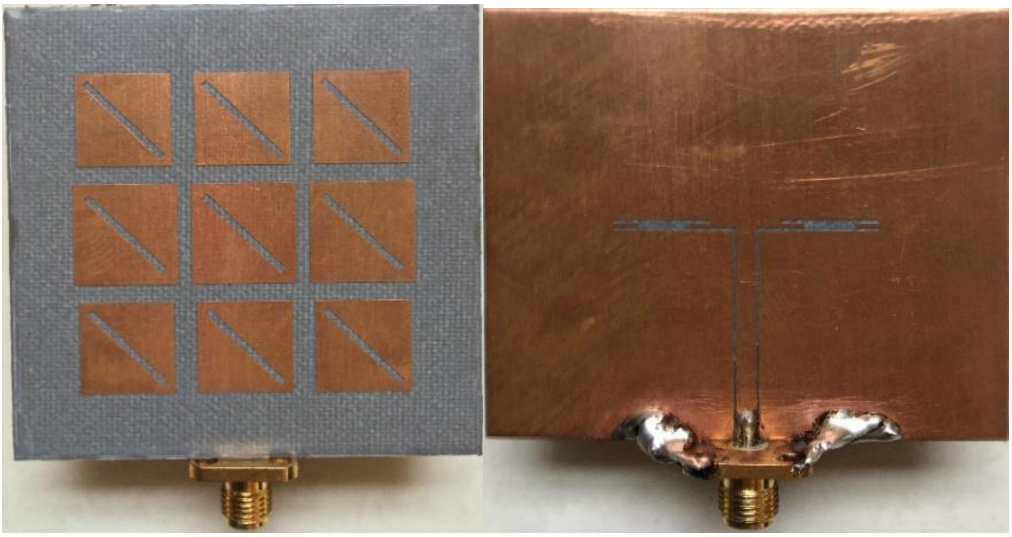

(a) (b)

Fig.5.19. Fabricated model of the proposed antenna (a) Top plane view (b) side plane view

The measured results for the reflection coefficient, gain, and the axial ratio is shown in fig. 5.20. The radiation pattern for the proposed antenna is displayed in fig. 5.21. The simulated and measured results are almost close to each other. There is slight variation due to errors in measurement setup and fabrication.

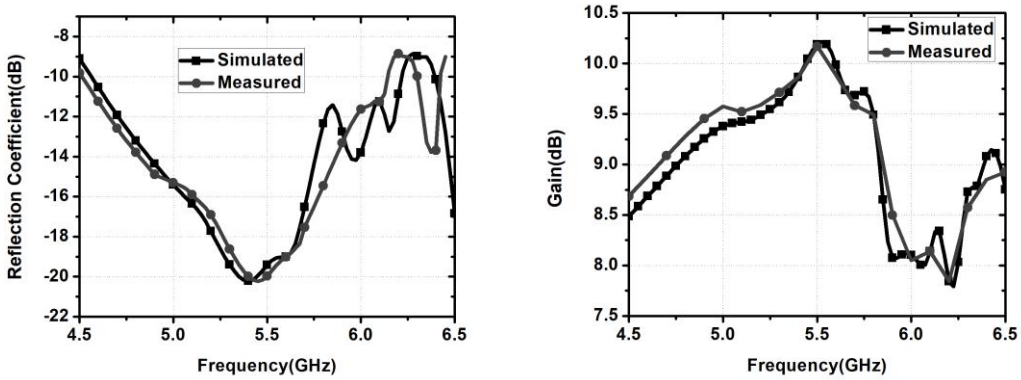

(a) (b)

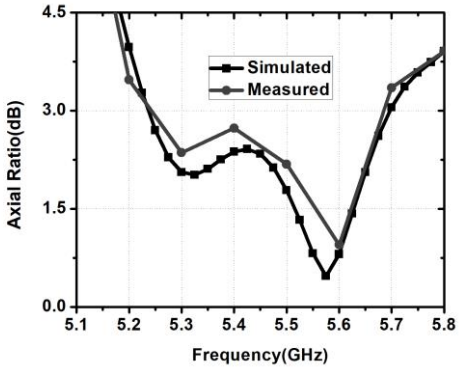

(c)

Fig.5.20. Simulated and measured results are compared for the (a) Reflection Coefficient (b) Gain (c) Axial ratio

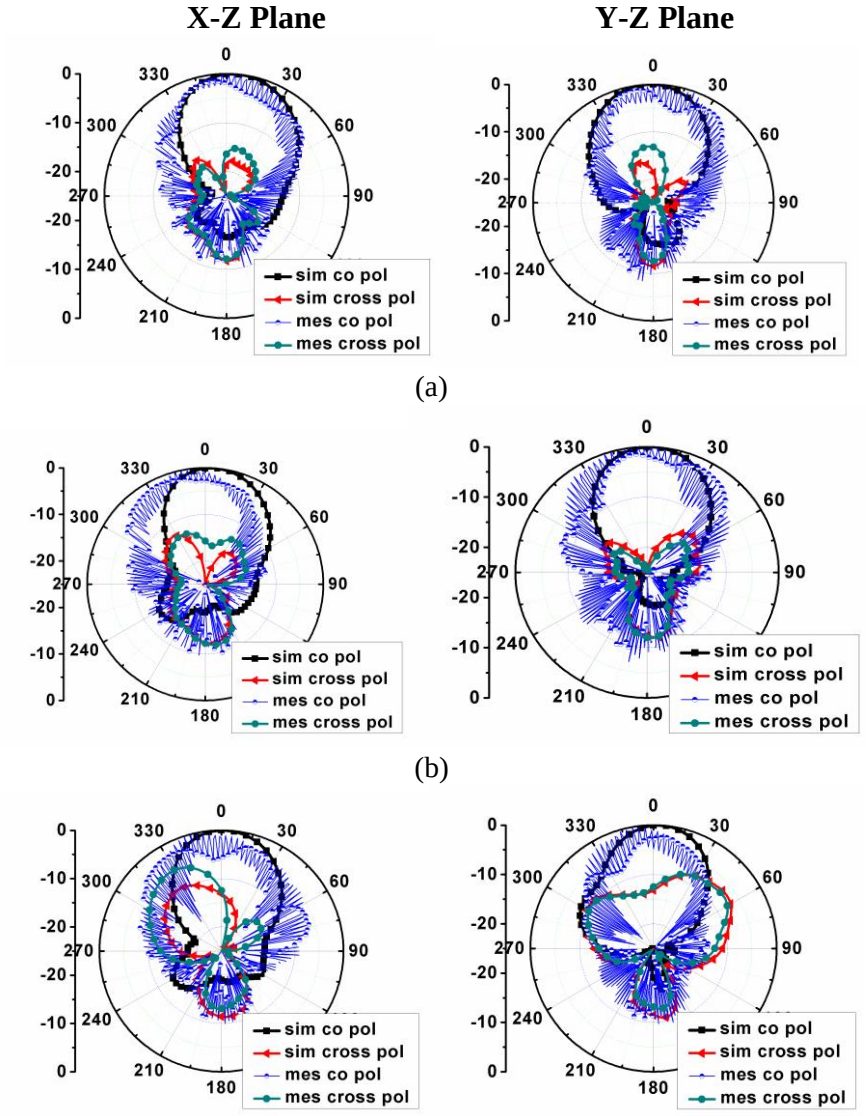

Fig.5.21. Radiation patterns for the proposed antenna at (a) 5.3GHz (b) 5.6GHz (c) 5.8GHz.

Table 5.3. Comparison with published literature

Ref	Substrates	Size(λ3)	Frequency range(GHz)	IBW (%)	Gain	AR (%)
[68]	Dual Layer	1.10λ×1.10λ×0.06λ	4.85-6.28	25	9.9 dBi	-
[69]	Dual Layer	1.10λ×1.10λ×0.06λ	4.60–6.17	29	9.8 dBi	-
[32]	Dual Layer	1.78λ× 1.78λ×0.07λ	4.8-6.2	31	14 dBi	-
[64]	Multilayer + Air gap	λ×λ×0.5λ	4.93-5.89	17.72	12.48	2.4
[65]	Multilayer + Air gap	λ×λ×0.5λ	4.81-6.63	31.8	10	18.9
[74]	Dual Layer	1.60λ×1.60λ×0.065 λ	7.88-12	41.45	13.5	23.16
[75]	Dual Layer	0.76 λ×0.76 λ×0.06λ	5-6.05	19	7.4-8.5	11.3
[36]	Single Layer	λ×λ×0.053λ	9.07-11.36	22.1	7.5 dBi	-
[37]	Single Layer	1.28λ×1.28 λ×0.09λ	4.81 -9.69	67.3	9.18 dBi	-
5.2	**Single Layer**	**λ×λ×0.052λ**	**4.5-6.63**	**38.2**	**10.37dBi**	**13%**
5.3	**Single Layer**	**λ×λ×0.052λ**	**4.56-6.21**	**30**	**10.20dBi**	**8.60%**

The proposed antenna simulation results are compared with published literature as shown in Table 5.3. To achieve broadband circular polarization, the published literature used a dual substrate layer, multilayer substrates, and an air gap. Few papers achieved a broadband circular polarization using parasitic patches to the radiating patches[76-79]. But they used probe feeding to the radiating patch. But the holes are required for the probe-fed radiating patch and soldering problems to the radiating patch. Such problems are avoided in some of the works to generate broadband linear polarization in single-layer substrates. In this thesis, the above noticed probelems are eliminated to create a high gain and broadband circularly polarized antenna in single layer substrate.

5.4 Summary

A truncated corner square patch metasurface antenna is designed with 3x3 array of truncated corner square patches and the metasurface is driven by an aperture CPW feed. In addition to that stubs are inserted in the uniform slot. Moreover, the central patch size in the metasurface is increased for enhancing the bandwidth of impedance bandwidth and 3dB axial ratio. Furthermore, truncation in surrounding patches is reduced to further enhance the bandwidth of impedance bandwidth and 3dB axial ratio.

The truncated corner square patches in the metasurface are replaced with 45^{o} rotated slot-loaded square patches. Moreover, the broadband bandwidth in impedance bandwidth and 3dB axial ratio are attained by increasing the size of the middle patches. Furthermore, the enhancement in the bandwidth of impedance bandwidth and 3dB axial ratio is attained by increasing the slot in the middle patches. The comparison of all antennas in this chapter is presented in Table 5.4. The antennas configured with the above specifications attain a broadband and high gain circularly polarized antenna in single layer planar substrate at 5GHz for Wi-Fi and Wi-Max applications.

Table 5.4. Comparison of all antennas

Antenna	Technique	S11 bandwidth	Gain	Axial Ratio(dB)
5.2	Truncated Corner Square Patch Metasurface Antenna with CPW fed Uniform Aperture	38.2 (4.5-6.63GHz)	10.37dBi	13%
5.3	45^{0} Rotated Slot Loaded Square Patch Metasurface Antenna with CPW fed Uniform Aperture	30 (4.56-6.21GHz)	10.21dBi	8.6%

Chapter 6

Overall Conclusion and Future Scope of The Work

6.1 Research findings of the thesis

The present research work is aimed at exploring novel antenna configurations leading to the designs and realizations of high gain and broadband circularly polarized antennas for 5 GHz Wi-Fi applications. The research work is focused on exploring bandwidth improvement using reactive impedance surface and gain improvement using different superstrates. Both techniques are applied simultaneously to enhance the impedance bandwidth and gain. In addition to that unconventional structures are proposed to achieve a broadband circular polarization. Later metasurface with aperture CPW feed techniques is opted to design high gain and broadband circularly polarized antennas in single layer substrate for 5GHz Wi-Fi applications. All the antennas are designed and simulated using high-frequency structure simulator software. These antennas are fabricated and measurements are performed. The measured results are found to be in good agreement with simulation results. All the high gain and broadband circularly polarized antennas have potential applications in 5GHz Wi-Fi applications.

In chapter 2, the microstrip square patch antenna is designed with an impedance bandwidth of 3.6 %(5.18-5.37GHz) and a gain of 3.5-3.63dBi. Impedance bandwidth of the antenna is enhanced to 6.9% (5.13- 5.50GHz) by using a reactive impedance surface and the average gain of the antenna is enhanced to 9.5-10.23dBi by using the dielectric lens to the microstrip square patch antenna. Instead of using the dielectric lens, the Fabry Perot resonator superstrates are studied and placed at a height half wavelength above the antenna to improve the gain of the antenna to 8.5dBi. In addition, circular polarization is achieved by truncating the pentagonal patch antenna and square patch antenna. The combination of the pentagonal patch with RIS and highly reflective superstrate has attained an impedance bandwidth of 17.72% (4.93-5.89GHz), the gain of 12.48dBi and an axial ratio bandwidth of 2.40% (5.01-5.14GHz. Furthermore, the truncated corner square patch is combined with RIS and high dense dielectric superstrate to achieve an impedance bandwidth of 18% (4.97-5.95GHz), the gain of 9.75dBi and an axial ratio bandwidth of 2.9% (5.15-5.30GHz).

In chapter 3, broadband circular polarization is achieved by using unconventional patch structures like E, C, H and S on reactive impedance surfaces with FR4 substrate. The feeding

position of these structures are adjusted to get broadband circular polarization. These structures are simulated and observed that the S shaped structure is providing good impedance matching over H, C and E structures. The S shaped patch with RIS has shown impedance bandwidth of 29.5% (4.68GHz-6.30GHz) and an axial ratio bandwidth of 15.1 %(5.09GHz-5.92GHz). But the gain of antenna is 1-3dBi only. It is not enough for present applications. In order to improve the gain of antenna, the positive phase gradient frequency selective surface superstrate is placed above the antenna. The S shaped patch with RIS and superstrate has shown impedance bandwidth of 31.8% (4.81GHz-6.63GHz) and gain of 10dBi. In addition to that an axial ratio bandwidth of 18.9 %(4.99GHz-6.03GHz).

In chapter 4, the realization of high gain and broadband circularly polarized antenna in single layer substrate is achived by using metasurface with aperture CPW feed technique. Initially, the metasurface is designed with 3x3 array of circle patches on top face of substrate and L shaped aperture CPW feed is designed on the bottom face of substrate. The stubs are added across the slot and central patch size in the metasurface is reduced to further enhance the impedance bandwidth and an axial ratio bandwidth. The antenna achieved an impedance bandwidth of 20.18% (4.9-6GHz), gain of 10.43dBi and an axial ratio bandwidth of 16.21%.

In chapter 5, instead of using L shaped aperture, the changes are made in the metasurface to design high gain and broadband circularly polarized antenna in single layer substrate. The metasurface is designed with 3x3 array truncated corner square patches on top face of substrate and uniform aperture CPW feed is designed on the bottom face of substrate. The stubs are added across the slot and central patch size is increased to further enhance the impedance bandwidth and an axial ratio bandwidth. Antenna has achieved an impedance bandwidth of 38.2(4.5-6.63GHz), an axial ratio bandwidth of 13% and gain of 10.37dBi. Instead of using truncated corner square patches in the metasurface, 3x3 array of 45^{o} rotated slot loaded square patches are used as a metasurface on the top face of substrate and uniform aperture CPW feed on the bottom face of substrate. The stubs are added across the slot and size of middle row patches are increased to further enhance the impedance bandwidth and axial ratio bandwidth. Antenna has achieved an impedance bandwidth of 30% (4.56-6.21GHz)), an axial ratio bandwidth of 8.6% and peak gain of 10.21dBi.

In this thesis, different types of techniques are expolred to achieve circular polarization. For probe feeding patches, truncation is applied to conventional structures like petagonal patch and square patch to get circular polarization. Unconventional structures like E,C,H and S are proposed to get broadband circualr polaization with RIS surface on FR4 substate. Later, the

circular polarization is generated for the metasurface antenna with aperture CPW feed technique. Initially, the L shaped aperture CPW feed is proposed to get broadband circular polaization. In the case of uniform aperture CPW feed, the metasurface is designed with array of truncated corner square patches or 45^{o} rotated slot loaded square patches.

In this thesis, different types of superstrates are also expolred to improve the gain of antennas such as highly reflective FSS superstrate , positive phase gradient FSS superstrate and high dense dielectric superstrate. Diffeent types of metasurfaces are also explored improve gain and bandwith simultaneously.

6.2 Future Scope of The Work

The FCC is assigning extra frequency bands to the Wi-Fi applications to meet the demand of present and future applications. Moreover, Wi-Fi antennas also need higher gain to provide signal to longer distances.

To explore the reseach work further, novel antenna design configurations can be explored by combining reflectors and other bandwidth enhancement techniques. The metamaterial structures can be incorporated in superstrate and parasitic elements can be added to the radiating element. In this thesis, the inductive type of feeding is given in aperture CPW feed. The results can be analysed using capacitive type of feeding in the aperture CPW feed. The changes can be done in the metasurface and aperture CPW feed to further enhance the results.

References

[1] Balanis, Constantine A. “Antenna theory: analysis and design 3rd edition” *John wiley & sons*, 2005.

[2] John D. Kraus and Ronald J.Marhefka. “Antennas for All Applications 3rd Edition.” *TATA McGraw – Hill edition*, 2003.

[3] Y. Huang and K. Boyle. “Antennas: from theory to practice.” *John Wiley & Sons*, 2008.

[4] Kumar, Girish, and Kamala Prasan Ray. “Broadband microstrip antennas.” *Artech house*, 2003.

[5]Gao, Steven Shichang, Qi Luo, and Fuguo Zhu. “Circularly polarized antennas.” *John Wiley & Sons*, 2013.

[6] Mosallaei, Hossein, and Kamal Sarabandi. "Antenna miniaturization and bandwidth enhancement using a reactive impedance substrate." *IEEE Transactions on antennas and propagation* 52, no. 9 (2004): 2403-2414.

[7] Qu, D., L. Shafai, and A. Foroozesh. "Improving microstrip patch antenna performance using EBG substrates." *IEE Proceedings-Microwaves, Antennas and Propagation* 153, no. 6 (2006): 558-563.

[8] Jash, Shyam Sundar, Chiranjib Goswami, and Rowdra Ghatak. "A low profile broadband circularly polarized planar antenna with an embedded slot realized on a reactive impedance surface." *AEU-International Journal of Electronics and Communications* 108 (2019): 62-72.

[9] Razi, Zahra Mousavi, Pejman Rezaei, and Arash Valizade. "A novel design of Fabry-Perot antenna using metamaterial superstrate for gain and bandwidth enhancement." *AEU-International Journal of Electronics and Communications* 69, no. 10 (2015): 1525-1532.

[10] Zheng, Yuejun, Jun Gao, Yulong Zhou, Xiangyu Cao, Huanhuan Yang, Sijia Li, and Tong Li. "Wideband gain enhancement and RCS reduction of Fabry–Perot resonator antenna with chessboard arranged metamaterial superstrate." *IEEE Transactions on Antennas and Propagation* 66, no. 2 (2017): 590-599.

[11]Vaid, Swati, and Ashok Mittal. "A low profile dual band resonant cavity antenna." *International Journal of RF and Microwave Computer-Aided Engineering* 27, no. 2 (2017): e21065.

[12] Abdelghani, Mohamed Lamine, Hussein Attia, and Tayeb Ahmed Denidni. "Dual-and wideband Fabry–Pérot resonator antenna for WLAN applications." *IEEE Antennas and Wireless Propagation Letters* 16 (2016): 473-476.

[13] Liu, ZhenGuo, WenXun Zhang, DaoLin Fu, YingYing Gu, and ZhiChen Ge. "Broadband Fabry-Perot resonator printed antennas using FSS superstrate with dissimilar size." *Microwave and Optical Technology Letters* 50, no. 6 (2008): 1623-1627.

[14] Feng, Pan, Xing Chen, and Kama Huang. "High performance resonant cavity antenna with non-uniform metamaterial inspired superstrate." *International Journal of RF and Microwave Computer-Aided Engineering* 27, no. 7 (2017): e21114.

[15] Xie, Peng, Guangming Wang, Xiangxin Kong, and Jiaheng Li. "Design of a novel metasurface for dual-band Fabry-Pérot cavity antenna." *International Journal of RF and Microwave Computer-Aided Engineering* 28, no. 2 (2018): e21181.

[16] Meriche, Mohammed Amin, Hussein Attia, Abderraouf Messai, Sheikh Sharif Iqbal Mitu, and Tayeb Ahmed Denidni. "Directive wideband cavity antenna with single-layer meta-superstrate." *IEEE Antennas and Wireless Propagation Letters* 18, no. 9 (2019): 1771-1774.

[17] Muhammad, Shoaib Anwar, Ronan Sauleau, Laurent Le Coq, and Hervé Legay. "Self-generation of circular polarization using compact Fabry–Perot cavity antennas." *IEEE Antennas and Wireless Propagation Letters* 10 (2011): 907-910.

[18] Muhammad, Shoaib Anwar, Ronan Sauleau, Guido Valerio, Laurent Le Coq, and Hervé Legay. "Self-polarizing Fabry–Perot antennas based on polarization twisting element." *IEEE Transactions on Antennas and Propagation* 61, no. 3 (2012): 1032-1040.

[19] Akbari, M., Sh Gupta, and A. R. Sebak. "High gain circularly-polarized Fabry-Perot dielectric resonator antenna for MMW applications." In *2016 IEEE International Symposium on Antennas and Propagation (APSURSI)*, pp. 545-546. IEEE, 2016.

[20] Zhang, Lei, and Tao Dong. "Low RCS and high-gain CP microstrip antenna using SA-MS." *Electronics Letters* 53, no. 6 (2017): 375-376.

[21] Sharma, Ankit, Deepak Gangwar, Binod Kumar Kanaujia, and Santanu Dwari. "Gain enhancement and RCS reduction of CP patch antenna using partially reflecting and absorbing metasurface." *Electromagnetics* 39, no. 2 (2019): 120-135.

[22] Li, Dongying, Zsolt Szabó, Xianming Qing, Er-Ping Li, and Zhi Ning Chen. "A high gain antenna with an optimized metamaterial inspired superstrate." *IEEE transactions on antennas and propagation* 60, no. 12 (2012): 6018-6023.

[23] Singh, Amit K., Mahesh P. Abegaonkar, and Shiban K. Koul. "High-gain and high-aperture-efficiency cavity resonator antenna using metamaterial superstrate." *IEEE Antennas and Wireless Propagation Letters* 16 (2017): 2388-2391.

[24] Zhang, Yu, Minquan Li, Xu Pan, Xiaopan Xia, Yanyang Liu, and Yingbo Wu. "High Gain Microstrip Antenna Based on Zero-index Metamaterials." In *2018 Progress in Electromagnetics Research Symposium (PIERS-Toyama)*, pp. 1088-1091. IEEE, 2018.

[25] Haider, Zain, Muhammad U. Khan, and Hammad M. Cheema. "A dual-band metamaterial superstrate for antenna gain enhancement." In *2018 IEEE International Symposium on Antennas and Propagation & USNC/URSI National Radio Science Meeting*, pp. 1017-1018. IEEE, 2018.

[26] Pandey, Ajay K., Monika Chauhan, Vinay K. Killamsety, and Biswajeet Mukherjee. "High-gain compact rectangular dielectric resonator antenna using metamaterial as superstrate." *International Journal of RF and Microwave Computer-Aided Engineering* 29, no. 12 (2019): e21968.

[27] Simruni, Mojtaba, and Shahrokh Jam. "Design of high gain, wideband microstrip resonant cavity antenna using FSS superstrate with equivalent circuit model." *AEU-International Journal of Electronics and Communications* 112 (2019): 152935.

[28] Mark, Robert, Neha Rajak, Kaushik Mandal, and Soma Das. "Metamaterial based superstrate towards the isolation and gain enhancement of MIMO antenna for WLAN application." *AEU-International Journal of Electronics and Communications* 100 (2019): 144-152.

[29] Li, Long, Shuo Lei, and Chang-Hong Liang. "Metamaterial-based fabry–perot resonator for ultra-low profile high-gain antenna." *Microwave and Optical Technology Letters* 54, no. 11 (2012): 2620-2623.

[30] Panda, Prakash Kumar, and Debalina Ghosh. "Isolation and gain enhancement of patch antennas using EMNZ superstrate." *AEU-International Journal of Electronics and Communications* 86 (2018): 164-170

[31]Usha, Priyanka, and Chitra Krishnan. "Epsilon near zero metasurface for ultrawideband antenna gain enhancement and radar cross section reduction." *AEU-International Journal of Electronics and Communications* 119 (2020): 153167.

[32] Lin, Feng Han, and Zhi Ning Chen. "Low-profile wideband metasurface antennas using characteristic mode analysis." *IEEE Transactions on Antennas and Propagation* 65, no. 4 (2017): 1706-1713.

[33] Bai, Hao, and Guang-Ming Wang. "A multistate high gain antenna based on metasurface." *International Journal of RF and Microwave Computer-Aided Engineering* 30, no. 8 (2020): e22330.

[34] Ta, Son Xuat, and Ikmo Park. "Low-profile broadband circularly polarized patch antenna using metasurface." *IEEE Transactions on Antennas and Propagation* 63, no. 12 (2015): 5929-5934.

[35] Sharma, Ankit, Deepak Gangwar, Binod Kumar Kanaujia, and Santanu Dwari. "RCS reduction and gain enhancement of SRR inspired circularly polarized slot antenna using metasurface." *AEU-International Journal of Electronics and Communications* 91 (2018): 132-142.

[36] Liao, Hsiu-Ping, and Shih-Yuan Chen. "Bandwidth and Gain Enhancement of CPW-Fed Slot Antenna Using A Partially Reflective Surface Formed by Two-Step Tapered Dipole Unit Cells." In *2019 IEEE Asia-Pacific Microwave Conference (APMC)*, pp. 1449-1451. IEEE, 2019.

[37] Wang, Junfang, Hang Wong, Zhuoqiao Ji, and Yongle Wu. "Broadband CPW-fed aperture coupled metasurface antenna." *IEEE Antennas and Wireless Propagation Letters* 18, no. 3 (2019): 517-520.

[38] Bernard, Loïc, G. Chertier, and Ronan Sauleau. "Wideband circularly polarized patch antennas on reactive impedance substrates." *IEEE Antennas and Wireless Propagation Letters* 10 (2011): 1015-1018.

[39] Nakamura, Teruhisa, and Takeshi Fukusako. "Broadband design of circularly polarized microstrip patch antenna using artificial ground structure with rectangular unit cells." *IEEE Transactions on Antennas and Propagation* 59, no. 6 (2011): 2103-2110.

[40] Nasimuddin, N., Zhi Ning Chen, and Xianming Qing. "Bandwidth Enhancement of a Single-Feed Circularly Polarized Antenna Using a Metasurface: Metamaterial-based wideband

CP rectangular microstrip antenna." *IEEE Antennas and Propagation Magazine* 58, no. 2 (2016): 39-46.

[41] Li, Q. L., S. W. Cheung, Di Wu, and T. I. Yuk. "Microwave lens using periodic dielectric sheets for antenna-gain enhancement." *IEEE Transactions on Antennas and Propagation* 65, no. 4 (2017): 2068-2073.

[42] Trentini, G. Von. "Partially reflecting sheet arrays." *IRE Transactions on antennas and propagation* 4, no. 4 (1956): 666-671.

[43] Zeb, B. A., R. M. Hashmi, and K. P. Esselle. "Wideband gain enhancement of slot antenna using one unprinted dielectric superstrate." *Electronics Letters* 51, no. 15 (2015): 1146-1148.

[44] Chatterjee, Ayan, and Susanta Kumar Parui. "Gain enhancement of a wide slot antenna using a second-order bandpass frequency selective surface." *Radioengineering* 24, no. 2 (2015): 455-461.

[45] Attia, Hussein, M. Lamine Abdelghani, and Tayeb A. Denidni. "Wideband and high-gain millimeter-wave antenna based on FSS Fabry–Perot cavity." *IEEE transactions on antennas and propagation* 65, no. 10 (2017): 5589-5594.

[46] Asaadi, Muftah, Islam Afifi, and Abdel-Razik Sebak. "High gain and wideband high dense dielectric patch antenna using FSS superstrate for millimeter-wave applications." *IEEE Access* 6 (2018): 38243-38250.

[47] Pitra, Kamil, Zbynek Raida, and Jaroslav Lacik. "Low-Profile Circularly Polarized Antenna Exploiting Fabry-Perot Resonator Principle." *Radioengineering* 24, no. 4 (2015).

[48] Orr, Robert, George Goussetis, and Vincent Fusco. "Design method for circularly polarized Fabry–Perot cavity antennas." *IEEE Transactions on Antennas and Propagation* 62, no. 1 (2013): 19-26.

[49] Ta, S. X., and T. K. Nguyen. "AR bandwidth and gain enhancements of patch antenna using single dielectric superstrate." *Electronics Letters* 53, no. 15 (2017): 1015-1017.

[50]Nguyen, T. K. "High-gain circularly polarised Fabry–Perot antenna with tapered frequency selective surface for X-band." *Electronics Letters* 55, no. 5 (2019): 241-242.

[51] Cao, Wenquan, Xinmeng Lv, Qianqian Wang, Yanhui Zhao, and Xiaoqin Yang. "Wideband circularly polarized Fabry–Pérot resonator antenna in Ku-band." *IEEE Antennas and Wireless Propagation Letters* 18, no. 4 (2019): 586-590.

[52] Bai, Bondili Kohitha. "Design and simulation of circularly polarized pentagonal-shaped microstrip patch antenna at RFID frequency 2.4 Hz." In *CS & IT Conference Proceedings*, vol. 2, no. 1. CS & IT Conference Proceedings, 2012.

[53] Yang, Fan, and Yahya Rahmat-Samii. "A low profile single dipole antenna radiating circularly polarized waves." *IEEE Transactions on Antennas and Propagation* 53, no. 9 (2005): 3083-3086.

[54] Chatterjee, Joysmita, Akhilesh Mohan, and Vivek Dixit. "Broadband circularly polarized H-shaped patch antenna using reactive impedance surface." *IEEE Antennas and Wireless Propagation Letters* 17, no. 4 (2018): 625-628.

[55] Wang, Naizhi, Qiang Liu, Changying Wu, Larbi Talbi, Qingsheng Zeng, and Jiadong Xu. "Wideband Fabry-Perot resonator antenna with two complementary FSS layers." *IEEE Transactions on Antennas and Propagation* 62, no. 5 (2014): 2463-2471.

[56] Yuan, Hang-Ying, Shao-Bo Qu, Jie-Qiu Zhang, Jia-Fu Wang, Hong-Ya Chen, Hang Zhou, Zhuo Xu, and An-Xue Zhang. "A metamaterial-inspired wideband high-gain F ABRY–P erot resonator microstrip patch antenna." *Microwave and Optical Technology Letters* 58, no. 7 (2016): 1675-1678.

[57] Zhang, Chen, Xiang-yu Cao, Jun Gao, and Si-jia Li. "Wideband high-gain and low scattering antenna using shared-aperture metamaterial superstrate." *Radioengineering* 27, no. 2 (2018): 379-385.

[58] Peddakrishna, Samineni, and Taimoor Khan. "Performance improvement of slotted elliptical patch antenna using FSS superstrate." *International Journal of RF and Microwave Computer-Aided Engineering* 28, no. 9 (2018): e21421.

[59] Vinnakota, Sarath Sankar, Runa Kumari, and Basudev Majumder. "Dual-polarized high gain resonant cavity antenna for radio frequency energy harvesting." *International Journal of RF and Microwave Computer-Aided Engineering* 29, no. 12 (2019): 22003.

[60] Zeb, Basit Ali, Nasiha Nikolic, and Karu P. Esselle. "A high-gain dual-band EBG resonator antenna with circular polarization." *IEEE Antennas and Wireless Propagation Letters* 14 (2014): 108-111.

[61] Liu, Zhen-Guo, Zhen-Xin Cao, and Le-Nan Wu. "Compact low-profile circularly polarized Fabry–Perot resonator antenna fed by linearly polarized microstrip patch." *IEEE Antennas and Wireless Propagation Letters* 15 (2015): 524-527.

[62] Ta, Son Xuat, Thi Hai-Yen Nguyen, Khac Kiem Nguyen, and Chien Dao-Ngoc. "Bandwidth-enhancement of circularly-polarized fabry-perot antenna using single-layer partially reflective surface." *International Journal of RF and Microwave Computer-Aided Engineering* 29, no. 8 (2019): e21774.

[63] Srinivas, Guthi, N. V. S. N. Sarma, and D. Vakula. "Gain and bandwidth improvement of circularly polarized pentagonal patch antenna." In *2019 TEQIP III Sponsored International Conference on Microwave Integrated Circuits, Photonics and Wireless Networks (IMICPW)*, pp. 274-277. IEEE, 2019.

[64] Srinivas, Guthi, and Damera Vakula. "High Gain and Wide Band Antenna Based on FSS and RIS Configuration." *Radioengineering* 30, no. 1 (2021).

[65] Guthi, Srinivas, and Vakula Damera. "High gain and wideband circularly polarized S-shaped patch antenna with reactive impedance surface and frequency-selective surface configuration for Wi-Fi and Wi-Max applications." *International Journal of RF and Microwave Computer-Aided Engineering* 31, no. 11 (2021): e22865.

[66] Shaw, Tarakeswar, Deepanjan Bhattacharjee, and Debasis Mitra. "Gain enhancement of slot antenna using zero-index metamaterial superstrate." *International Journal of RF and Microwave Computer-Aided Engineering* 27, no. 4 (2017): e21078.

[67] Sheersha, Jils A., N. Nasimuddin, and Arokiaswami Alphones. "A high gain wideband circularly polarized antenna with asymmetric metasurface." *International Journal of RF and Microwave Computer-Aided Engineering* 29, no. 7 (2019): e21740.

[68] Liu, Wei, Zhi Ning Chen, and Xianming Qing. "Metamaterial-based low-profile broadband mushroom antenna." *IEEE transactions on antennas and propagation* 62, no. 3 (2013): 1165-1172.

[69] Liu, Wei, Zhi Ning Chen, and Xianming Qing. "Metamaterial-based low-profile broadband aperture-coupled grid-slotted patch antenna." *IEEE transactions on antennas and propagation* 63, no. 7 (2015): 3325-3329.

[70] Cao, Wen-quan, Bangning Zhang, Wei Hong, and Jun Jin. "L-shaped slot coupling-fed low-profile broadband circularly polarized patch antenna with metasurface." *Journal of ElEctromagnEtic WavEs and applications* 31, no. 1 (2017): 111-120.

[71] Menzel W, Grabherr W. A microstrip patch antenna with coplanar feed line. *IEEE Microwave and Guided Wave Letters,* Vol. 1, No. 11, November 1991

[72] Deng SM, Wu MD, Hsu P. Impedance characteristics of microstrip antennas excited by coplanar waveguides with inductive or capacitive coupling slots. *IEEE microwave and guided wave letters*. 1995 Nov;5(11):391-3.

[73] Giauffret L, Laheurte JM, Papiernik A. Study of various shapes of the coupling slot in CPW-fed microstrip antennas. *IEEE Transactions on Antennas and Propagation*. 1997 Apr;45(4):642-7.

[74] Ta, Son Xuat, and Ikmo Park. "Planar wideband circularly polarized metasurface-based antenna array." *Journal of ElEctromagnEtic WavEs and applications* 30, no. 12 (2016): 1620-1630.

[75] Liu, Yuan, Yu-Xuan Huang, Zhan-Wei Liu, Shu-Ting Cai, Xiao-Ming Xiong, and Jing Guo. "A new broadband circularly polarized antenna with a single-layer metasurface." *International Journal of RF and Microwave Computer-Aided Engineering* 30, no. 7 (2020): e22226.

[76] Zheng, Yue-Jun, Jun Gao, Yu-Long Zhou, Xiang-Yu Cao, Li-Ming Xu, Si-Jia Li, and Huan-Huan Yang. "Metamaterial-based patch antenna with wideband RCS reduction and gain enhancement using improved loading method." *IET Microwaves, Antennas & Propagation* 11, no. 9 (2017): 1183-1189.

[77] Liang, Zhipeng, Jun Ouyang, and Feng Yang. "Low-profile wideband circularly polarised single-layer metasurface antenna." *Electronics letters* 54, no. 24 (2018): 1362-1364.

[78] Tran, Huy Hung, Niamat Hussain, and Tuan Tu Le. "Single-layer low-profile wideband circularly polarized patch antenna surrounded by periodic metallic plates." *International Journal of RF and Microwave Computer-Aided Engineering* 29, no. 12 (2019): e21969.

[79] Hussain, Niamat, Huy Hung Tran, and Tuan Tu Le. "Single-layer wideband high-gain circularly polarized patch antenna with parasitic elements." *AEU-International Journal of Electronics and Communications* 113 (2020): 152992.

[80] https://www.radartutorial.eu/06.antennas/pic/dipole.png

[81] https://www.researchgate.net/profile/Thamer-Almoneef 2/publication/267406861/figure/fig5/AS:634117590876164@1528196823906/The-fabricated-microstrip-line-fed-patch-antenna_Q640.jpg

[82] https://www.researchgate.net/profile/Mahmoud-Moubadir/publication/303106848/figure/fig7/AS:646574241759236@1531166720582/Radiation-pattern-of-a-patch-antenna-in-3D.png

[83] https://ae01.alicdn.com/kf/HTB1YBr7KpXXXXcrXpXXq6xXFXXXE/GSM-CDMA-outdoor-yagi-antenna-12dBi-N-female-868M-7elements-roof-top-yagi-antenna.jpg

[84] https://www.l3harris.com/sites/default/files/styles/625_x_570/public/2020-09/sas-ma-product-AS-48435-antenna-hero-1250x1140.png?itok=QNLJFxon

[85] https://cpimg.tistatic.com/00975242/b/5/Satellite-Offset-Dish-Antenna-w410.jpg

[86] https://www.ahsystems.com/EMC-formulas-equations/images/Antenna-gain-dBi.png

[87] https://www.emedicalprep.com/wp-content/uploads/2-types-of-polarization.png

[88] https://qph.cf2.quoracdn.net/main-qimg-1b1ebd87848d086ca17ab254096c31bf.webp

[89] https://www.wifi-shop24.com/cyberbajt-24-12-yagi-directional-antenna-outdoor-12dbi

[90] https://www.wifi-shop24.com/alfa-network-aga-2424t-wifi-grid-antenna-24dbi

[91] https://www.wifi-shop24.com/interline-panel-17-directional-weatherproof-wifi-antenna-17dbi

[92] https://www.wifi-shop24.com/24-GHz-WiFi-Omnidirectional-Antenna-RP-SMA-Connector-2dBi

[93] https://www.wifi-shop24.com/5ghz-wifi-omni-antenna-5dbi-gain-rpsma-connector

[94] https://www.wifi-shop24.com/interline-panel-23-5ghz-directional-panel-antenna-abs-23dbi

[95]https://www.dvcomm.in/media/catalog/product/cache/2/image/9df78eab33525d08d6e5fb8d27136e95/c/p/cpe610.jpg

[96] https://www.wifi-shop24.com/dualband-wifi-antenna-ceiling-mounr-black-30cm-cable-rpsma-connector-5dbi

[97] http://www.ecsystem.cz/ec_system/download/point-to-point-profi-5ghz-6ghz.pdf

[98] http://www.ecsystem.cz/content/news/thumbs/2016-20-01-11-09-46-1920-450-20-135-point-to-point-ec-link.jpg

[99] http://www.ecsystem.cz/content/news/thumbs/2016-20-01-11-10-20-1920-450-20-137-point-to-multipoint-ec-multipoint.jpg

[100]https://www.researchgate.net/publication/330300933/figure/fig2/AS:1086037552037894@1635942938088/Selected-functionalities-of-metasurfaces-a-band-pass-frequency-selective-surface-b.jpg

Publications

International Journals - Published

1. Guthi, Srinivas, and Vakula Damera. "High Gain and Broadband Circularly Polarized Antenna using Metasurface and CPW fed L-Shaped Aperture." *AEU-International Journal of Electronics and Communications* (2022): 154109. (SCI- ELSEVIER PUBLISHER)

2. Guthi, Srinivas, and Vakula Damera. "High gain and wideband circularly polarized S-shaped patch antenna with reactive impedance surface and frequency-selective surface configuration for Wi-Fi and Wi-Max applications." *International Journal of RF and Microwave Computer-Aided Engineering* 31, no. 11 (2021): e22865. (SCI- WILEY PUBLISHER)

3. Guthi Srinivas, and Damera Vakula, “Aperture Coupled CPW Feed for High gain and Broadband Circularly Polarized Slot Loaded Square Patch Metasurface Antenna,” *Microwave and optical technology letters*, .2022; 64:809–815. (SCI- WILEY PUBLISHER)

4. Srinivas G, Vakula D “High Gain and Wide Band Antenna Based on FSS and RIS Configuration.” *Radio engineering*. 2021 Apr 1;30(1). (SCI-CZECH TECHNICAL UNIVERSITY)

5. Srinivas G, Vakula D “Broadband and High Gain Circularly Polarized Truncated Corner Square Patch Metasurface Antenna using Aperture CPW Feed” *Journal of Electromagnetic Waves and Applications*, (2022): 1-13. (SCI- TAYLOR AND FRANCIS)

6. Guthi Srinivas, and Vakula Damera. "High Gain and Wide Band Fabry Perot Resonator Antenna." *International Journal of system assurance engineering and management*, (2022): 1-9. (ESCI- SPRINGER).

International Conferences – Presented & Published in Conference Proceedings

1. Srinivas Guthi, N. V. S. N. Sarma, and D. Vakula. "Gain and Bandwidth Improvement of Circularly Polarized Pentagonal Patch Antenna." *2019 TEQIP III Sponsored International Conference on Microwave Integrated Circuits, Photonics and Wireless Networks (IMICPW)*. IEEE, 2019.

2. Guthi Srinivas, N. V. S. N. Sarma, and D. Vakula," Gain and Bandwidth Enhancement of Patch Antenna", *Photonics & Electromagnetics Research Symposium* (PIERS). 2019.

3. Guthi Srinivas, and D Vakula, "High Gain and Wide Band Fabry Perot Resonator Antenna." *13th International Conference* (ATMS – 2021 Virtual Platform).